FAIRCHILD HILLER
REPUBLIC AVIATION DIVISION
FARMINGDALE, LONG ISLAND, NEW YORK

Prepared for:

Office of Naval Research
Code 468
Acoustics Programs
Washington, D.C. 20360

Prepared by:

William J. Guman
Burton G. Humphrey Jr.

FAIRCHILD HILLER CORPORATION
REPUBLIC AVIATION DIVISION
Farmingdale, New York 11735

Reproduction, dissemination, or use of information contained herein is permitted for any purpose of the U. S. Government. Research was sponsored by the Office of Naval Research, Code 468 under contract No. Nonr 4741(00), Authority No. NR-185-706.

Period of Performance: 1 December 1964 - 31 October 1968

PCD-TR-68-16
FHR 2229-7
PC088R0004
December 31, 1968

Studies on an Electric Discharge Underwater Sound Source

FINAL REPORT

Contract No. Nonr 4741(00)

CONTENTS

ILLUSTRATIONS

Figure No.		Page
52	Current and Light Probe Reading (40 KV)	80
53	Two Capacitor Discharges in Fresh and Salt Water	81
54a	Current Waveform Shaping in Fresh Water	82
54b	Current Waveform Shaping in Fresh Water	83
55a	Current Waveform Shaping in Salt Water	85
55b	Current Waveform Shaping in Salt Water	86
56	Normalized Energy Spectrum	87

ABSTRACT

Operation of the inverse pinch geometry in underwater electrical discharges, viewed as acoustic sources, has been evaluated. The basic characteristics of the signal radiated (e.g., distance dependence, waveform, etc.) are similar to general underwater discharges and explosive sources. Critical dependence of the energy efficiency on the electrical damping characteristics of the discharge circuit (including the discharge itself) was found. However, high speed optical investigations disclosed that, under the achievable energy and configuration limitations, it was not possible to produce a discharge of the desired cylindrical symmetry.

Auxiliary investigations demonstrated that the configuration produced satisfactory strong (arc-like) discharges in water equivalent in salinity to sea water; however, the increased energy loss during initiation of the arc, due to the higher conductivity of the water, tended to decrease overall efficiency in saline solutions. It was also demonstrated that near field acoustic signals may be shaped to a considerable extent by tailoring the waveform of the electrical discharge (with significantly decreased energy efficiency, however).

SECTION I

INTRODUCTION

A. OBJECTIVES OF PROGRAM

The work summarized in this report deals with exploratory development of a system for generating strong acoustic pulses in water by discharge of high voltage capacitively stored electrical energy into an underwater electrode pair. An inverse pinch electrode geometry, such as has been successfully employed in low pressure gas discharge experiments [1,2] was employed. The outwardly directed force on the conducting plasma column of the discharge, produced by the interaction of the current with its self-generated magnetic field in a suitable geometry, appears to offer a means of augmenting the pressure exerted on the expanding water-plasma boundary. Such an increase in the acceleration driving the initial stages of generation of the acoustic pulse in the water should increase its magnitude.

An evaluation of the practical feasibility of the use of inverse pinch geometry in underwater discharge acoustic work was therefore attempted. In addition to exploration of the practical problems involved, determination of conditions for optimizing energy transfer to the water was attempted as well as investigation of correlation between discharge circuit characteristics and the waveform of the acoustic pulse.

B. MAGNETICALLY AUGMENTED ELECTRIC DISCHARGE SOUND SOURCES

One of the objectives of the present study was to attempt to use the self-generated magnetic field energy created by the underwater electric discharge to augment the acoustic signal radiated. This objective can, in principle, be most effectively accomplished by studying an inverse-pinch electrode geometry sound source. In such an axisymmetric geometry the magnetic field produced by the electric current is confined and utilized to do work against the surrounding water by interacting with the cylindrical plasma sheet generated during the electric discharge. The radiated acoustic signal is produced by the expansion and ultimate collapse of the plasma and the bubble into which it evolves.

Figure 1 shows a schematic representation of the inverse-pinch electric discharge sound source. Upon closing switch S, the electric energy stored in capacitor C is discharged into the interelectrode region of the electrode assembly. The electric current (denoted by arrows) generates a circumferential magnetic field. Because the circumferential magnetic field interacts with the current-carrying plasma, a magnetic force is exerted on the plasma. This force acts normal to the plane containing the magnetic induction vector and the current density vector. Unlike ordinary spark discharges, the net resultant magnetic force acting on the plasma in the inverse-pinch electrode configuration is always directed radially outward (with respect to the axis of symmetry) even during electric current oscillations. This force is exerted on the plasma only while current flows and generally is independent of the magnitude of the thermodynamic gas pressure within the plasma. For the geometry under study, the magnetic force-per-unit-volume acting at any radial location r (measured from the axis of symmetry) varies directly as the square of the net total current passing through the circular plane of radius r, and inversely as the square of the radius r. The net total current at any radius r is equal to the magnitude of the total current passing through the center electrode (see Figure 1) minus the current density of the return current passing through the plasma integrated over all elements of area $2\pi r\,dr$, the limits of integration extending from the radius of the inner surface of the plasma to the radius r. It is postulated here that the return current is carried by the whole plasma sheet. As a result of the magnetic-force-per-unit-volume which acts on the

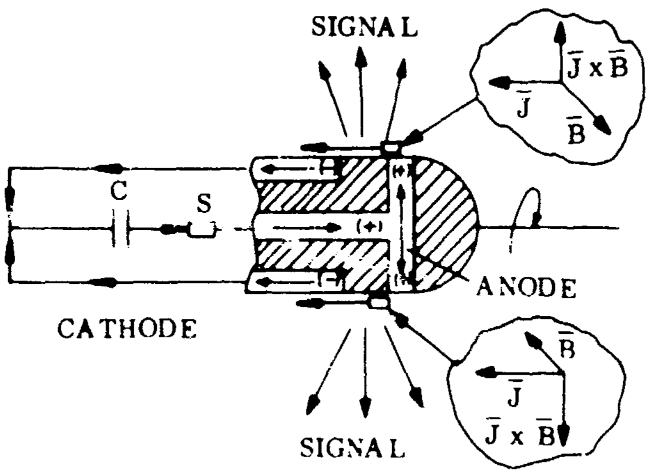

Figure 1. Schematic of Inverse-Pinch Sound Source

plasma, the pressure at the inner boundary is reduced and the pressure at the outer boundary is increased with respect to those pressures which would have resulted from the thermal conditions alone. It is the increase in pressure at the outer boundary, of course, which is the more directly and obviously related to the production of the sound pulse.

Analytically the effect of the magnetic pressure is examined as follows. Neglecting gravitational, electric and viscous forces, the equation of motion of an element of the plasma column reads:

$$\rho \frac{D\bar{u}}{Dt} = - \nabla p + \bar{j} \times \bar{B}$$

with ρ, p, $\bar{j}$ and $\bar{B}$ denoting mass density, static pressure, electric current density and magnetic field intensity, respectively. The term $D\bar{u}/Dt$ is the total time derivative of the velocity. The term $\bar{j} \times \bar{B}$ represents the magnetic force per unit volume and ∇p is the pressure gradient across the element being examined. From Maxwell's equation (neglecting displacement currents), one has:

$$\nabla \times H = \bar{j}$$

with $\bar{B} = \mu \bar{H}$

The term $\bar{j} \times \bar{B}$ can therefore be rewritten as:

$$\bar{j} \times \bar{B} = - \mu \bar{H} \times (\nabla \times \bar{H}) = - \nabla \left(\frac{B^2}{2\mu} \right) + \mu (\bar{H} \cdot \nabla \bar{H})$$

The equation of motion is therefore quite generally given by:

$$\rho \frac{D\bar{u}}{Dt} = - \nabla \left(p + \frac{B^2}{2\mu} \right) + \mu (\bar{H} \cdot \nabla \bar{H})$$

The term $B^2/2\mu$ is more commonly referred to as the "magnetic pressure". For a cylindrical geometry, such as the inverse pinch geometry being studied, only one component of $\bar{H}$ exists and $\nabla \bar{H}$ is normal to $\bar{H}$. Thus $\bar{H} \cdot \nabla \bar{H} = 0$ for the geometry being considered.

The term $B^2/2\mu$ ("magnetic pressure") can be rewritten in terms of the total current as follows: From Stokes theorem one has:

$$\int \bar{H} \cdot ds = \int (\nabla \times \bar{H}) \cdot dA$$

Substituting Maxwell's equation, this becomes:

$$\frac{1}{\mu} \oint \bar{B} \cdot ds = \int \bar{j} \cdot d\bar{A} = I$$

where $\bar{j} \cdot dA$ is the total current I enclosed by the area A. The left expression of the last equation gives the integral of the magnetic field along any closed path enclosing area A. Since the discharge is assumed cylindrically symmetric, a circular path concentric about the axis of symmetry of the acoustic source is selected. Thus $\bar{H}$ is a constant along this path (because of cylindrical symmetry) and one finds:

$$\frac{1}{\mu} \oint B \cdot ds = \frac{B_\theta}{\mu} \oint ds = \frac{B_\theta}{\mu} 2\pi r = I$$

with B_θ the azimuthal magnetic field intensity. The magnetic force per unit volume in the equation of motion therefore reads:

$$\frac{B^2}{2\mu} = \frac{\mu I^2}{8\pi^2 r^2}$$

or

$$j \times B = -\nabla \left(\frac{B^2}{2\mu}\right) = -\frac{\partial}{\partial r} \left(\frac{\mu I^2}{8\pi^2 r^2}\right)$$

It should be noted from this latter expression that the driving action of the magnetic force in the plasma is radially outward directed and contributes in the same manner as the hydrostatic pressure in expanding the bubble. In ordinary exploding wires this magnetic pressure is radially inward directed and tends to reduce the acoustic effect.

Some simple calculations can now be carried out to establish the magnitude of the "magnetic pressures" likely to be encountered. Figure 2 presents the magnitude of the magnetic pressure experienced by the conducting plasma shell whose radius

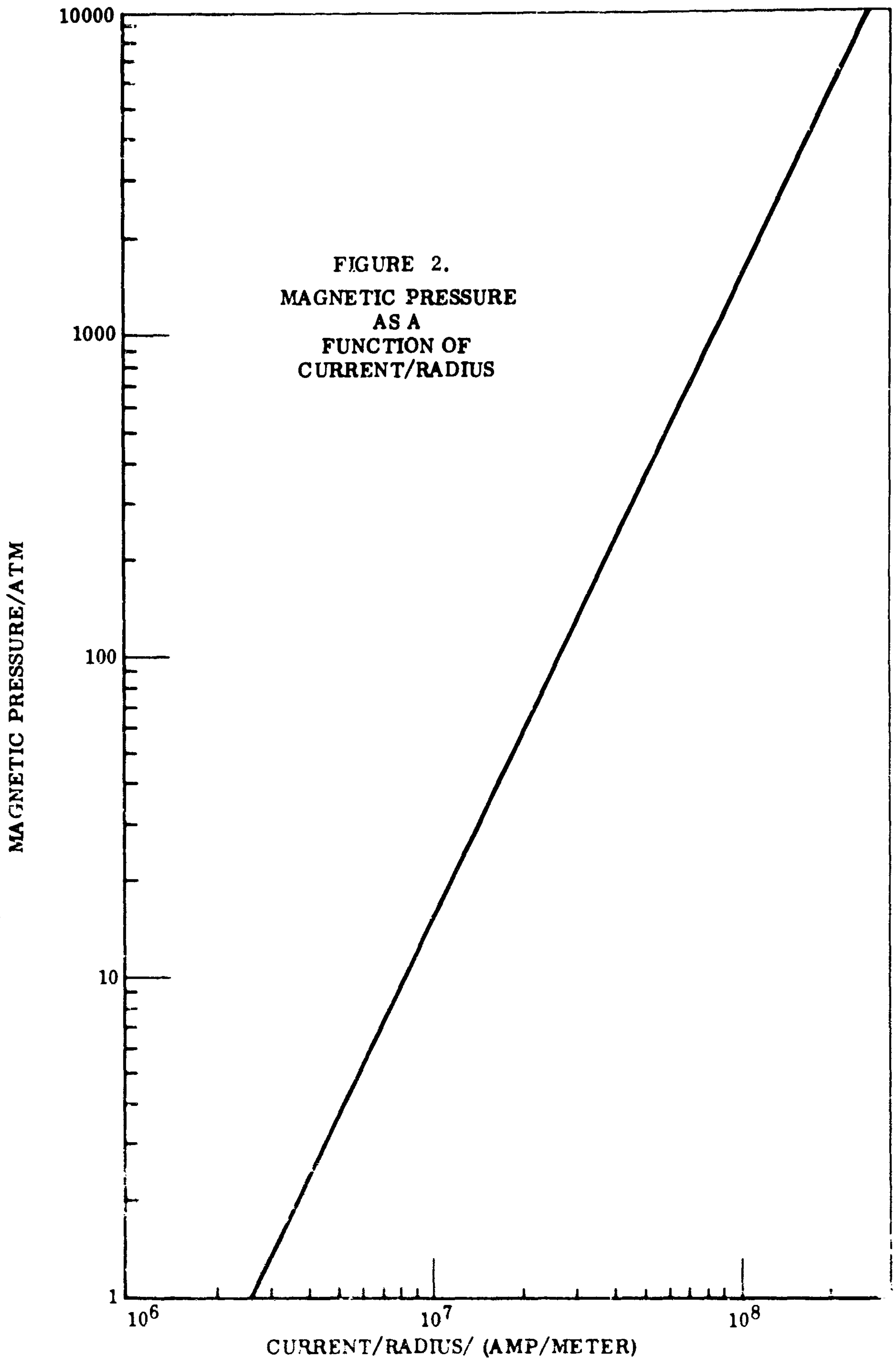

FIGURE 2.
MAGNETIC PRESSURE
AS A
FUNCTION OF
CURRENT/RADIUS
10000
1000
100
10
1
MAGNETIC PRESSURE/ATM
10^6
10^7
10^8
CURRENT/RADIUS/ (AMP/METER)

is r as a function of the current to radius ratio. It is seen that the magnetic contribution to the pressure at the outer boundary is not large in comparison with that associated with the thermal effects. For example, with a current of 300,000 amperes in an electrode 0.75 cm in diameter the total magnetic-force-per-unit-area (i.e., the combined magnitudes of the pressure shifts at the inner and outer boundaries of the plasma) is about 1,000 atmospheres independent of the thermodynamic gas pressure existing in the plasma. In addition, unless the plasma sheet is a perfectly closed surface and of extremely high electrical conductivity much of the time-varying magnetic field energy is dissipated in the water surrounding the electrodes. Nevertheless some augmentation (roughly 10%) of the acoustic effect might be anticipated which would not occur in exploding wire studies for example.

Efforts of the present program have concentrated on producing as large a current as possible, with a given quantity of stored energy in the capacitor. Fortunately, both the thermodynamic gas pressure and the magnetic-force-per-unit-area are increased as one increases the amplitude of the current. The former is accomplished by ohmic dissipation of electric energy in the plasma while the latter is automatically self-induced. The thermodynamic pressure is related by an appropriate equation of state to internal thermal energy while the magnetic-force-per-unit-area is proportional to the square of the local magnetic induction. For the thin plasma sheet being considered, it is equal to the "magnetic pressure" which exists at the inner boundary of the plasma.

Besides the inverse pinch electrode geometry, there are other electrode configurations in which magnetic augmentation of the acoustic effect might be anticipated. Of these, a line discharge in which the current flows in opposite directions in two adjacent conductors is perhaps the simplest scheme. In essence the force experienced by the plasma column of the line discharge (similar to that generated by an exploding wire, for example) is magnetically repelled by the counterflowing electric discharge current flowing in the return lead located immediately behind the line discharge. The magnetic force acting in the line discharge is then known to be:

$$F = \frac{\mu I^2 L}{2 \pi s}$$

with μ , i, L, s denoting the permeability, electric current, length of the discharge column, and the spacing between the line discharge and the return lead behind it.

Based upon the high speed photographic results obtained in this study it is believed that one, and in some rare instances, two line discharges are formed on the periphery of the inverse pinch electrode assembly studied. In initiating the discharge it appears that a series of streamers spread out in the water and that the main discharge takes place in that streamer (or those) that bridges the two electrodes of the acoustic source. As energy is deposited into this streamer by the external circuit, there is a tendency of the streamer to spread peripherally around the electrode surface while expanding away from the electrodes. In no case was a cylindrical plasma sheet formed. Therefore, any magnetic augmentation found in this study is arrived at more from the repulsion of two current carrying line elements rather than the expansion of a cylindrical plasma sheet under the action of magnetic pressure.

SECTION II

DESCRIPTION OF EXPERIMENTAL FACILITIES

A. TESTING TANK

All underwater discharge experiments were performed in the laboratory in an approximately 8-foot high, 8-foot diameter metal tank. When filled to the 7-foot overflow level, the tank contains approximately 2500 gallons. The frame of the tank is electrically strapped directly to a ground bus for safety considerations. The interior is coated with an insulating protective epoxy marine paint, both for corrosion resistance and for reduction of the electric current leakage path to ground from the electrical discharge apparatus; it was found with the highly conductive salt solutions that appreciable leakage existed nevertheless. Careful grounding procedure was found to eliminate any ground loop difficulties from this source, however. A circulating and filtering system was used to maintain clarity of the water, and it performed satisfactorily throughout the course of the work. This system was operated only when no tests were being performed.

The principal disadvantages to testing impulsive acoustic sources in laboratory scale tanks rather than in a free-field environment are the limited period of reception of the direct signal before the arrival of reverberation signals from the free surface, bottom and tank walls, and the possibility that near field effects may be significant. The maximum signal duration free of boundary reverberation effects available in the above tank geometry for a 3-foot separation of source and detector, for example, is approximately one millisecond, when placed equidistant from the axis at a depth of 3.5 feet. This period of time is insufficient to record unperturbed pressure signals generated by the collapse of the discharge gas bubble, since time of the order of 5-10 milliseconds would be required for this latter phenomenum at the energy levels used in this work (above 100 joules). On the other hand, the primary positive pressure pulse from the discharge itself was found generally to be confined to a time span of 100 microseconds or less, with the pressure decaying gradually thereafter, in accordance with the requirement that the time integral of the complete pressure pulse must vanish.

Accordingly, the primary pressure pulse was the only part of the acoustic signal which was studied in this work. Since the optimum source-transducer location (in terms of signal duration) would not have sufficed to show the bubble pulse, the source was placed, for operational convenience, always at varying depths along the axis of the tank. Signal durations adequate for displaying the primary pressure pulse were always obtained.

Most of the earlier developmental work was performed in fresh water; ordinary tap water was used for this purpose. Operation of the acoustic source in salt water was also investigated, and for this purpose a series of simulated sea water solutions of varying degrees of salinity was prepared by dissolving in situ the requisite amounts of "Instant Ocean" synthetic sea salts*. The manufacturer's instructions specify the quantity necessary to prepare a solution capable of supporting marine life. A normal salinity of 35 promille was assumed for the purpose of solution preparation, and proportioned amounts of the components used to prepare solutions of the desired salinity.

The solutions as prepared were characterized by measurement of their electrical conductivity. A standard AC Wheatstone bridge arrangement was used, employing a parallel circular disc platinized electrode conductance cell standardized with 0.1 N KCl. A schematic of the circuit is shown in Figure 3. An approximate correlation with the more common parameter, salinity (S), was made using the data on sea water conductance contained in Dietrich (Reference 3, page 83). In addition, measurements on the pH of the solution were made using an L&N glass electrode system and crude density measurements were made using a simple hydrometer float. The results of all the above measurements are summarized in Table 1.

The agreement of S_η with S (nominal) is regarded as generally satisfactory, although the divergence seems to increase at higher values of S at a linear rate,

---

* Aquarium Systems, Inc., 1489 East 289th Street, Wickliffe, Ohio. See Appendix I for composition.

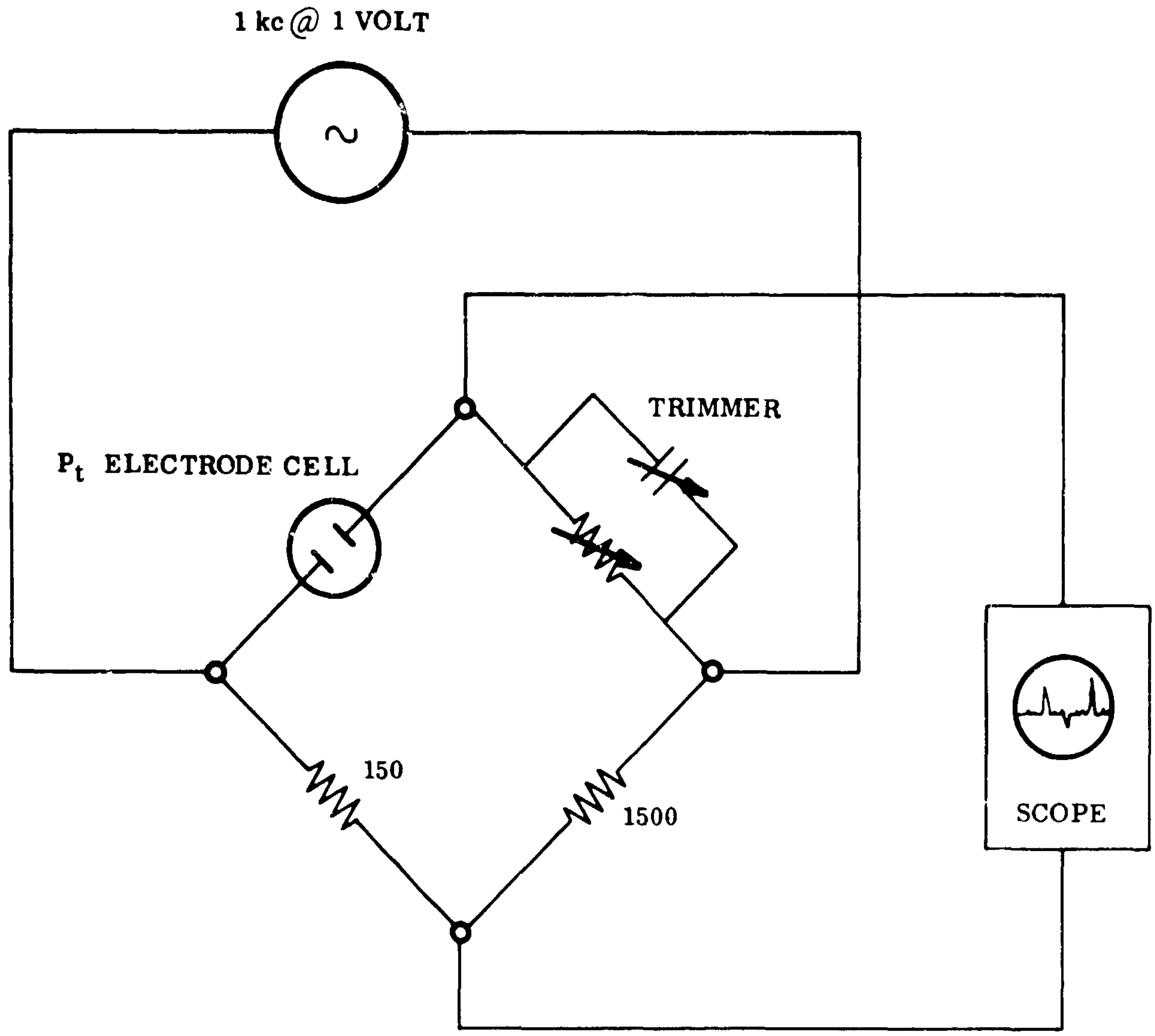

Figure 3. Conductivity Bridge Schematic

Table 1: Salt Solution Properties

Soln. No.	S(nominal) °/₀₀	$10^3 \kappa_{20°C}$ mho/cm	S_κ °/₀₀	ρ g/cm^3	S_ρ °/₀₀	pH
I	2.2	3.9	1.9	0.999	2.2	---
II	4.4	7.3	4.2	1.006	10.5	---
III	8.9	12.9	8.2	1.008	13.0	7.78
IV	17.5	24.4	16.4	1.014	21.0	8.25
V	26.2	35.1	24.6	1.020	28.9	8.25
VI	35.0	43.9	31.3	1.026	36.5	8.60

probably due to some systematic error in the measurement or solution preparation. The divergence of the last point (VI) is more marked; this may be associated with observed difficulty in dissolving the last batch of salt. A small amount of insoluble residue or precipitate was observed.

B. ELECTRICAL SYSTEM

1. Description of General Circuit

The general configuration of the capacitive discharge electrical circuit is shown in Figure 4. The variable high voltage supply was a model HV-140 unit made by Electrostatic Ionic Corporation, Garfield, New Jersey, rated at 140 kV/5ma. Various capacitors were used during the course of the work depending on the voltage level, energy and mechanical requirements of particular experiments; the bulk of the work was performed using Cornell-Dublier 15 μfd, 20 KV low units for lower voltages (up to 18 KV) and Axel 50E104, 1 μ fd 50 KV low inductance units for the higher voltages. The portions of the circuit below the dotted line which provide the capability of providing delayed energy input, were not used except during the pulse shaping experiments described in Section III-F. The maximum energy capability of the system was approximately 9000 joules.

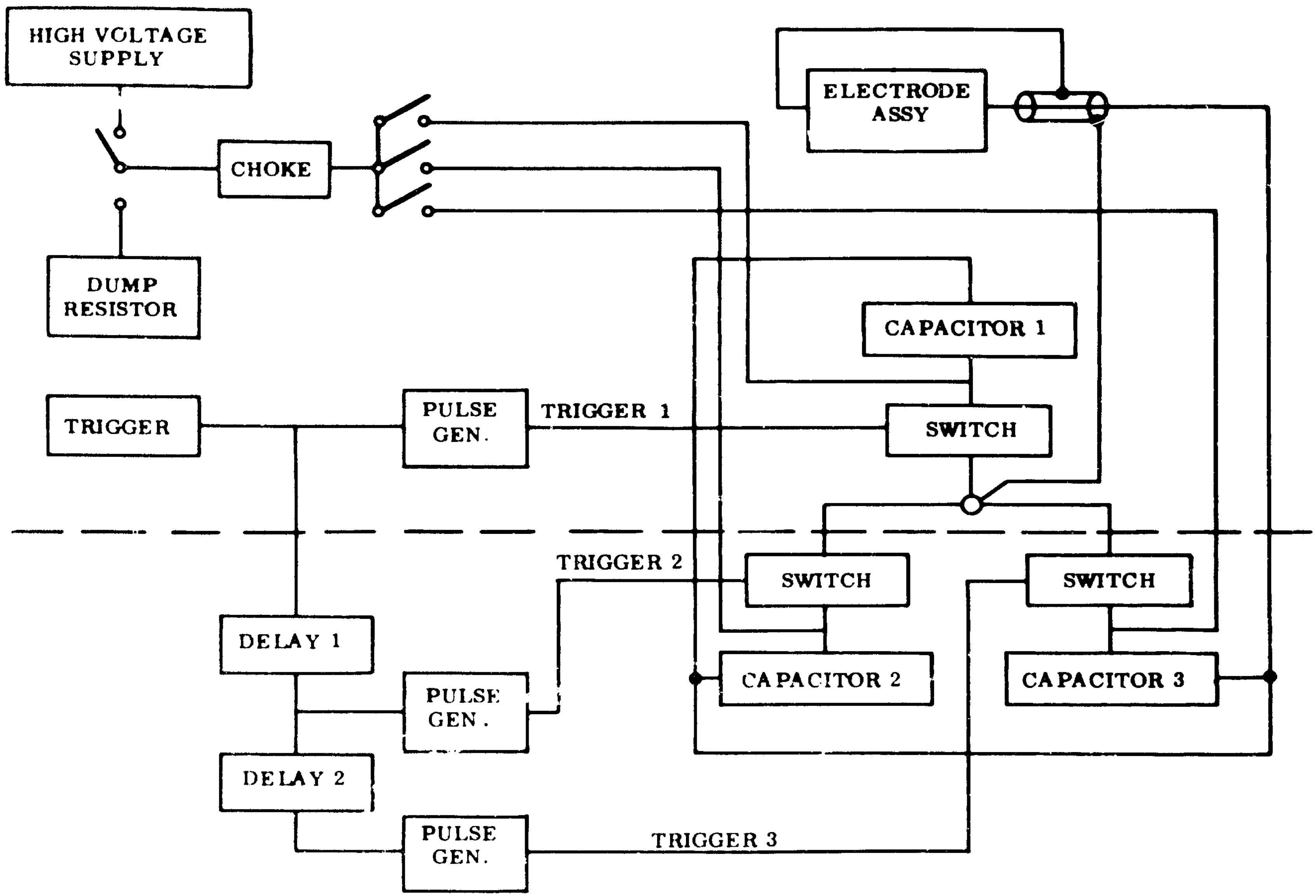

Figure 4. Main Electrical Circuit Schematic

High voltage switching of the capacitor energy into the underwater discharge electrodes (acoustic source) was accomplished by use of ignitrons, specifically the G.E. Model GL 7703 (up to 20 KV) and the Model Z-7428 (up to 35 KV). Usually in order to minimize resistive and inductive losses, the ignitron was mounted directly onto the "hot" post of its capacitor. Controlled ignition of the ignitron was effected by use of an approximately 2.5 KV pulse produced from the trigger pulse generator circuit shown in Figure 4. A circuit capable of providing delays of up to 300 microseconds from receipt of the primary firing pulse was used to provide the input to these pulse generators; Figure 5 shows the circuitry employed. Considerable attention to shielding and isolation was necessary in order to avoid premature triggering of the pulse generators by induced transients from capacitors discharging earlier in the sequence when the delay circuits were used.

Coupling of the capacitor to the underwater discharge electrodes was accomplished, for the bulk of this work, by the use of low inductance dual coaxial high voltage cable. Minimization of inductance associated with parallel coupling of several capacitors was minimized through use of two large, closely spaced collector plates, one of which was connected to the output of each ignitron, and the other providing a return to the capacitor cases through wells enclosing the ignitrons. This latter feature provided a low inductance configuration for the discharge path through the ignitrons. Figure 6 illustrates the arrangement.

Measurements were routinely made of the discharge current and voltage at the capacitor end of the coaxial cable. Voltage was measured by use of a Tektronix P 6015 1000X High Voltage Probe, rated at 40 KV, connected to the ignitron output. Currents were measured through use of calibrated Rogowsky coils placed around the ignitron output lead prior to entry into the coaxial cable leading to the discharge electrodes. A simple passive R-C integrating network was used to convert the induced coil voltage to a signal proportional to the current; calibration of the system was accomplished by simultaneous measurement of the voltages from the Rogowsky coil and a series precision resistor during passage of an under damped oscillatory current generated in the calibration circuit by a capacitor discharge. Circuit inductance was shown to be negligible by the absence of phase shift between the two signals.

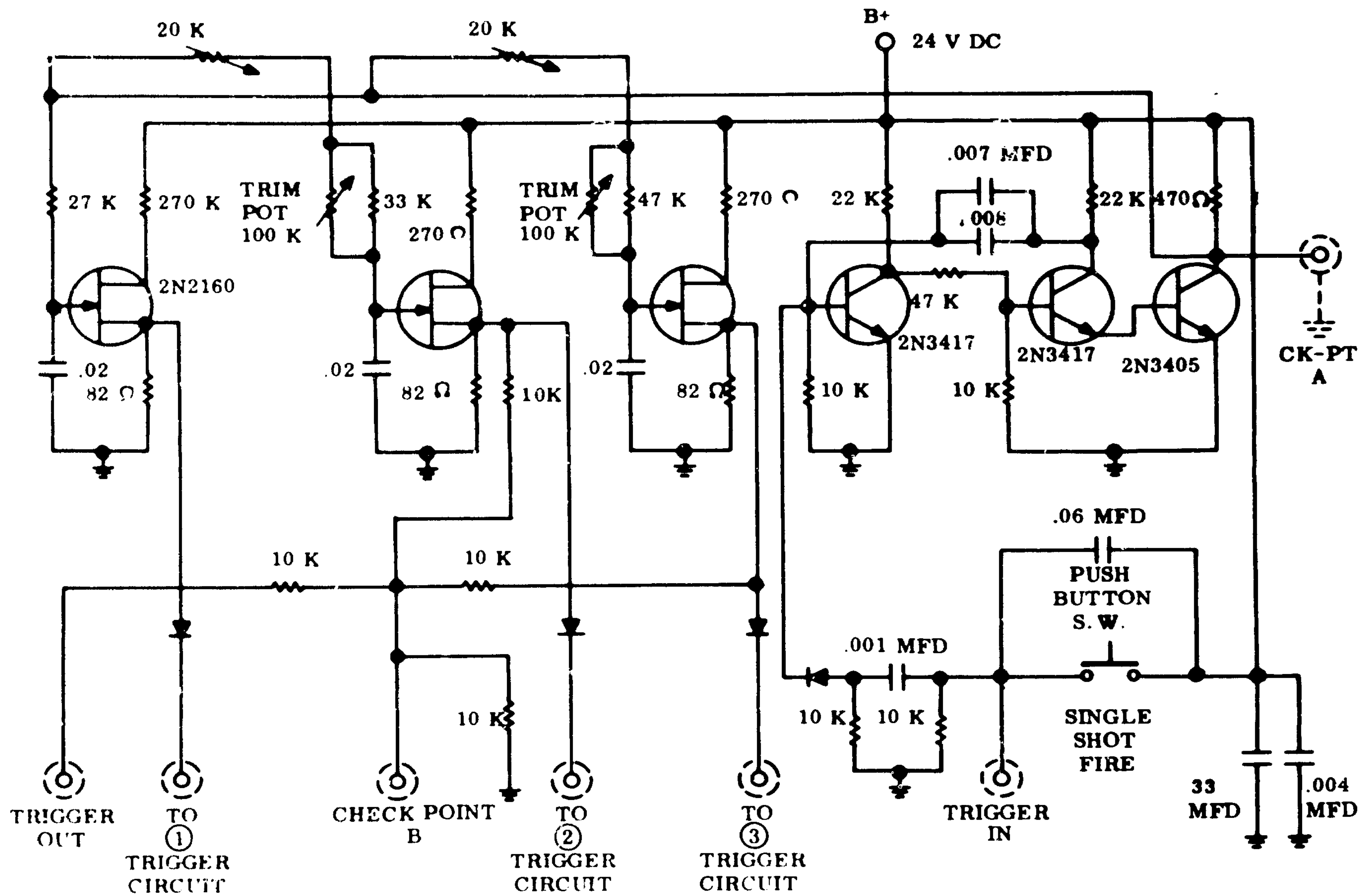

Figure 5. Trigger Delay Circuit

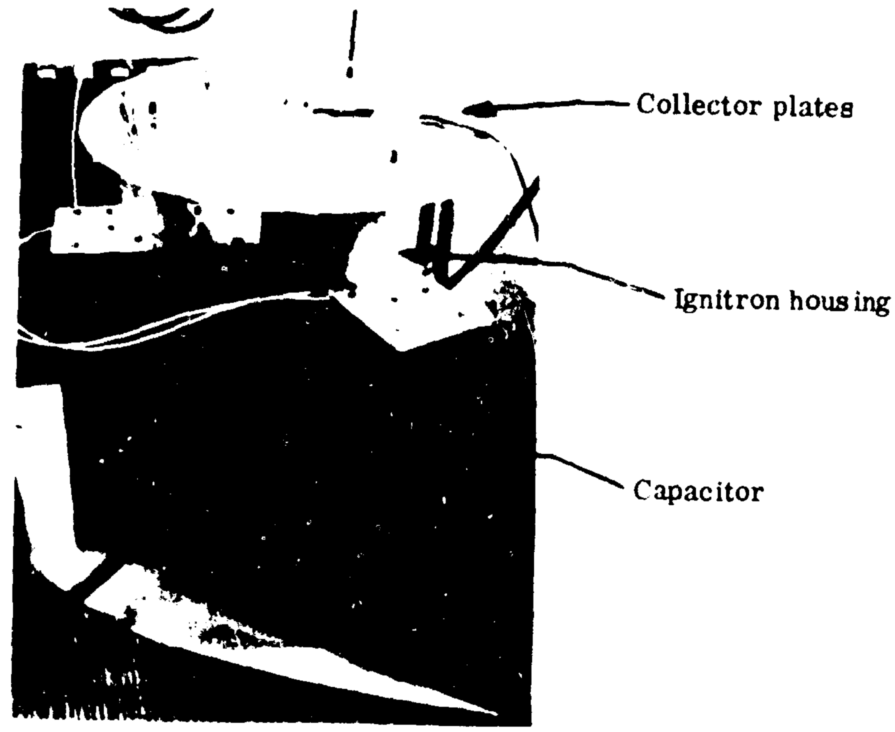

Figure 6a: Capacitor Bank Assembly

Figure 6b: Ignitron in Housing

Data generated during the underwater discharges was acquired by Tektronix Models 551 or 555 oscilloscopes using Polaroid recording cameras. Careful avoidance of ground loops by use of isolation transformers and single path grounding was necessary to avoid erroneous noise signals during the high voltage discharge. Triggering of the oscilloscope sweep was achieved by a trigger pulse generated by the firing switch (using the delay circuit of the Tektronix 555 scope as required by the discharge initiation period) or by a signal generated by a simple phototube circuit arranged so as to be illuminated by the discharge.

2. Low Inductance Network

During earlier parts of this study, it was found that the acoustic intensity was found to correlate with peak current. It is known that the peak current generated by a circuit such as that shown in Figure 4 varies as:

$$i_{max} \propto \sqrt{\frac{E}{L_o}}$$

with E the energy initially in the capacitor and L_o the circuit inductance. Therefore, it is reasonable to believe that the acoustic effect for a given capacitor energy can be increased by decreasing the inductance of the discharge circuit. Peak currents of 50,000 amperes have been generated with the discharge circuit utilizing 25 feet long coaxial cables. The maximum current that can theoretically be achieved with the ignitron and the capacitor currently in such a discharge circuit can be readily evaluated. The inductances of the ignitron* and capacitor** are given as 50 milli μ henries and 40 milli μ henries, respectively. Assuming the electrode assembly (with an inductance calculated to be about 75 milli μ henries) to be fastened directly to the ignitron and the ignitron directly to the capacitor, the theoretical maximum peak current that can be obtained with these components is found to be about 200,000 amperes. Because this value of the peak current is roughly four times

----

* Personal communication, M. Begun, Power Conversion Department, Republic Aviation Division/Fairchild Hiller Corporation.

** 1965-66 Component Selecter, Cornell-Dublier Electronics, 50 Pine Street, Newark, New Jersey larger than the value that was attained with the 25 feet long coaxial cables, it was decided to assemble a very low inductance discharge circuit.

Figure 7 shows the assembled low inductance discharge circuit including the acoustic source.

Figure 7. Assembled Low-Inductance Discharge Circuit (3 kilojoules)

The overall circuit inductance was evaluated from a current trace obtained by shorting the electrode assembly with a strap which made contact around the complete circumference of both the anode and the cathode of the source. Measurements indicate an overall circuit inductance below 1.5×10^{-7} to 2.8×10^{-7} henries.

To prevent axial shock loads from damaging the ignitron, the electrode assembly was shock isolated by means of a spring assembly.

Besides shock isolating the ignitron from the acoustic field, it was also necessary to prevent spurious electric discharges from taking place within the coaxial current-carrying assembly surrounding the ignitron. Originally adequate spacing was provided between current paths to prevent a discharge from occurring between these paths. It was found, however, that when the assembly was immersed in cold water, condensation of entrained air would cause electrical discharges to take place within the enclosure surrounding the ignitron. In an attempt to eliminate this problem, this spacing was filled with transformer oil. It is believed that because of the incompressibility of the transformer oil pressure pulses generated in the surrounding water were transferred to the ignitron casing and may possibly have contributed to the failure of one ignitron. The problem of internal arcing was resolved by filling the spacing with a very pliable silicone rubber. After pouring the silicone rubber into the spacing between conductors, the assembly was degassed in a vacuum chamber. Besides electrically isolating the current paths from each other, the silicone rubber also provides some vibration isolation. An additional feature of this technique is that the potting compound provides some hermetic sealing of the ignitron should the evacuated glass envelope of the ignitron break. No spurious discharges between the ignitron and the surrounding casing have been observed since the ignitron assembly has been potted.

C. PRESSURE MEASUREMENT

Measurements of the underwater discharge pressure pulse, which represent the principal source of quantitative information for this work, were made using, primarily, a pair of calibrated Atlantic Research Corporation Model LC 32 hydrophones, serial numbers 317 and 445, kindly provided by the U. S. Navy Underwater Sound Reference Laboratory, Orlando, Florida. These transducers have the following nominal characteristics:

Voltage Sensitivity	.49 volts/psi (-103 db/1volt/μ bar)
Transverse Directivity @ 100 khz	± 1.0 db
Axial Directivity @ 25khz	± 4.0 db
Frequency Response	Flat to 60 khz - 12 db @ 100 khz
Maximum Static Pressure	500 psi

They possess the positive attributes of high reliability and wide acceptance.

The transducers were used to record the waveform of the primary pressure pulse generated by the initial plasma expansion in the near field region (one to three feet from the discharge). The relatively small size of the testing tank, by creating a large amount of extraneous reflection noise, made investigation of bubble pulse phenomena generally impractical, as was noted above. Completely accurate portrayal of the waveform of a fast rise pressure pulse may be compromised particularly by two transducers properties: rise time (frequency response), and transit time across the transducer face. The rise time of the LC 32 hydrophone, calculated on simple linear low pass filter considerations and the given frequency response, would be on the order of ten microseconds. The diameter of the active transducer section is 0.75 inches, and its length is approximately 1.5 inches; thus the transit time is between 10 and 25 microseconds, depending on orientation. Thus the instrument is not suitable for accurate measurement of pulse waveform below 20 microseconds.

Theoretical[4] and experimental[5] investigations demonstrate that underwater discharges or any impulsive high energy release generate a steep-fronted shock wave in water which propagates outward. Accurate investigation of the structure of this pressure front would require a transducer with better than one microsecond response; moreover, such information would have little practical utility relative to use of the underwater discharge as an acoustic source. Accordingly, the LC 32 instrument was employed from the point of view of providing a relative measure of the peak pressure of the initial shock wave, thus providing a tool for evaluation of changes in electrode geometry and materials, energy source characteristics, etc. Generally, the rise time of signals recorded was found to be of the magnitude dictated by the transducer characteristics; the peak pressures recorded thus may be regarded as conservative; i.e., smaller in magnitude than the actual shock pressure.

D. OPTICAL TECHNIQUES

1. High Speed Photography

a) Framing Camera

A high speed framing camera was used to examine the initiation and growth of the luminous plasma bubble. From phototube studies that were carried out, it was known that the luminousity radiated by the underwater plasma correlated well with the electric current variation and that for the energy levels being studied the total duration of luminosity persisted up to about 200 microseconds. A Beckman-Whitley Model 189 framing camera was found to be well suited for such a correlation and symmetry of discharge study. This camera is capable of taking 25 pictures at a maximum framing rate of 1,200,000 frames per second. An inspection of experimental data indicated that it would be desirable to examine the entire initiation and energy deposition phase. The entire period was examined because phototube studies of the period of interest indicated that no light was detected by the phototubes during the initiation period while high speed streak photographs did show the presence of light during this period. Therefore, a mirror speed of the camera was selected to spread the total writing time for the 25 frames over the period of interest, namely 100 μ second. The framing rates selected ranged between 200,000 and 250,000 frames per second, giving approximately four to five μ seconds between each of the 25 frames. Since the size of the electrode and the luminous bubble encompassed an area of only a few square inches, the camera was moved to within the closest focusing distance for which the event to be photographed would fill up a complete film frame. At a distance of 7.1 feet, the field size photographed is about 1.3" x 3.7" thus affording the maximum resolution within a frame.

The Beckman-Whitley camera does not have a fast acting shutter, and it is, therefore, necessary to use an event-triggering pulse output provided by the camera to properly start the event to be observed relative to the period that is seen by the film. Sequencing of events in this manner to within a few microseconds was found to be somewhat difficult to accomplish with the underwater discharge. The time interval that existed between application of the triggering pulse to the ignitron firing circuit which switches the capacitor bank across the electrodes and commencement of the energy deposition phase was found to vary in some cases by as much as 50 microseconds for the 20 KV (15 μfd) system studied.

Before high speed photographs were taken, a series of exploratory runs with phototubes were taken. The purpose of these runs was to determine the most probable time lag that would arise for each applied energy (or voltage) level of operation. Using this technique it was possible to "preset" the camera to start photographing the discharge at a time the discharge just starts. Even with this technique it was not always possible to catch the discharge from the instant it started. In order to be able to correlate events depicted by high speed photography with discharge current, a light probe viewing the discharge and a discharge current waveshape were displayed simultaneously on an oscilloscope. The trigger output of the Beckman-Whitley camera was used to switch the capacitor bank across the electrode of the acoustic source and also to start the sweep speed of the oscilloscope. Knowing the sweep speed of the high speed camera it was possible to correlate the discharge current, the high speed photographs and the phototube observation within a reasonable degree of accuracy.

Figure 8 shows the positioning of the framing camera relative to the water tank. Because the camera must be used in a horizontal position, a mirror located in the center of the tank was used to view the electrode assembly along the axis of symmetry. Viewing the discharge in this manner provides information of the peripheral symmetry of the electric discharge as well as information on the radial expansion of the plasma. In order to preclude excess fogging of the film from light that is scattered by the water and from ripples generated on the surface of the water, a light shield comprised of a glass plate at the bottom of a box was floated on the surface. Most of the glass of the light shield was masked with black tape so that only the region of interest around the electrode could be seen by the camera. At no time did the discharge either break or crack the floating glass plate. Figure 9 shows the relative positioning of the mirror, light shield, and electrode assembly. In addition to these features, it was found necessary to use No. 0.5, No. 2, and No. 3 Wratten neutral density filters to prevent the light intensity from overexposing the film (Eastman-Double X). With these filters it was possible to examine most of the luminous growth of the plasma during the energy deposition phase. However, the filters excluded any light from exposing the film that may have been present during the initiation phase.

2. <u>Phototube System</u>

A simple tool for examining the variation of luminousity of the plasma bubble is had by using a phototube to view the underwater discharge. An RCA IP-42 vacuum phototube was found convenienct for this purpose. The simplicity of the circuit is shown in Figure 10.

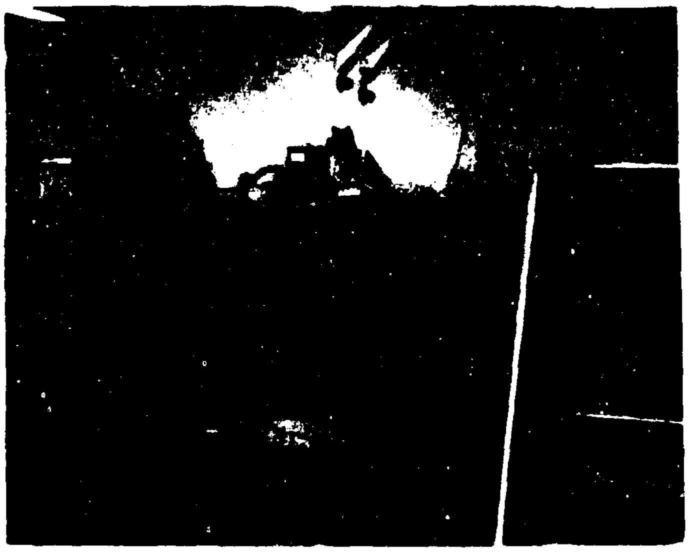

Figure 8. High-Speed Framing Camera in Position

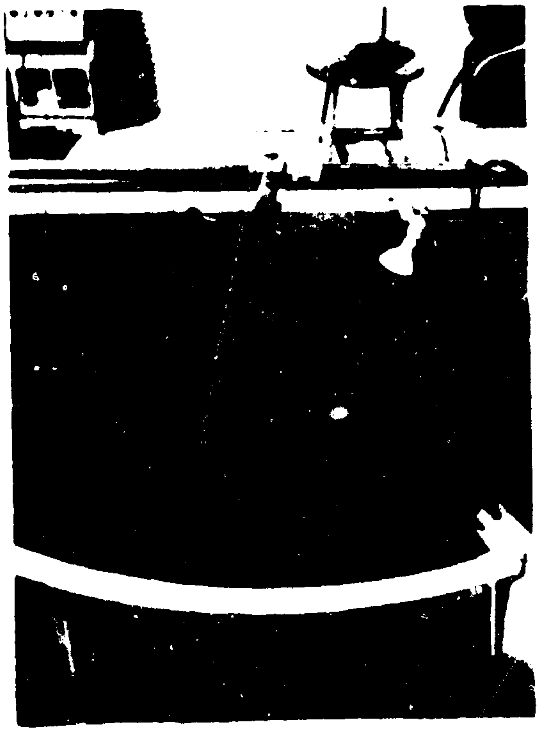

Figure 9. Mirror, Light Shield, and Acoustic Source

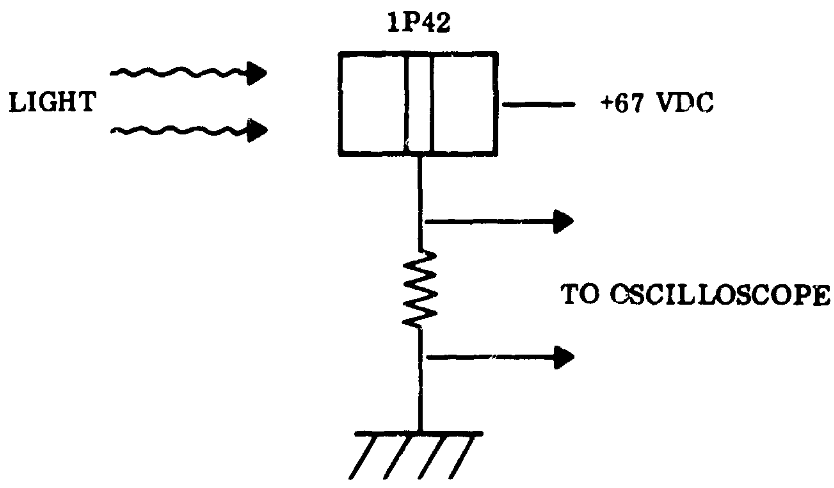

Figure 10. Schematic of Phototube Circuit

Figure 11 shows a typical experimental setup that was used with the phototube. A long narrow tube was aimed at the region of discharge. A 1P-42 phototube (and circuit) was positioned at the end of the tube located the farthest from the discharge. This tube served to narrow the viewed region of the discharge as seen by the phototube. Current traces and phototube output due to the luminosity radiated by the plasma bubble were displayed simultaneously on a dual beam oscilloscope.

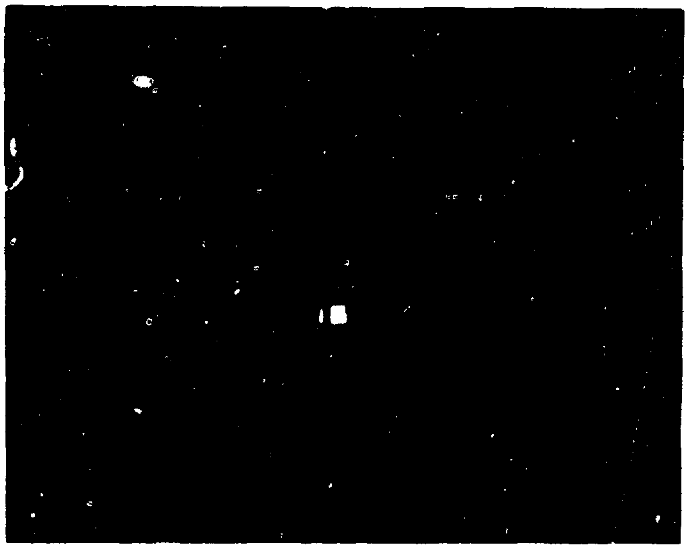

Figure 11. Phototube Setup

SECTION III

EXPERIMENTAL RESULTS

A. GENERAL ASPECTS

1. Physical Aspects of Generating an Underwater Acoustic Signal by an Electrical Discharge:

For convenience of analysis and experimental studies, it is possible to consider the events occurring in water as a consequence of discharging energy across two electrodes quite generally as involving four phases:

i The Initiation Phase: During this phase a high voltage is suddenly applied by means of a switch across the electrodes. Because of the small conductivity of the water, electric current flows across the interelectrode spacing and a small voltage drop is observed on the energy storage capacitor. This phase terminates rather abruptly with the formation of a distinct plasma column in the water. The duration of this initiation phase was found to be on the order of 1μ sec when 40 KV was applied and as long as 150μ sec when 10 KV was applied across the electrodes. Very few measurements were made of events occurring during the initiation phase for the course of work presently being reported upon.

Figure 12 shows the drop in voltage in the capacitor bank during this initiation phase. Both the electric current that flows and the light that may exist during the initiation phase are too small to be determined with the diagnostic equipment that was used during the present studies. Streak photographs, however, taken with a rotating mirror camera indicate that some light is emitted during this initiation phase.

ii Energy Deposition Phase: During this second phase, the remaining electric energy stored in the capacitor bank is rapidly discharged into the plasma column and also is dissipated in the external electrical circuitry. Large voltage changes which rapidly decay to zero, large electric current, and light generation in the plasma are encountered during this second phase. The duration of this energy deposition phase was found to depend upon the duration of electric current oscillations. At a given salinity these oscillations were found to depend upon the

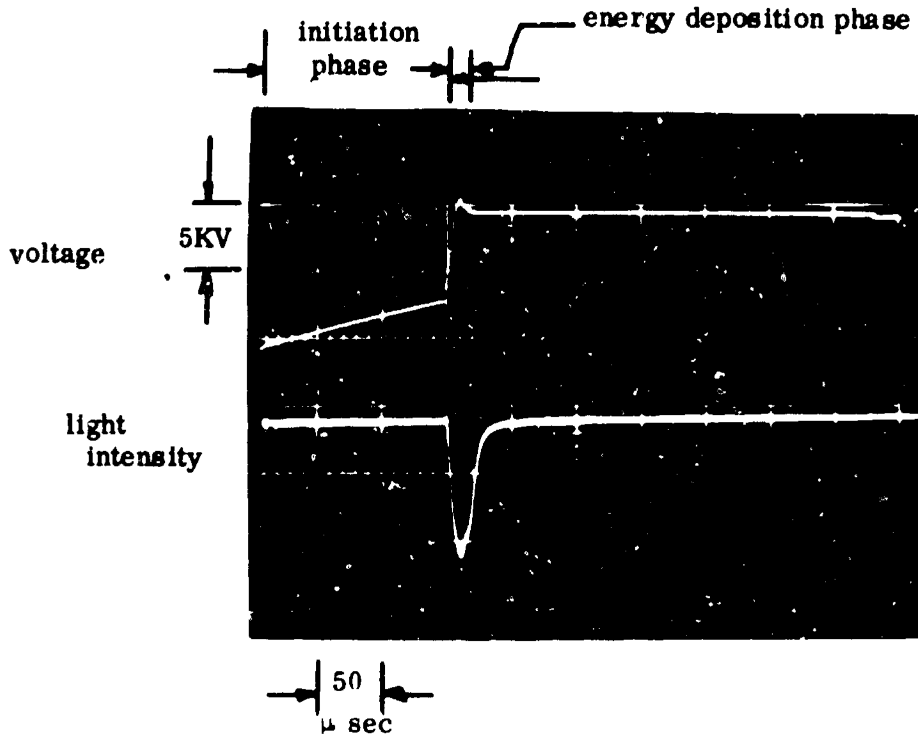

Figure 12. Discharge Behavior (10 KV)

interelectrode spacing and the initial voltage on the capacitor. This energy deposition phase was found to last approximately 10 μ sec for a critically damped discharge and more than 100 μ sec for a discharge which exhibited damped current ringing over a number of cycles.

For the critically damped discharge shown in Figure 12, the voltage is seen to drop to zero in about 10 μ sec. Light is emitted for a period of about 30 μ sec by the plasma that was generated.

Figure 13 shows the electric current variation and the variation in light intensity emitted by the plasma during a typical critically damped discharge occurring at 10 KV. It has been found that some correlation appears to exist between the type of current variation that is encountered and the light intensity radiated by the plasma. These results will be discussed in more detail in Section III-E.

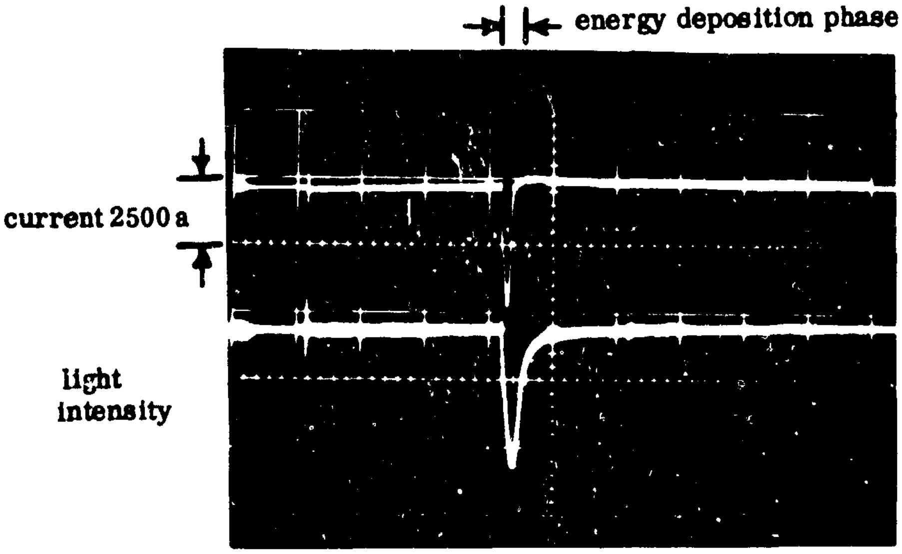

Figure 13. Energy Deposition Phase (10 KV)

Because some correlation has also been observed between electric current variations and acoustic pressure signals in the water, it is suspected that this energy deposition phase strongly influences the subsequent bubble expansion phase. Therefore, it was decided to examine the growth of the luminous plasma by a Beckman-Whitley Model 189 framing camera. Some of the results that were obtained with this camera are also presented in Section III-E of this report. An elementary idealized analysis of the initial motion of the energized plasma bubble is reported in Reference 6, for example.

iii <u>Bubble Expansion Phase</u>: Due to the large inertia of the water only a small displacement of water occurs during the energy deposition phase (the acceleration of the plasma-water interface, however may be very large). Most of the displacement of water by the electric discharge takes place during this bubble expansion phase. Because the plasma luminosity was found to persist essentially only during the period of current oscillation (i.e., the energy deposition phase) photographic studies of the bubble expansion necessitate the use of either a Schlieren or a Shadowgraph system in order to detect the growth of the bubble boundary. Such studies have not as yet been carried out in this program. Inasmuch as the expansion bubble boundary is analogous to a piston, the acoustic pressure that exists some distance away from the source can be related by means of incompressible fluid dynamic theory to the dynamics of the bubble boundary as a reasonably good first approximation. Typical analytic studies of this phase are presented in Reference 6, for example.

iv. Bubble Contraction and Subsequent Oscillations: After the expanding bubble has transferred its energy to the surrounding water, the bubble contracts under the action of the external hydrostatic pressure. This implosion also radiates strong acoustic signals into the external fluid. The magnitude of the peak pressure and the wave shape of the radiated pulse generation by the implosion depends significantly upon how instantaneously the imploding water is brought to rest. Entrained water vapor in the collapsing bubble limits the peak pressure that is generated. An accurate calculation requires knowing the amount of gas entrained at any instant of the implosion, the geometry and size of the electrode, etc. However, a simple calculation can be readily carried out which presents the largest possible peak pressure obtainable. Such a calculation includes compressibility of the water. As water is brought instantaneously to rest a pressure rise relative to local ambient is generated equal to:

$$\Delta P = \rho a \Delta u$$

with ρ, a, Δu, the mass density of water, the speed of sound of water, and the change in volocity of water that is brought to rest. The velocity Δu will be equal to $\sqrt{2 gh}$ with h the depth below the free surface. Thus,

$$\Delta P = \rho a \sqrt{2 gh}$$

For example, at a depth of 1000 feet below the free surface, ideally a peak pressure of 17,280 psi is generated at the source of this implosion.

After this first implosion, additional rapidly decaying minor expansions and contractions may occur.

While it is convenient for experimental purposes to consider the generation of acoustic signals by an electric discharge in water to be comprised of the four phases described, it has not yet been possible to formulate an analysis encompassing all four phases taking into consideration the external electric circuitry.

Generating an acoustic impulse by an underwater electric discharge requires that as much of the initially stored electric energy be delivered usefully to the source as possible. Some considerations of the energy transfer process will now be presented.

Typically, simple series LCR electric discharge currents as shown in Figure 14 are used in underwater electric discharge studies.

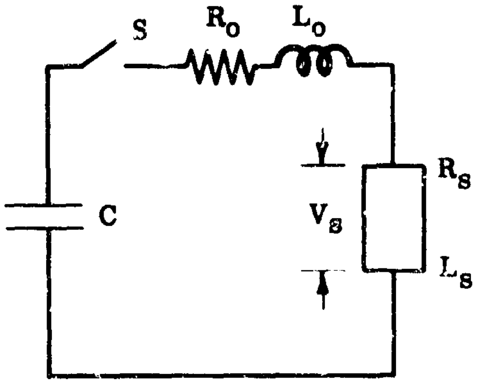

C	energy storage capacitor
S	switch
R_o	external circuit resistance (fixed)
L_o	external circuit inductance (fixed)
R_s	resistance of acoustic source
L_s	inductance of acoustic source
V_s	voltage drop across acoustic source.

Figure 14. Schematic of Discharge Circuit

The differential equation governing the dynamic behavior of the electric discharge circuit is written as:

$$-\frac{d}{dt}\left(\frac{q^2}{2C}\right) = \frac{d}{dt}\left(\frac{1}{2} L_o i^2\right) + i^2 R_o + iV_s$$

(1) (2) (3) (4)

where:

(1) is the rate of decrease of electrostatic energy in the capacitor

(2) is the rate of change of magnetic field energy in the external circuit

(3) is the joulean dissipation within the external circuit

(4) is the instantaneous power going into the acoustic source.

Terms (2) and (3) represent energy losses in converting electric energy to acoustic energy. To transfer the maximum quantity of available energy into the acoustic source, it is quite obvious that the external circuit inductance and resistance should be kept as small as possible.

The voltage drop V_s across the acoustic source in the above equation can be expanded to read:

$$V_s = \frac{d}{dt}(L_s i) + IR_s$$

(capacitive effects can be considered negligible). The first term on the right side of this expansion multiplied by the current is the power input to the inductance of the discharge. This term includes the rate at which work is done on the plasma by the magnetic force, i.e., $\frac{\mu i^2 \ell}{4\, 4\pi r} \frac{dr}{dt}$ for the inverse pinch geometry being studied. The second term multiplied by the current expresses the rate at which energy is dissipated in the plasma resistance. This latter dissipation of electric energy manifests itself as a change of internal energy of the plasma. The internal energy, however, is related through an appropriate equation of state valid at high pressures and high temperatures, to the gas dynamic pressures. The inductive term L_s, which is a function of plasma geometry, and the instantaneous plasma resistance term R_s are the two terms which couple the dynamic behavior of the external electric circuit to the dynamic behavior of the plasma bubble during the electric energy transfer process. For the inverse pinch electrode geometry under study, the inductive term L_{as} is given by:

$$L_{as} = \frac{\mu \ell}{2\pi} \ln \left(\frac{r}{h}\right)$$

with μ the magnetic permeability, ℓ the fixed separation between electrodes, r the instantaneous outer radial position of the plasma (a variable), and h the fixed inner radius of the returning current path. Caulfield[7] finds the plasma resistance R_s essentially constant in his studies while Martin[8] finds the plasma resistance to vary by about a factor of ten during the flow of electric current. Once a suitable expression for the plasma resistance $R_s = R_s(i)$ is substituted into an alternate form of the circuit equation, i.e.,

$$\frac{d^2 i}{dt^2}\left[L_o + \frac{\mu \ell}{2\pi}\,\ell n\,\frac{r}{h}\right] + \frac{di}{dt}\left[R + \frac{\mu \ell}{\pi r}\,\frac{dr}{dt} + R_s\,(i)\right]$$

$$+\, i\left[\frac{1}{C} + \frac{\mu \ell}{2\pi r}\,\frac{d^2 r}{dt^2} - \frac{\mu \ell}{2\pi r^2}\left(\frac{dr}{dt}\right)^2 + \frac{dR_s(i)}{dt}\right] = 0$$

the nonlinear differential equation of the electric circuit becomes expressed in terms of the independent variables, current i and plasma radius r. Couplied with an appropriate momentum equation, energy equation, continuity of mass equation, (see Reference 6, for example), and an equation of state, it should, in principle, be possible to analyze the dynamic behavior of the plasma under the action of the self induced magnetic field.

Experimental results of the present study indicate that magnetic effects apparently do not play a significant role at the energy level studied. The electric circuit equation therefore reduces to one neglecting any changes in inductance due to plasma motion. Indeed, in comparison to the circuit inductance, it is even reasonable to neglect the inductance term of the source altogether. Electric energy is transferred into the streamer (plasma) by ohmic dissipation of electric energy alone. For maximum energy transfer into the electric discharge acoustic source, the external circuit resistance and inductance should be as small as possible. This latter observation motivated that a very low inductance, low resistance discharge circuit be built and tested. The results obtained with this circuit were gratifying in that the peak acoustic power generated for a given initial energy appear to be significantly larger than those reported by other investigators when compared at the same energy level.

For efficient transfer of electric energy into acoustic energy by an underwater electric discharge it was also found that the electric current discharge waveshapes having a critically damped waveform resulted in the largest peak pressure at a given energy level. From high speed photography it appears that in an osciliatory type of discharge a new plasma arc is initiated at the electrodes each time the electric current passes through a zero.

2. <u>General Observations</u>

During the earlier part of the program it was observed that either of two types of discharges could occur:

(a) Essentially critically damped electric circuit oscillation

(b) Current oscillations (ringing)

The amplitude and waveform of the pressure signal radiated by the discharge was found to depend significantly upon which type of electric current waveform prevailed. Quite generally, it was found that at a given energy level the critically damped discharge produced a higher level of pressure than an oscillation discharge. Studies were carried out to determine under what conditions either type of discharge would occur. The results of these studies are summarized in Figure 15.

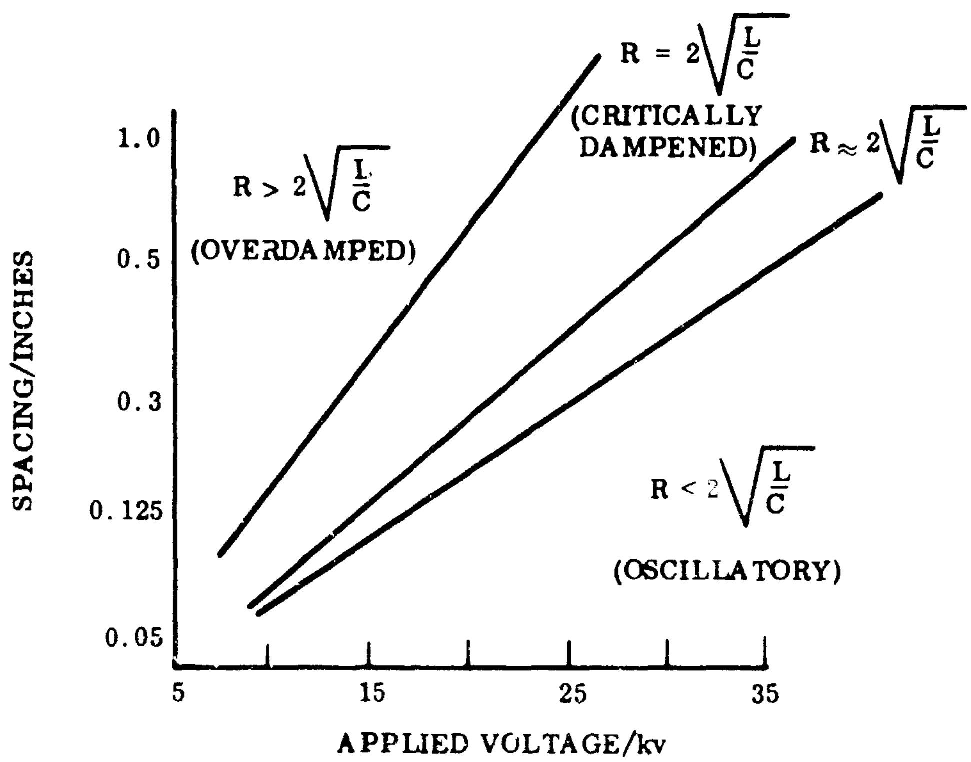

Figure 15. Typical Variation of Electric Current as a Function of Electrode Spacing and Initial Voltage

Several important observations may be noted:

- As the applied voltage is increased across a fixed interelectrode spacing the current is found to vary from an underdamped discharge ($R_o > 2\sqrt{L/C}$ through a critically damped discharge ($R_o < 2\sqrt{L/C}$). "Explosive-like" discharges radiating measurable acoustic signals are found to occur only with the latter two types of current variation.

- As the interelectrode spacing is increased holding the applied voltage constant, the current is found to vary from an underdamped discharge through a critically-damped discharge to one which is overdamped "explosive-like" discharges were found to occur only with the first two types of discharges.

These observations have shown the spacing between electrodes to be one of the most important parameters governing the amplitude of an acoustic signal. Varing the interelectrode spacing changes the electric resistance and, to a smaller extent, the inductance of the electric network. The variable resistance introduced is that of the water initially located between the electrodes. It is strongly suspected that, analogous to transmission line studies, by varying the resistance of the load it is possible to match the impedance of the load (acoustic source) to that of the energy storage circuit so that an optimum transfer of energy results from the latter to the former.

B. ELECTRODE ASSEMBLY

1. Electrode Design

Three different electrode configurations were studied. In all three cases some augmentation of the acoustic pressure by self-magnetic effects was anticipated. The first design that was studied evolved from inverse pinch studies in plasma physics and is shown schematically in Figure 16. An actual electrode is shown in Figure 17. In this configuration the electric current remains in a coaxial

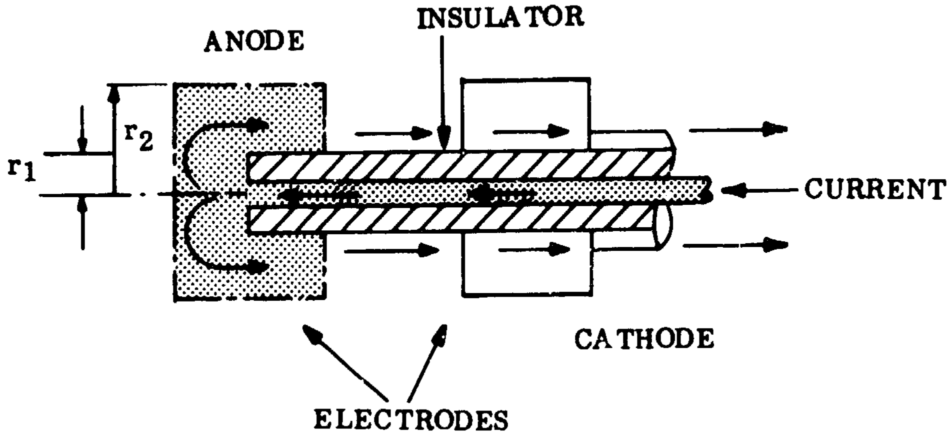

Figure 16. Schematic of First Electrode Assembly

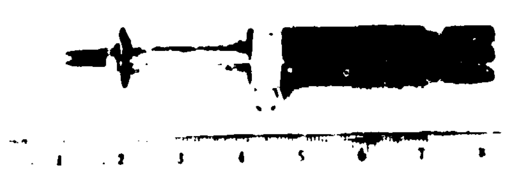

Figure 17. Electrode Assembly with Confined Discharge

configuration. The electric discharge takes place at the insulator between the two disc shaped electrodes. With this configuration it was found that the acoustic pressure located between the two disc shaped electrodes would tend to separate these and frequently bend the center conductor. Furthermore, it was found that the acoustic pressure generated was not as large as the pressure that was generated by the same configuration but eliminating confinement of the discharge (i.e., $r_2/r_1 = 1$). This second configuration is shown schematically in Figure 18. Most of the experimental results of this program were obtained with this second configuration. An actual electrode assembly is shown in Figure 19. It should be noted that the axially directed shock loading is significantly reduced by incorporating a coil spring in the outer electric current path (even though the inductance is increased somewhat). This spring and part of the electrode assembly are subsequently plotted in an elastomer as shown in Figure 19.

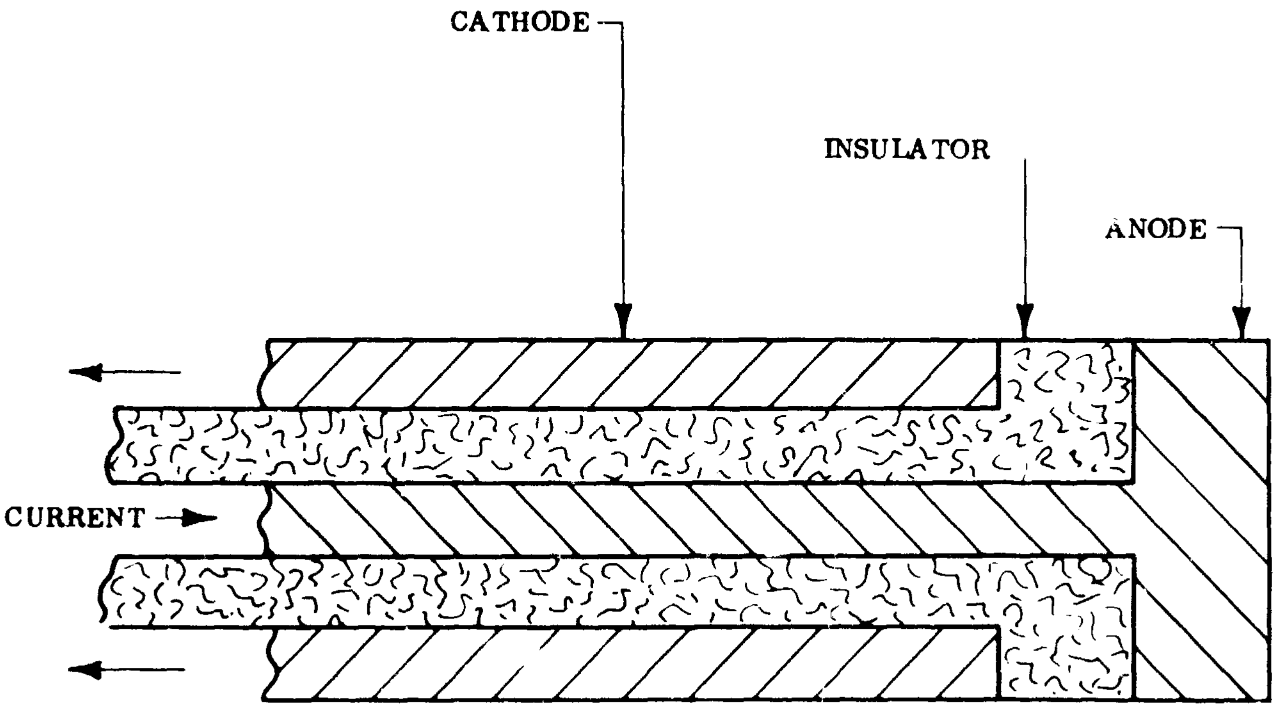

Figure 18. Schematic of Unconfined Electrode Assembly

----

* PRC-PR-1431 Type 11, Product Research Company, 410 Jersey Avenue, Gloucester City, New Jersey

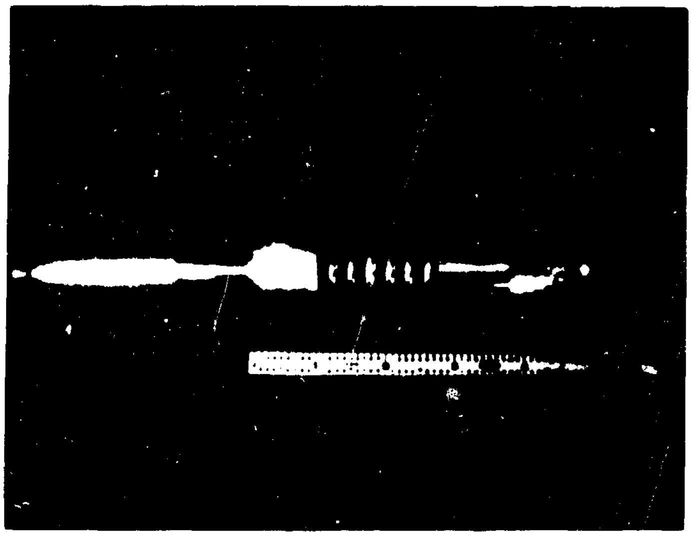

Figure 19. Variable Gap Electrode Assembly.

This potting insulates the assembly from the water and also seals it from water penetration.

In either electrode configuration described above, the most critical element was found to be the insulator located between the two electrodes. Material that was found to withstand reasonably well the sudden shock loading at extremely high pressure levels were Tygon* and Adiprene**. After roughly 100 discharges at the 3000 joule discharge level even these pliable insulations would develop surface cracks. Life tests at lower energy levels were not carried out. Most other rigid dielectric substances like Teflon, Micarta, Kel-F and Dynel were found to rupture within a few discharges. The third electrode assembly briefly tested is shown schematically in Figure 20. In this coaxial assembly the discharge takes place across the end face and is referred to as a "button geometry".

-----

* Compound 167 DuPont Company, Elastomer Chemicals Dept. Wilmington, Delaware, 19898

** The United States Stoneware Company, Akron, Ohio 44309

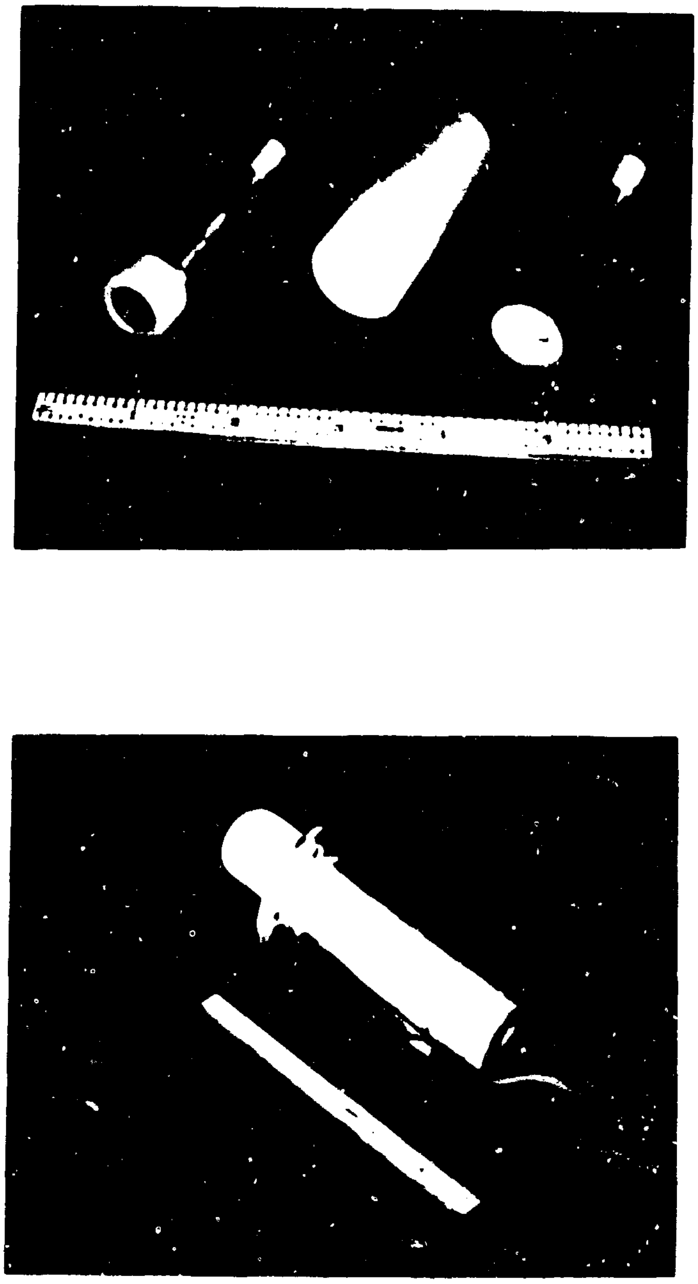

Figure 20. Button Geometry

C. ACOUSTIC ENERGY VARIATION

1. Effect of Geometric Parameters

a) Pressure as a Function of the Distance from the Electrode

The peak pressure variation as a function of radial distance from the source was determined for two electrode configurations. One of these was an inverse pinch type assembly while the second was a conventional sparker system. All pressure measurements were taken at varying radial distances from the source but at one azimuthal location relative to the source. The initial discharge energy was kept at 450 joules. Pressure readings were taken at 6-inch intervals starting from an initial location of 6 inches from the source. The data obtained indicated that peak pressure (P) varied with distance (r) from the source in accordance with the relation:

$$P = K r^{-1.035}$$

b) Azimuthal Pressure Variation

An azimuthal pressure survey was also carried out. This survey was performed at one fixed radial distance (3 feet) from the axis of symmetry in a plane normal to the axis. Since only two pressure transducers were available for these measurements two pressure recordings, separated by 180° in the reference plane were taken per discharge. The azimuthal pressure variation was then established by accumulating the results of a number of discharges with the pressure transducer positioned in a new azimuthal location each discharge. The results of this azimuthal pressure variation confirmed the results of high speed photographic studies of the discharge. In either case it was found that the discharge and the resultant pressure field was not perfectly axisymmetric. Since the electric discharge does not form at the same place on the electrode each discharge it was observed that reproducibility of the peak pressure at a given azimuthal location could vary by ±10%.

c) Electrode Spacing

The spacing between the electrodes was found to be one of the most important parameters governing the amplitude of the acoustic signal. The dependence of acoustic energy on interelectrode spacing can be comprehended by noting that the area under the pressure squared-time trace is proportional to the acoustic energy. The behavior of relative acoustic energy as a function of inter-electrode spacing holding the capacitively stored energy constant is shown in Figure 21 for one typical discharge circuit.

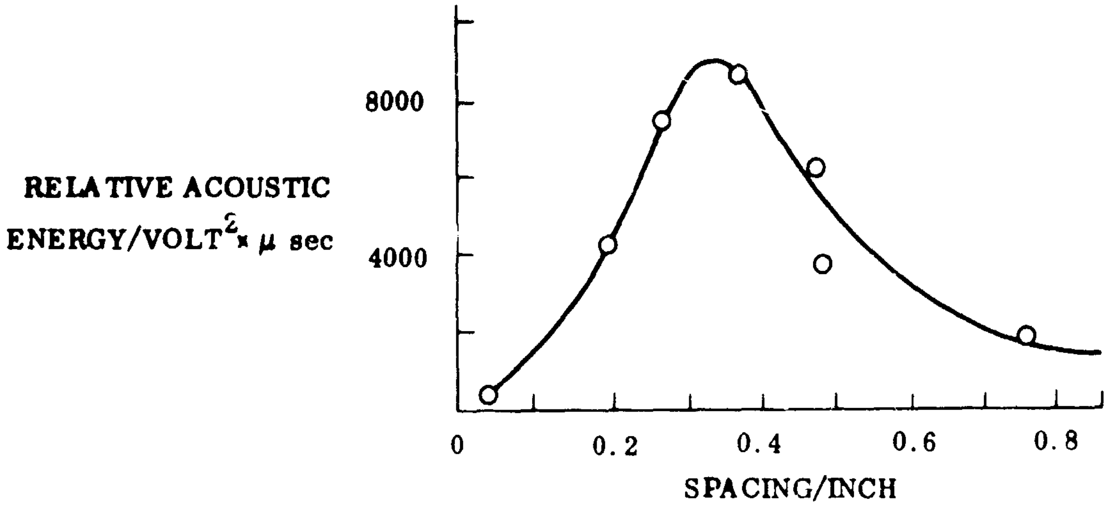

Figure 21. Relative Acoustic Energy as a Function of Interelectrode Spacing (3 μfd, 20 kw)

The effect of interelectrode spacing in electric current wave formed was already discussed in Section III A. In that section general observations were presented showing how interelectrode spacing affected electric discharge wave shape and how the wave shape related to the type of electric discharge to be expected. From the general information presented in Figures 15 and 21 respectively, it should be possible to readily ascertain the steps to be taken to optimize the acoustic output of any given electrode type electric discharge acoustic source.

d) Electrode Geometry

Basically two different types of electrode geometries were studied. One of these is the inverse pinch geometry described in more detail in Section 1-C. The second electrode geometry briefly used as a button geometry. With either electrode configuration certain geometric factors (other than the very important electrode spacing) appear to be relevant. With the inverse pinch geometry it was found that the radius ratio outer radius of electrode (R) to outer radius of insulator (r) (see Figure 22), was relevant. With $r/R < 1$ it was found that

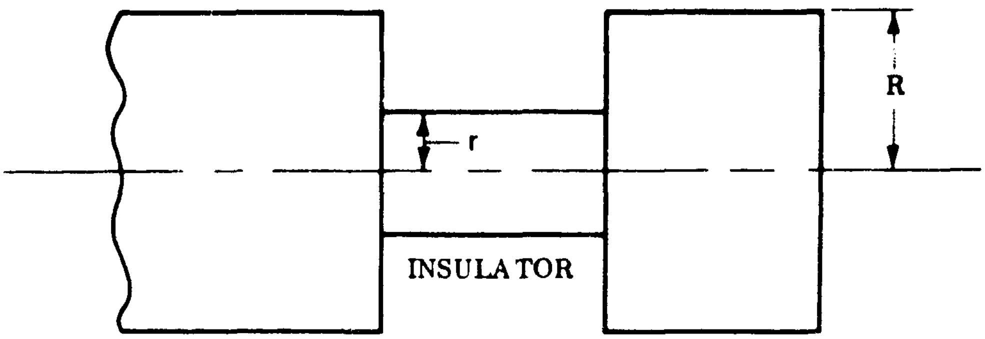

Figure 22. Geometric Variables of Inverse Pinch Electrode Geometry

for otherwise identical conditions the peak pressure radiated by the source was less than the value observed when $r/R = 1$. This observation is shown clearly by the results presented in Figure 24, to be described in more detail. While a systematic study of this variable was not carrie... the significantly higher pressures obtained for the geometry of $r/R = 1$ ...nted using that geometry almost exclusively. Besides producing larger peak pressure, it was also found that fewer structural problems were encountered for geometries having $r/R = 1$ than with geometry $r/R < 1$.

With button geometries the electric discharge takes place between two coaxial electrodes. Two geometric variations were briefly examined during the course of study being reported upon. In one of these the discharge occurred between the electrode, while in the second case the insulator was extended so that the discharge takes place across the end face of the assembly. Figure 23 shows the parameter h which is believed relevant for such button geometries. It was found that when $h > 0$ the discharge would be confined between the electrodes and structural problems were encountered. No structural

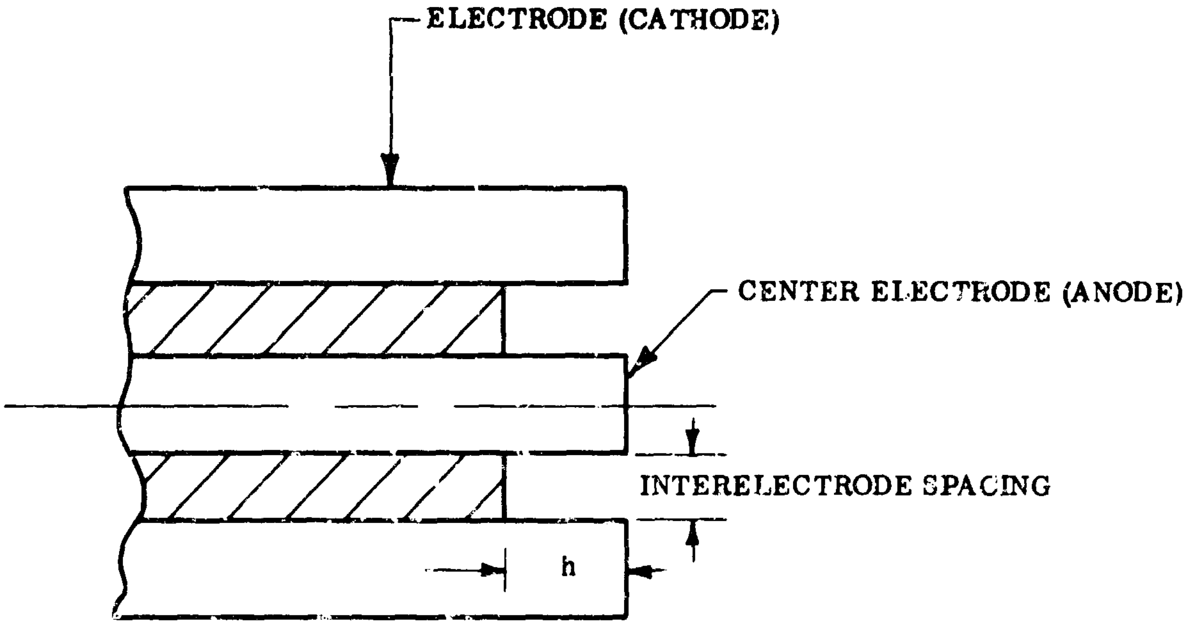

Figure 23. Coaxial Button Geometry

problems were encountered when $h = \infty$. As with the coaxial electrode geometry, it was found that the discharge would occur as a line discharge between the two electrodes rather than a planar discharge. The peak pressure radiated by the coaxial button geometry appeared to be about the same as with the inverse pinch geometry. An insufficient number of experiments were carried out with the coaxial button geometry to make any detailed comparisons with the inverse pinch geometry.

Since it was observed that underwater electric discharges tend to occur as line discharges, there does not appear to be any particular advantage in using electrode geometries which are designed to produce sheet discharges. While no experiments have been performed with electrode geometries which are designed to produce line discharges, it is suspected that a low inductance electrode configuration utilizing a back stop for self-magnetic augmentation would perhaps produce the same results as produced by either inverse pinch electrodes or button geometries.

2. Effect of Electrical Parameters

a) Energy

During this study the dependence of radiated peak pressure on initial capacitor energy was examined. Some of the results that have been obtained are shown in Figure 24. The data shown in this figure was obtained with two different electrode configurations, three different electric networks, and a large number of different interelectrode spacing. The two electrode configurations tested are shown in Figures 11 and 18, respectively. One of the electric networks, 3-CD (OSC)-25, used a 3 μfd capacitor bank and a coaxial cable 25 feet long to connect the capacitor to the acoustic source. The second network, 15-CD(OSC)-25, used a 15 μfd capacitor instead of a 3 μfd capacitor. The third network, 15-CD-0, that was studied is the one shown in Figure 7. The inductance of this latter circuit, 2×10^{-7} henries, is about a decimal order-of-magnitude lower than either of the other two networks that have been tested. By varying the interelectrode spacing it was possible to get either a critically-damped (CD) or an oscillatory discharge (OSC). The lines in Figure 24 are drawn to facilitate locating any given set of data. Some general observations can be made from the data presented in Figure 24.

1) At a given energy level the peak pressure radiated by an unconfined discharge was found to be larger than that radiated by a discharge confined between electrodes. (The confined discharge in this case is for an inverse pinch geometry with $r/R < 1$).

2) For given energy level, cable length, and electrode diameter, a larger peak pressure is radiated by a discharge in which the interelectrode spacing has been adjusted to produce a critically damped current than radiated by an oscillatory current.

3) The highest peak pressure observed at any energy level tested was obtained with the network having essentially no cable between the capacitor and the acoustic source and having the interelectrode spacing adjusted to provide an essentially critically-damped discharge.

A typical pressure-time oscilloscope trace being obtained in water of zero salinity with the low-inductance network (see Figure 7) is shown in

Figure 25a. The experimental data currently being obtained with this network is shown in Figure 24 grouped about the line labeled 15-CD-0. Three typical data points are also presented in Table 2 below:

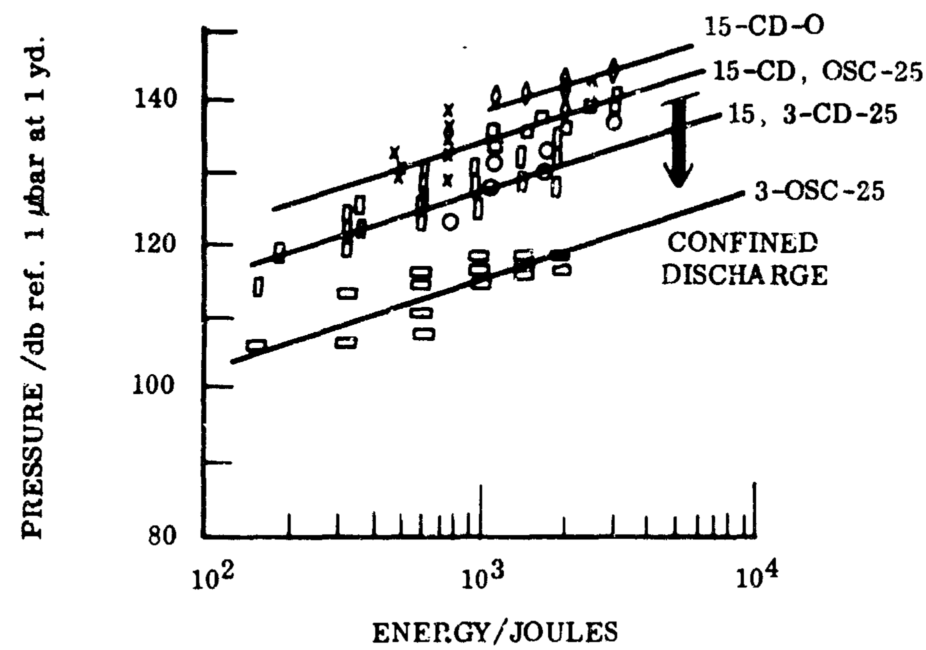

Figure 24. Pressure as a Function of Capacitor Energy

TABLE 2. TYPICAL DATA FOR LOW-IMPEDANCE NETWORK

Electrical Quantities			Peak Acoustic Pressure at 1 Yard	
Initial Potential Kilovolt	Initial Energy Joule	Peak Current Ampere	Pressure psi	20 Log_{10} (Pressure/μbar)
10	750	32400	84.5	135.2
14	1470	48000	169.0	141.2
16	1920	63000	206.0	143.1

In all cases it is found that a time-delay exists between voltage application and the onset of large electric currents. This delay is associated with the initiation period in which streamers are formed between the electrodes of the source. If this delay is long (i.e., 25 to 300 microseconds) it is found that a significant amount of energy is extracted from the energy initially stored in the capacitor before the explosive-like discharge occurs. Figure 12 shows a typical oscilloscope trace of the voltage variation taking place for a case involving a long initiation period.

Generally, it was found that peak pressure correlates with discharge energy (independent of salinity or duration of initiation period) if the discharge energy is taken to be the capacitor energy at the instant of the "explosive-like" discharge.

b) Circuit Inductance

In the present studies it was found that as the circuit inductance was decreased, while maintaining a critically damped discharge, the peak acoustic pressure at a given energy level would increase. This result is shown in Figure 23. As indicated in the previous section the highest peak pressure that was observed at any energy level was obtained with the discharge circuit having essentially no cable between the capacitor and the acoustic source. The total inductance of this latter network was found to be between 1.5×10^{-7} to 2.8×10^{-7} Henries. This value of inductance is roughly a factor of 10 below the value of 1.5×10^{-6} Henries measured with the discharge circuit using a 25 foot coaxial cable between the capacitor and the acoustic source and which produced a known value of peak pressure.

It is believed that high inductance circuits prevent the peak electric current from being optimized at a given energy level with corresponding energy losses occurring in the leads and that an efficient power transfer cannot be achieved between the energy source and the acoustic source (i.e., the load) in cases where the electric discharge is not critically damped. An analysis of these latter items would be in order in an attempt to explain the observed experimental results.

c) **Salinity (Conductance) of Water and Correlation of Results**

Discharges were performed at three voltages: 12, 15 and 18 KV in each of the six salt solutions (presented in Table 1). A fixed electrode spacing was used for all shots (see above). Representative samples from the 15 KV and 18 KV series oscilloscope records are shown in Figures 25 and 26. The first set of Figure 25a shows for reference a typical record at the two-foot range of a fresh water discharge, with a peak pressure of 240 psi; scaled to three feet by $r^{-1.08}$ (the dependence previously found in this work), this corresponds to a peak pressure of 156 psi (140.6 db re 1 dyne/cm^2) at one yard for an initial energy of 1.7 k joules. This record was triggered by a photocell viewing the discharge region due to a long initiation period in fresh water (typically 300-500 microseconds) which would otherwise preclude the obtaining of good time resolution on the records. All other records are triggered directly, thus showing the complete discharge history, including the initiation period.

Shot B42 (Figure 25a) shows the principal features of the operation of the electrode in salt water (Solution II of Table 1). Immediately upon application of voltage to the electrodes by the ignitron firing, a leakage current, whose magnitude is a function of the medium conductivity (ca 1000 amps for this case, and ca 6000 amps for solution VI (Figure 26b) drains off the capacitor charge. After an initiation period which was found to be both inversely dependent on the medium conductivity and subject to some statistical fluctuation as in fresh water, transition to the regular low resistance strong discharge occurred. However, the capacitor voltage at this point has been substantially reduced, resulting in reduced peak current and pressures.

It is of particular noteworthiness that the leakage current flowing during the induction period produces a detectable acoustic output, approximately 10 psi here. The generation of a gas bubble in the interelectrode region prior to the strong discharge has been clearly demonstrated in fresh water[9] the implication of the relatively larger acoustic output is that a much larger gas bubble is found, due to the greater rate of energy dissipation in conducting media. If one assumes that an essential condition for transition to a strong discharge is the presence of a gas bubble bridging the two electrodes (for example, the coalescing of bubbles formed individually around each electrode), the hypothesis of a greater rate of gas evolution is consistent with the reduced initiation period observed in salt water.

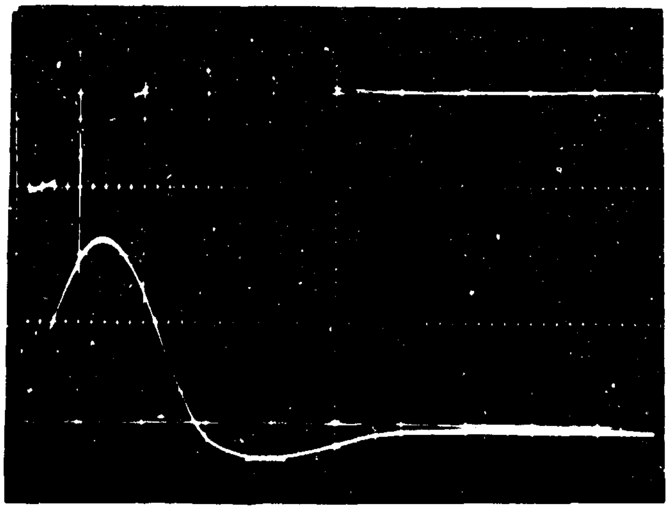

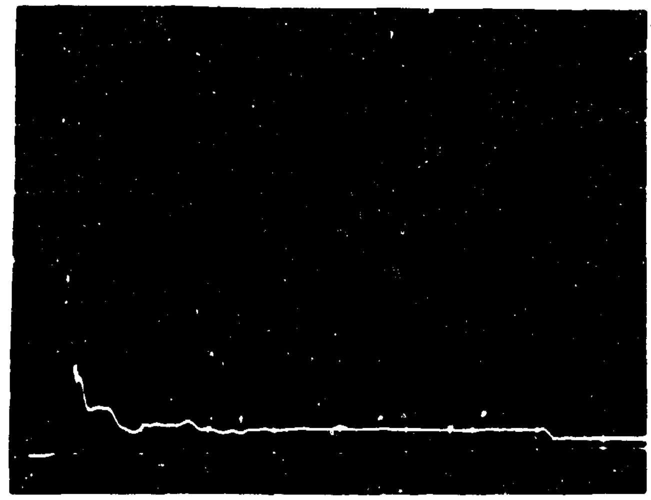

Upper, voltage = 10kV/div
Lower, current = 10^4 amps/div
Sweep = 5μsec/div
Photocell trigger

Pressure = 100 psi/div
Range = 2 feet
Sweep = 100 μsec/div

Shot B12 - Fresh Water

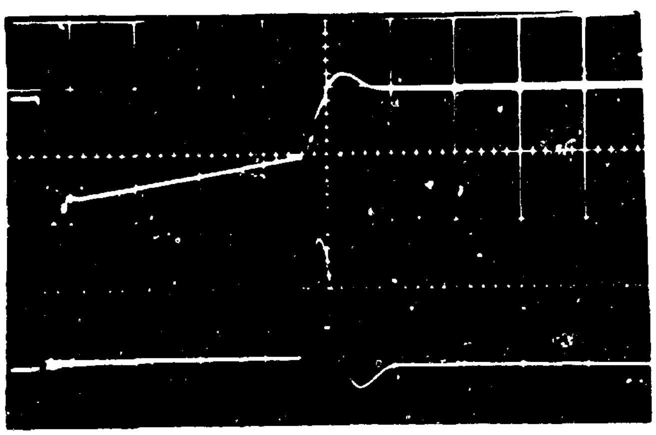

Upper, voltage = 10kV/div
Lower, current - 10^4 amps/div
Sweep = 20 μsec/div
Direct trigger

Pressure = 50 psi/div
Range = 2 feet
Sweep = 50 μsec/div

Shot B42 - Solution No. II

FIGURE 25a. 15 kV SERIES

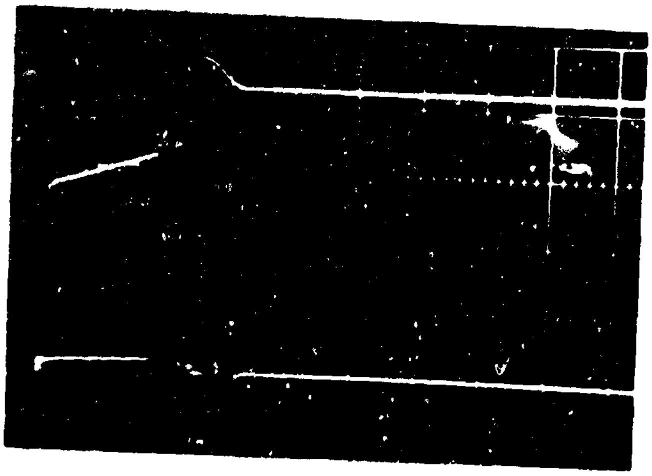

Upper, voltage = 10 kV/div

Lower, current = 10^4 amps/div

Sweep = 20 μsec/div

Direct Trigger

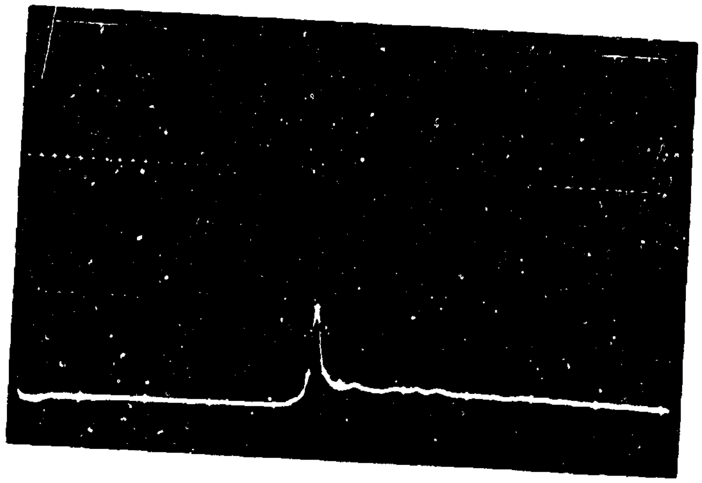

Pressure = 100 psi/div

Range = 2 feet

Sweep = 100 μsec/div

Shot B67 - Solution No. III

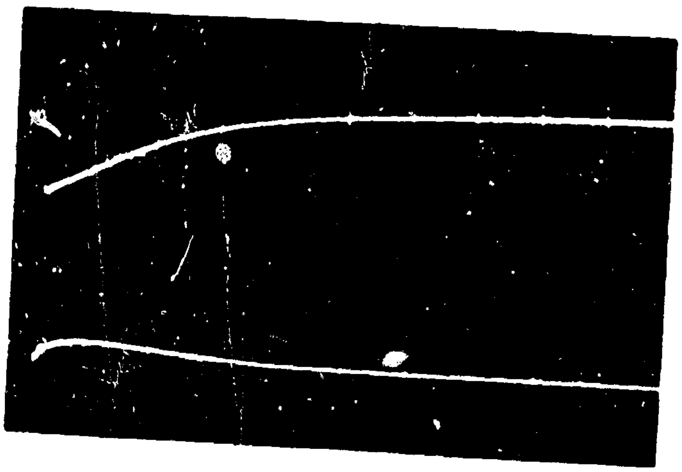

Upper, voltage = 10 kV/div

Lower, current = 10^4 amps/div

Sweep = 20 μsec/div

Direct Trigger

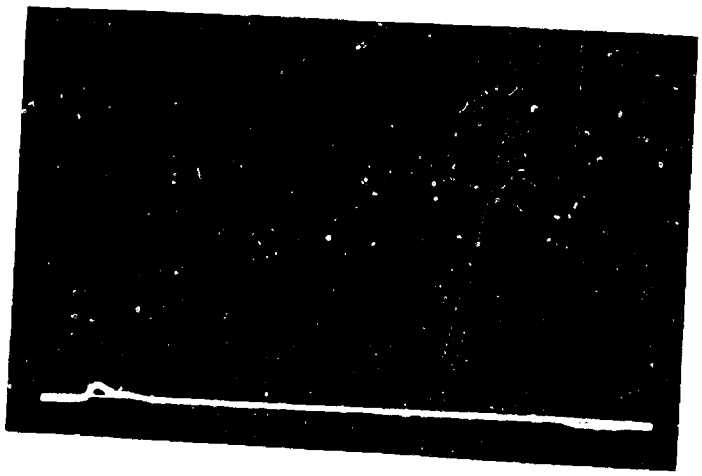

Pressure = 50 psi/div

Range = 2 feet

Sweep = 100 μsec/div

Shot B78 - Solution No. IV

Figure 25b: 15 kV Series

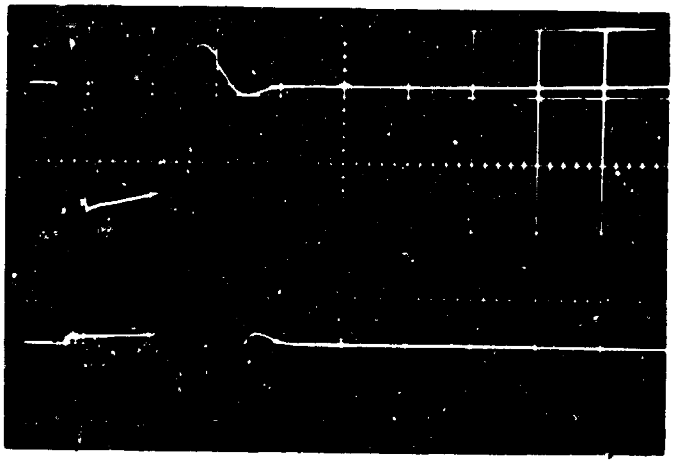

Upper, voltage = 10 kV/div
Lower, current = 10^4 amps/div
Sweep = 20 μsec/div
Direct Trigger

Pressu e = 50 psi/div.
Range = 2 feet
Sweep = 50 μsec/div

Shot B43 - Solution No. II

Upper, voltage = 10 kV/div.
Lower, current = 10^4amps/div
Sweep - 20 μsec/div
Direct Trigger

Pressure = 50 psi/div.
Range = 2 feet
Sweep = 50 μsec/div

Shot B79 - Solution No. IV

FIGURE 26a. 19 kV SERIES

Upper, voltage = 10 kV/div
Lower, current = 10^4 amps/div
Sweep = 20 μ sec/div
Direct Trigger

Pressure = 50 psi/div
Range = 2 feet
Sweep = 50 μ sec/div

Shot B97 - Solution No. VI

Figure 26b. 18 KV Series

The initial leakage current can be seen to increase markedly with increasing salinity; the result in the 15 KV series was the inability to generate a strong (explosive-like) discharge at salinities above 15 promille; shot B78 (Figure 25b) shows the nature of the weak discharge and signal obtained. Strong discharges were obtained with 18 KV up to the maximum salinity tested (Figures 26a and 26b) with results otherwise in concordance with the above. The initiation period was, as expected, shorter; however, the rapid rate of leakage still resulted in appreciable reduction of the peak acoustic output relative to fresh water.

d) Correlation of Salt Water Results

The qualitative similarity in form between the pressure waveforms and the current in the above examples makes it of interest to see whether the pressure peak, which apparently results from the strong discharge or arc, can be correlated among discharges in water of varying salinity, including fresh water. A crude correlation of this sort was attempted using the relevant data samples obtained in this series. The obvious parameters: initial energy, peak current, energy at arc initiation produced generally a large scatter. The product (voltage at arc initiation) x (peak current), however, produced a surprisingly good (almost linear) correlation (Figure 27); the four abnormally low points could be ascribed to the occurrence of the arc at an azimuth different from that of the transducer. The fresh water points fit smoothly into the curve, leading to the tentative conclusion that the effect of salinity on the present electrode configuration is generally to reduce by leakage the voltage (energy) available at the critical point of arc initiation. Reduction of this loss by some mechanism of inducing earlier development of the arc is thus essential to obtain optimum energy efficiency.

The principal results may be summarized as follows:

1) Operation of the present electrode design in salt water results in considerably reduced initiation periods, the duration varying in an inverse manner with the electrical conductivity of the medium and, presumably associated with a greater rate of gas evolution.

2) The energy drain on the capacitor during this initiation period is very large, making desirable development of means for reducing its duration in order to achieve reasonable energy efficiency.

3) Approximate empirical correlation of the peak pressure is obtained in both fresh and salt water using the product of maximum current and voltage at the start of the "explosive-like" discharge.

D. SPECTRAL ENERGY VARIATION

Two typical pressure traces obtained with the low inductance discharge circuit are shown in Figure 28. These traces display the pressure variation three feet from the acoustic source measured in a plane normal to the axis of symmetry of the acoustic source. All of the pressure traces generated by discharges ranging from 10 KV to 20 KV (i.e., a discharge energy ranging from 750 joules to 3000 joules) have essentially the same general form as the two traces shown in Figure 28. Typically, it is found that the pressure rises rapidly from zero to peak pressure in about 20 microseconds. In another 20 to 30 microseconds the pressure drops from the peak value down to some low value typically 15% to 25% of the peak value. This latter pressure level is reduced by about 50% of its

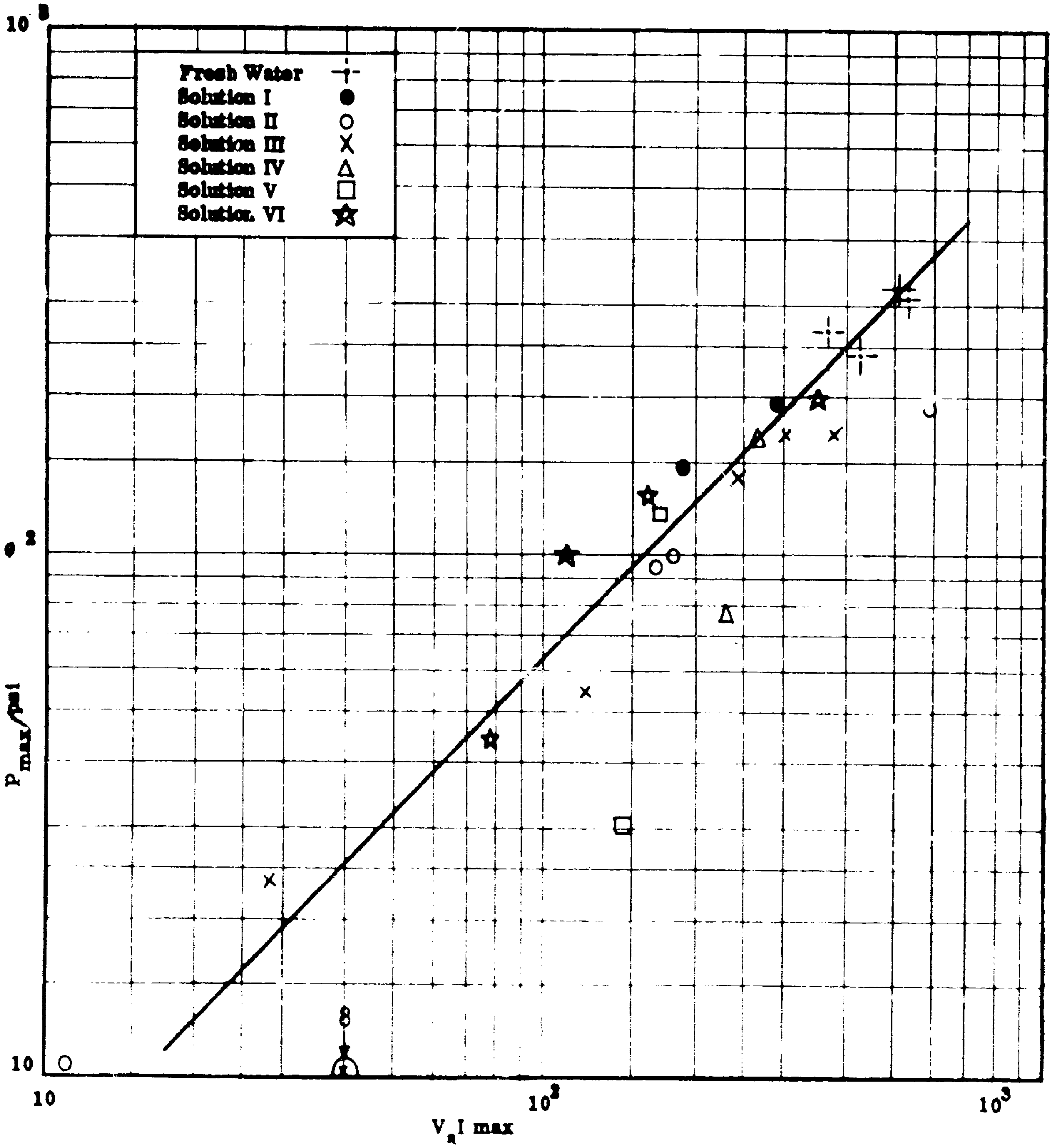

Figure 27. Peak Acoustic Pressure as a Function of the Product (Voltage at Arc) x (Peak Current)

original value over a period of about 400 microseconds after which it drops to very nearly zero. The period during which these pressure variations occur are free from reflections from any of the surfaces of the tank.

The form of the pressure traces that have been observed lend themselves in a rather straightforward manner to spectral analysis.

The temporal pressure variations that have been observed (see Figure 28 for example) suggests that an analytic spectral analysis can be carried out by considering the pressure variation to be represented by a series of connected straight line segments. Consider a typical pressure variation to be given in the form shown by Figure 29.

In the interval of time $\Delta t = t_{i+1} - t_i$ the pressure is given by the relation:

$$p(t) = P_i + \frac{P_{i+1} - P_i}{t_{i+1} - t_i} (t - t_i)$$

This relation is of the form:

$$p(t) = A_i t + B_i$$

with

$$A_i = \frac{P_{i+1} - P_i}{t_{i+1} - t_i}$$

$$B_i = P_i - A_i t_i$$

The energy density flux is defined as:

$$S(w) = \frac{2}{\rho c} \left| F(w) \right|^2$$

with ρ, c, and $F(w)$ the mass density, sound velocity and

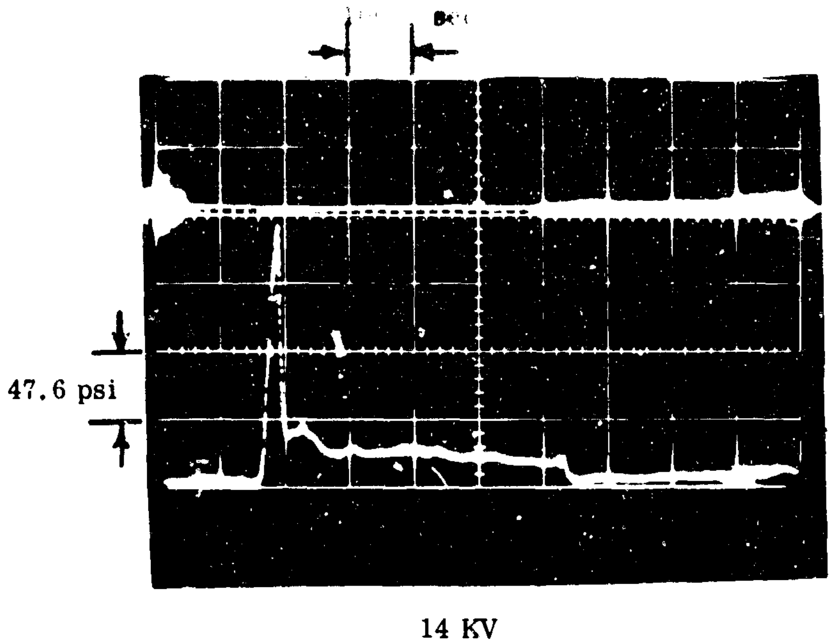

Figure 28. Pressure Trace at 1 Yard from the Acoustic Source
(Low Inductance Discharge Circuit)

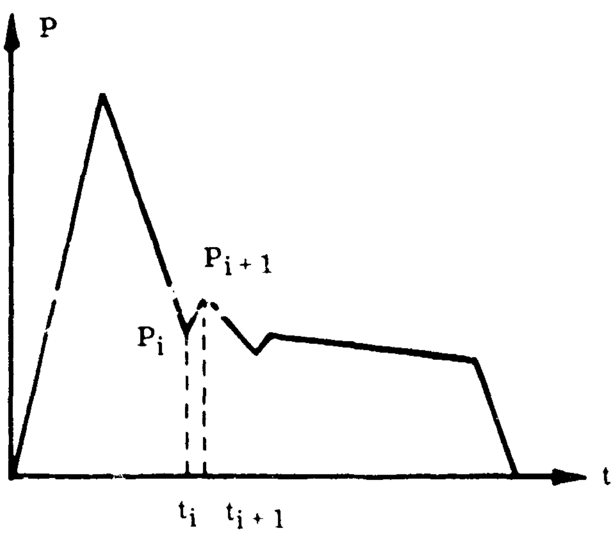

Figure 29. Typical Pressure Variation

$$F(w) = \int_{-\infty}^{\infty} p(t)\, e^{-jwt}\, dt = \sum_{i=0}^{n} F_i(w) = \sum_{i=0}^{n} \alpha_i - j \sum_{i=0}^{n} \beta_i$$

respectively. Now

$$\alpha_i = \int_{t_i}^{t_{i+1}} (A_i t + B_i) \cos wt \, dt$$

$$\beta_i = \int_{t_i}^{t_{i+1}} (A_i t + B_i) \sin wt \, dt$$

Integrating these latter two expressions and simplifying the resulting expression gives:

$$\alpha_i = 2\,\Delta_i \left\{ (\cos w\tau_i) \left(\frac{\sin w\,\Delta_i}{w\,\Delta_i} \right) (P_i + A_i\,\Delta_i) + (A_i\,\tau_i) \left(\frac{\sin w\tau_i}{w\,\tau_i} \right) \left(\cos w\Delta_i - \frac{\sin w\,\Delta_i}{w\,\Delta_i} \right) \right\}$$

$$\beta_i = 2\,\Delta_i \left\{ (\sin w\tau_i) \left(\frac{\sin w\,\Delta_i}{w\,\Delta_i} \right) (P_i + A_i\,\Delta_i) - (A_i\,\tau_i) \left(\frac{\cos w\,\tau_i}{w\,\tau_i} \right) \left(\cos \Delta_i - \frac{\sin w\,\Delta_i}{w\,\Delta_i} \right) \right\}$$

with

$$\Delta_i = \frac{t_{i+1} - t_i}{2}$$

$$\tau_i = \frac{t_{i+1} + t_i}{2}$$

$$w = 2\pi f$$

with f the frequency.

The spectral energy distribution can then be readily evaluated on a computer by noting that:

$$S(w) = \frac{2}{\rho c} \left[\left(\sum_{i=0}^{n} \alpha_i \right)^2 + \left(\sum_{i=0}^{n} \beta_i \right)^2 \right]$$

These latter relations were used to spectral analyze the pressure distributions presented in Figure 28. The results of this analysis are presented in Figure 30.

The acoustic energy radiated by the acoustic source can be determined from a pressure survey carried out at all points of a spherical surface of radius r whose center is at the source and subsequently carrying out a double integration over all frequencies and over the surface area surveyed. Only in the very special case of a perfectly spherically symmetric discharge will the energy radiated across a spherical surface of radius r be given by:

$$E = 4 \pi r^2 \int_0^{\infty} S(w)\, df$$

An accurate evaluation of the acoustic energy radiated by the source under investigation has yet not been carried out. Such a measurement is most meaningfully carried out in an unconfined environment. Only in such an environment is it possible to have confidence in having determined the correct low frequency portion of the spectrum radiated.

The results of the above analysis were programmed for a computer to present the acoustic energy per unit area per unit cycle as a function of frequency. It is realized that because of the finite size of the tank (8-foot diameter) in which tests were conducted the calculated frequency data below about 2000 Hz is not meaningful. It is hoped that pressure readings in the ocean could be carried out so that the complete spectrum generated by the acoustic source could be had. Similarly, as noted earlier, it should be noted that because of wall interactions all pressure traces presented do not include the pressure signal radiated by the bubble collapse.

Figure 30 presents the results of spectral analyzing the pressure data presented in Figure 28 as well as an additional pressure trace that was taken at

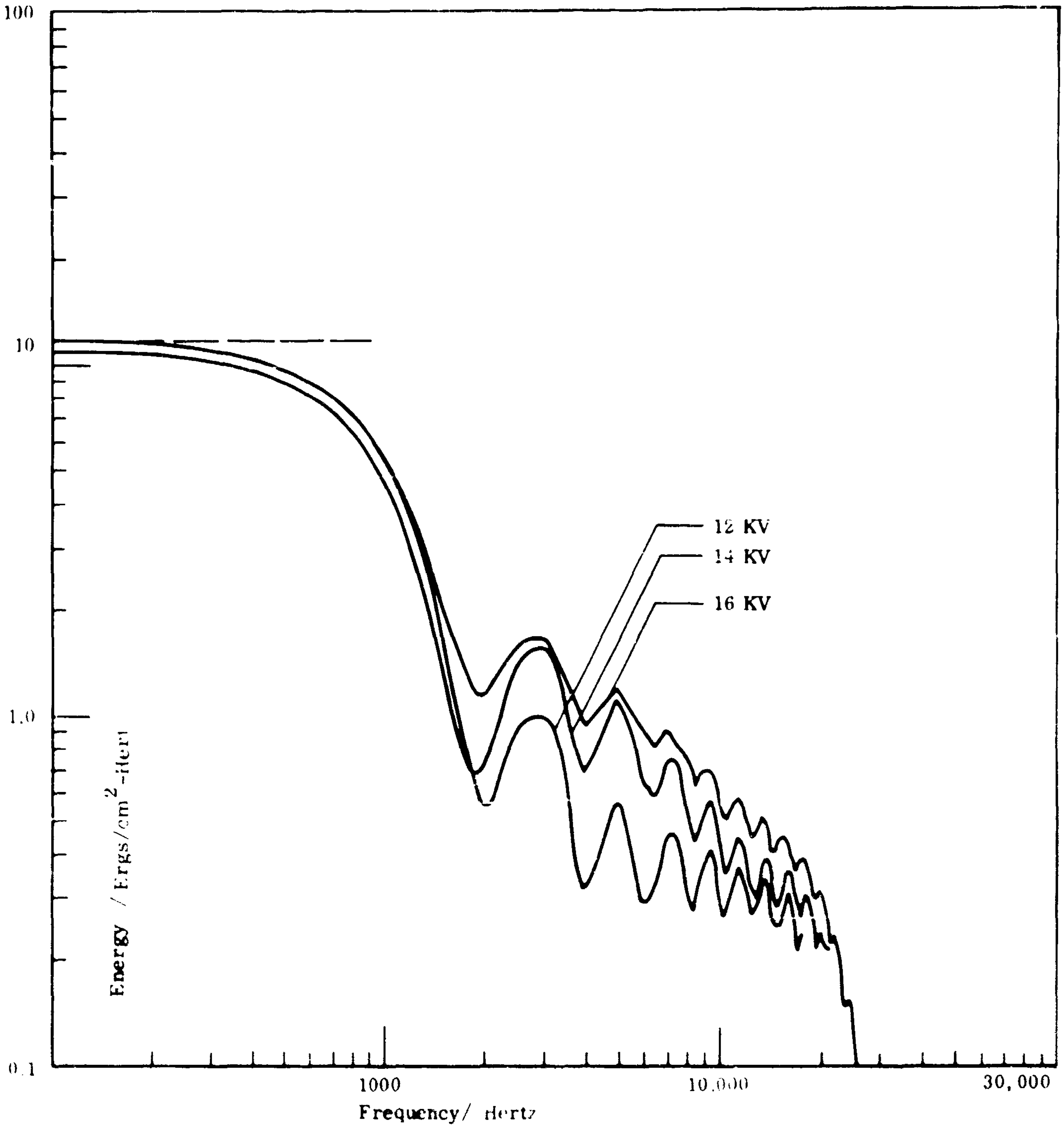

Figure 30. Spectral Analysis of Pressure Traces

16 KV. Because of the size of the tank in which tests were carried out the calculated energy radiated at low frequencies is not valid. It is not known whether the peak spectral energy density that was generated occurs at about 2800 Hz or if the peak occurs somewhere near 1300 Hz before the energy density variation merges into the correct asymptotic behavior at low frequencies. Tests carried out in either a lake or in the ocean should provide the exact location of the peak of the spectrum as well as the correct asymptotic behavior at low frequencies. Since in all three cases the variation of pressure with time was essentially of the same shape (see Figure 28), it is not surprising to observe that all three energy spectral variations are similar in shape.

It is believed that a spectral analysis of the complete pressure-time histories taken in an environment (i.e., lake or ocean) where free surface or bottom reflections are absent are more meaningful than those presented under laboratory conditions.

E. LUMINOSITY STUDIES

1. High Speed Photographs

The technique used for observing the underwater discharge by means of high speed photography was presented in Section II D-1. Some of the more pertinent results will now be presented.

Figures 31 through 35 show electric current and light intensity variation seen by a phototube of the discharge sequences presented in Figures 36 through 40, respectively. Calculations indicate that the time interval denoted by arrows in Figures 31 through 35 should be the period during which the high speed Beckman-Whitiey camera photographed the plasma.

An inspection of Figures 36 through 39 shows the presence of luminous streamers extending radially into the water besides the presence of the plasma. These streamers can be seen in Frames 1 through 6 in Figures 36a and in Frames 1 through 4 in Figure 38a. These streamers last for about 30 microseconds. The discharge shown in Figure 39a shows these streamers to be initially nearly uniformly distributed over the periphery of the electrodes while they are found to be localized in the discharges shown in Figures 36a, 37a, and 38a. Mel'nikov, et al [10]

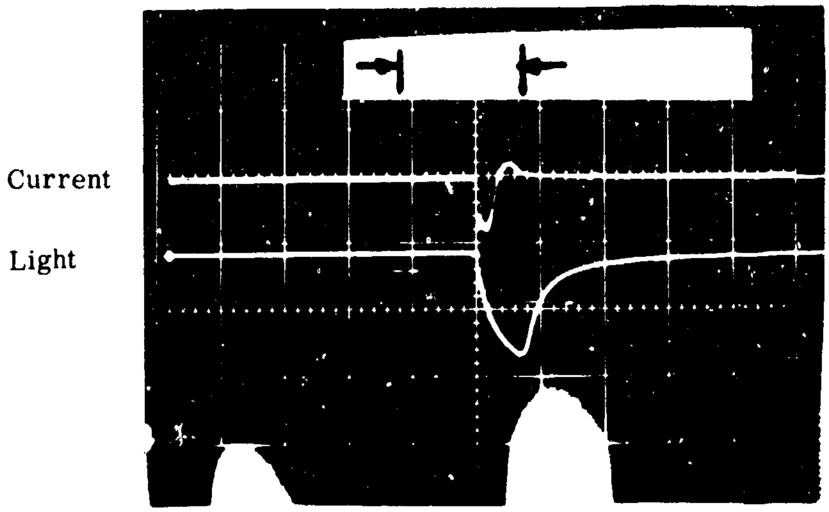

Figure 31. Current and Light Probe Traces for Log 50

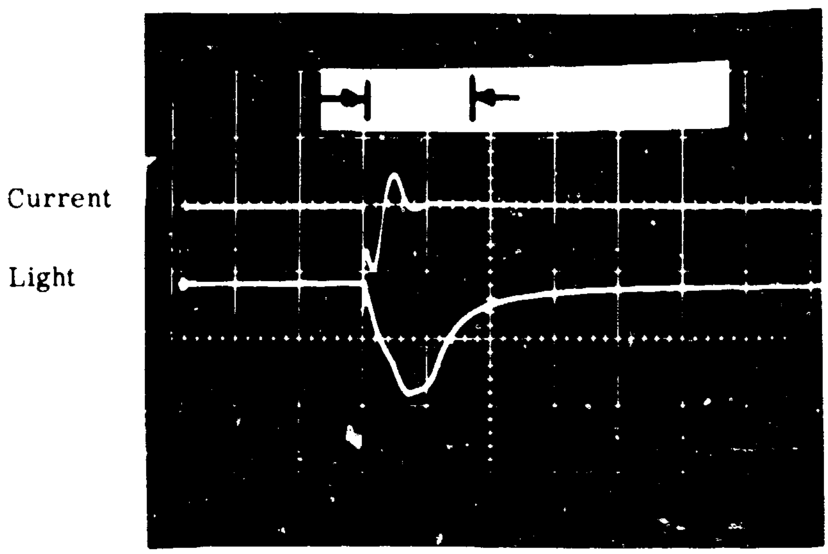

Figure 32. Current and Light Probe Traces for Log 51

Additional Information: 50, 000 amperes/cm for all current traces
50 μsec/cm sweep speed for all current and light probe traces

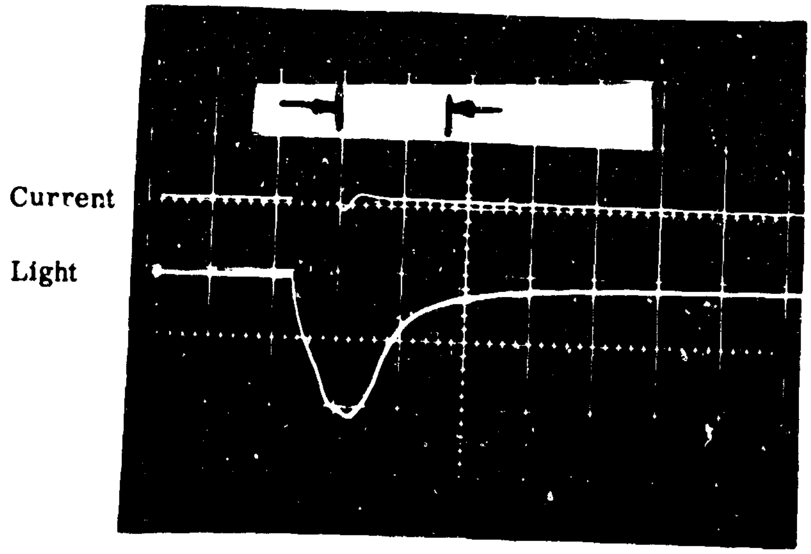

Figure 33. Current and Light Probe Traces for Log 34

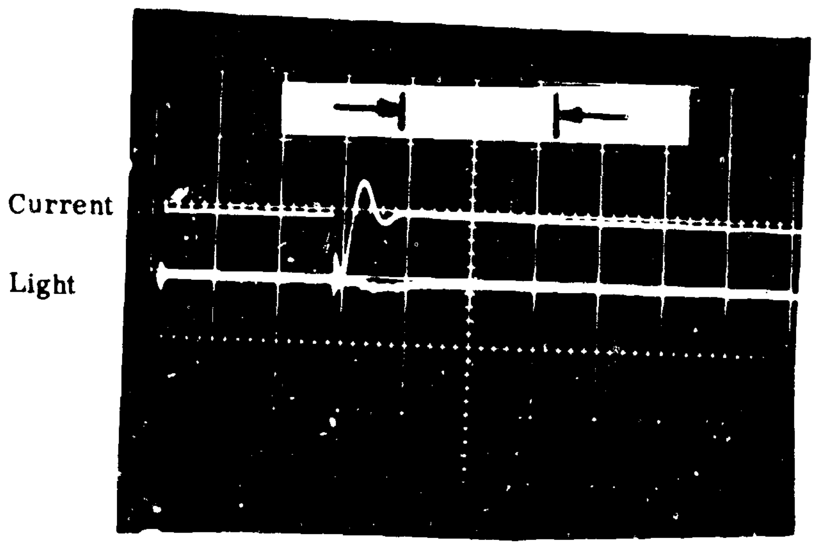

Figure 34. Current and Light Probe Traces for Log 54 (Light Probe was not viewing the Discharge)

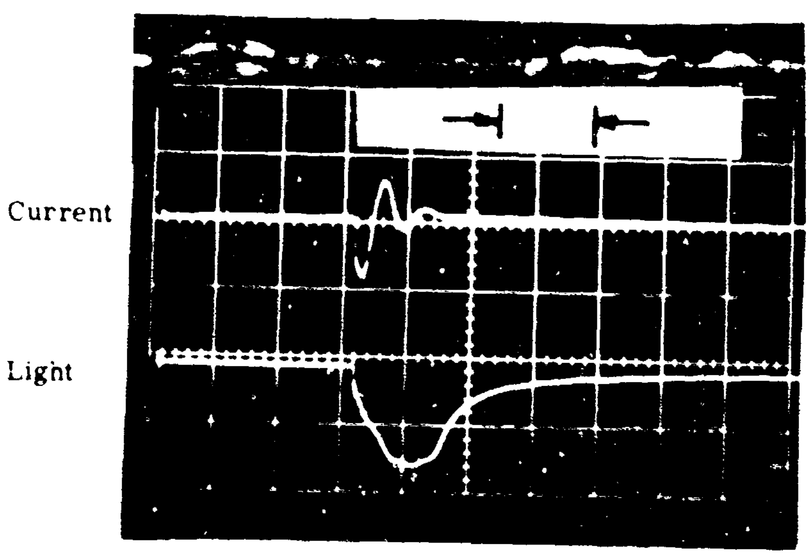

Figure 35. Current and Light Probe Traces for Log 23

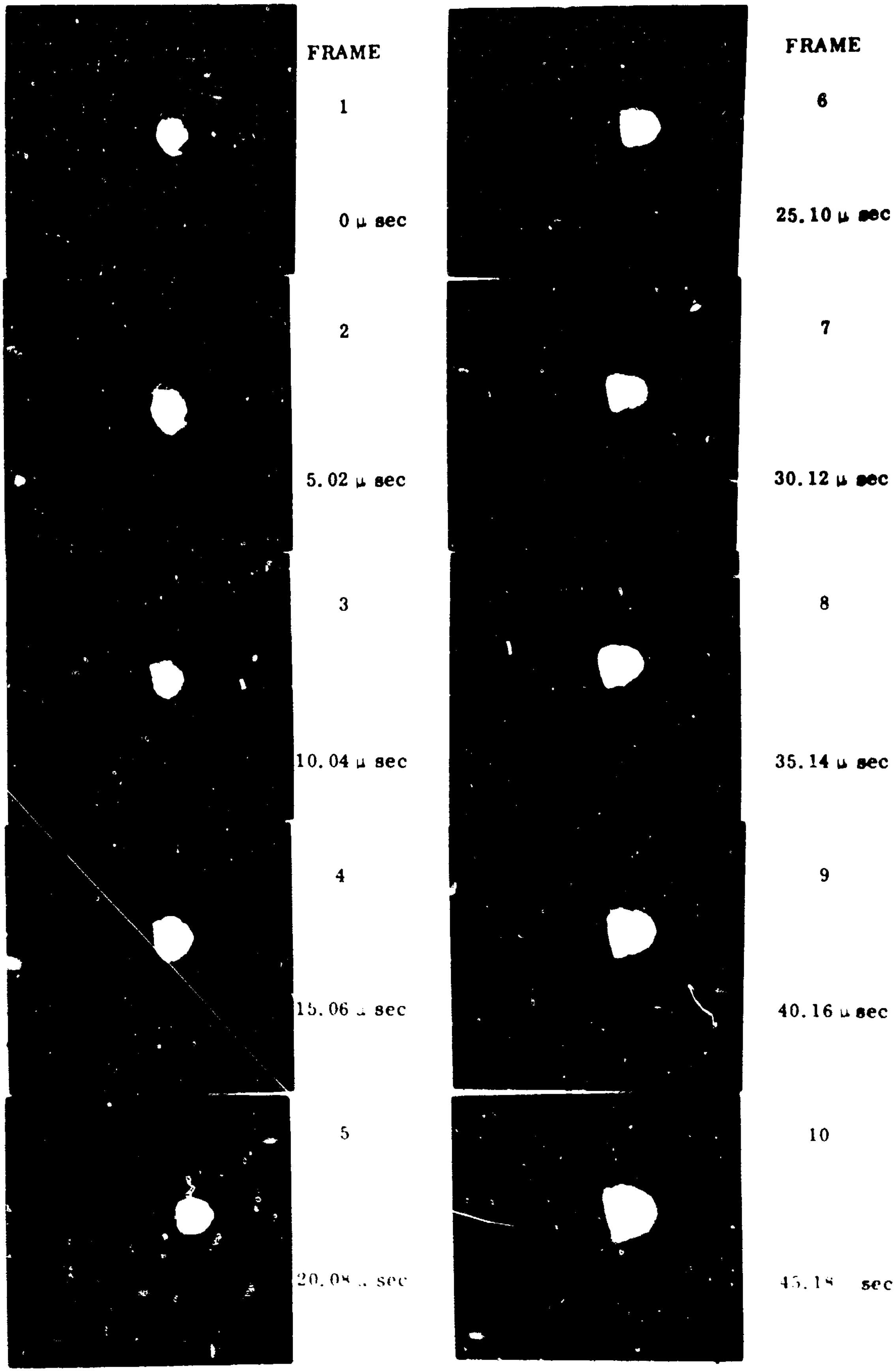

Figure 36a. High Speed Photographs of Plasma Growth (Log 50, 199,000 fps)

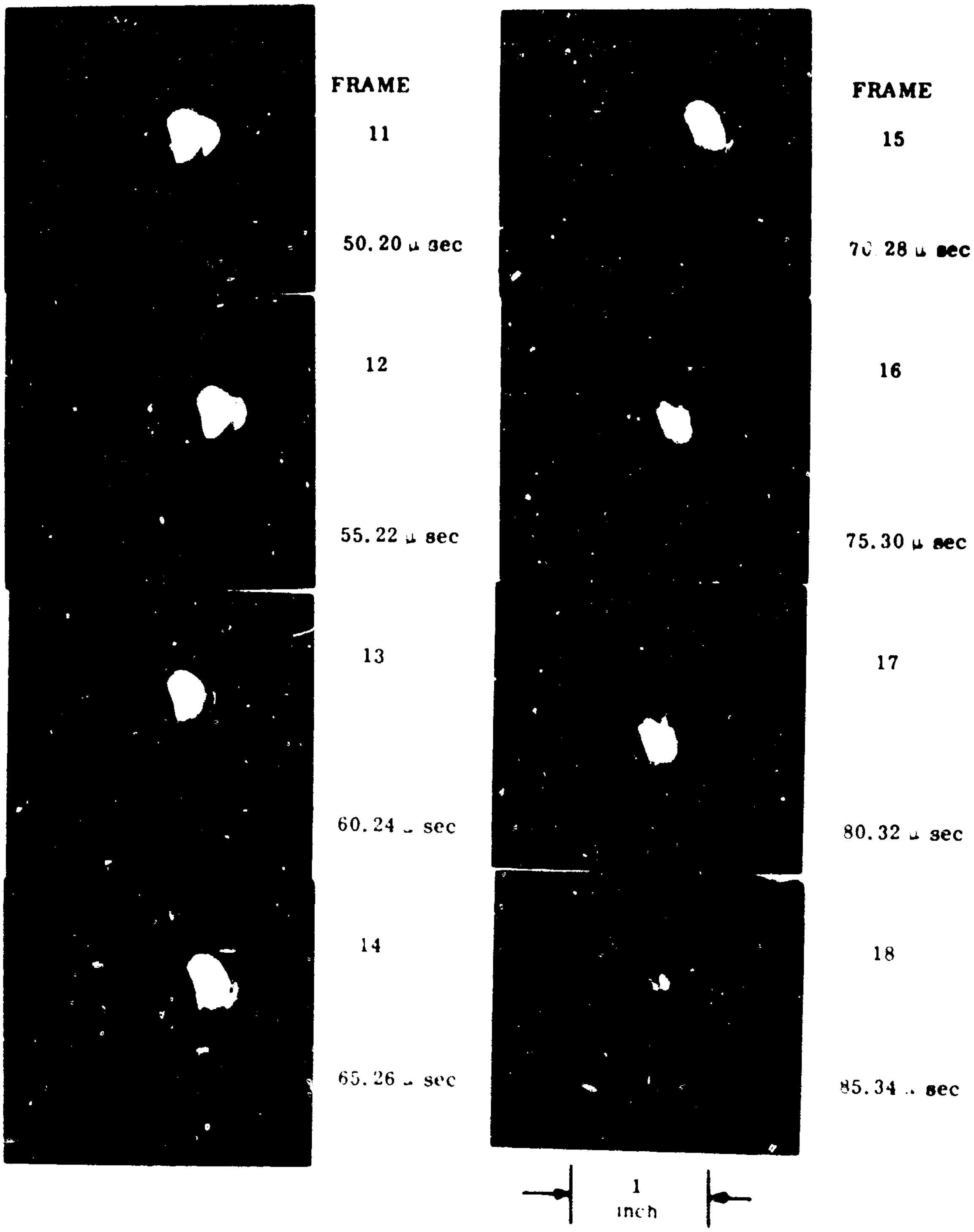

Figure 36b. High Speed Photographs of Plasma Growth (Log 50, 199000 fps)

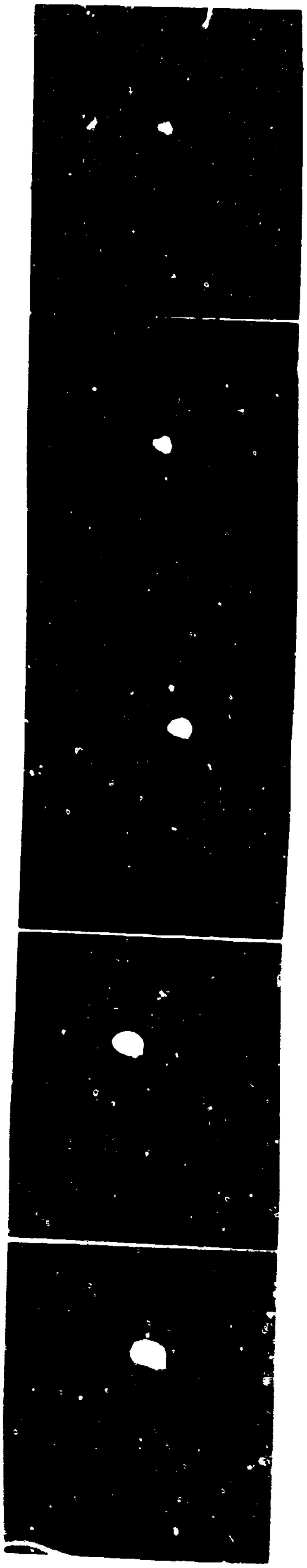

FRAME

1

0 µ sec

2

4.3 µ sec

3

8.7 µ sec

4

13 µ sec

5

17.3 µ sec

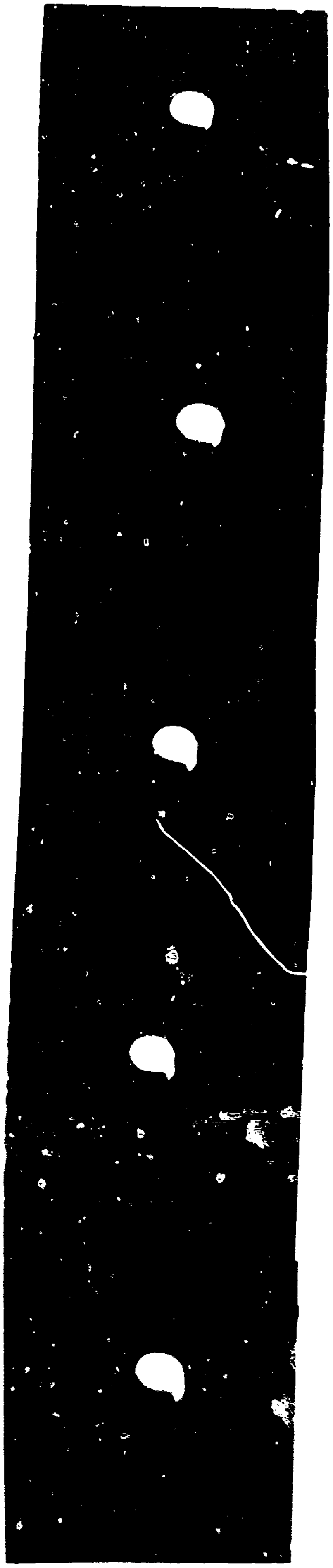

FRAME

6

21.6 µ sec

7

26 µ sec

8

30.3 µ sec

9

34.6 µ sec

10

38.9 µ sec

Figure 37a. High-Speed Photographs of Plasma Growth
(Log 51, 231,000 fps)

FRAME

11

43.3 μ sec

12

47.6 μ sec

13

52 μ sec

14

56.3 μ sec

15

60.6 μ sec

FRAME

16

65 μ sec

17

69.3 μ sec

18

73.7 μ sec

19

78 μ sec

Figure 37 b. High-Speed Photographs of Plasma Growth
(Log 51, 231,000 fps)

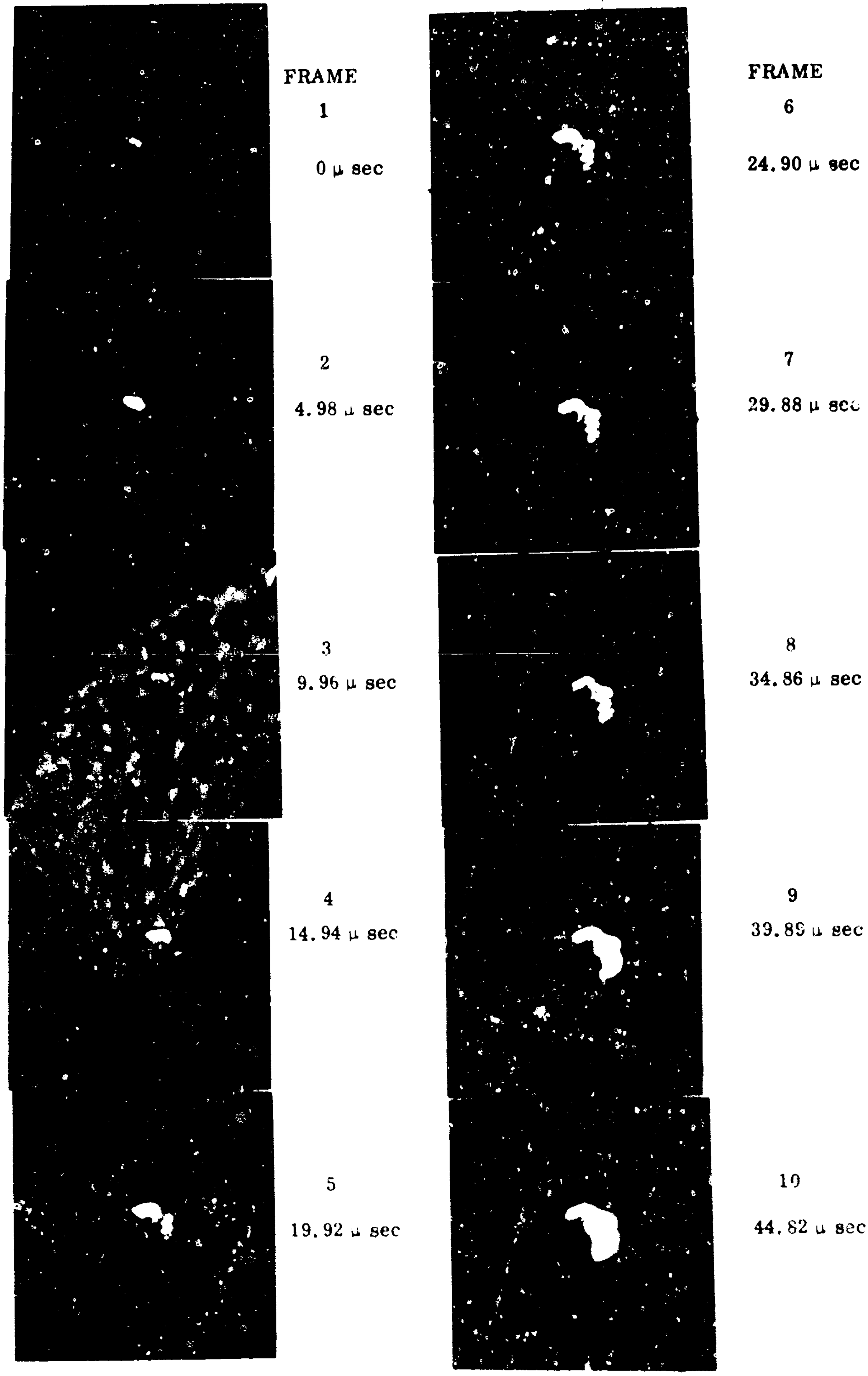

Figure 38a High-Speed Photographs of Plasma Growth
(Log 34, 201,000 fps)

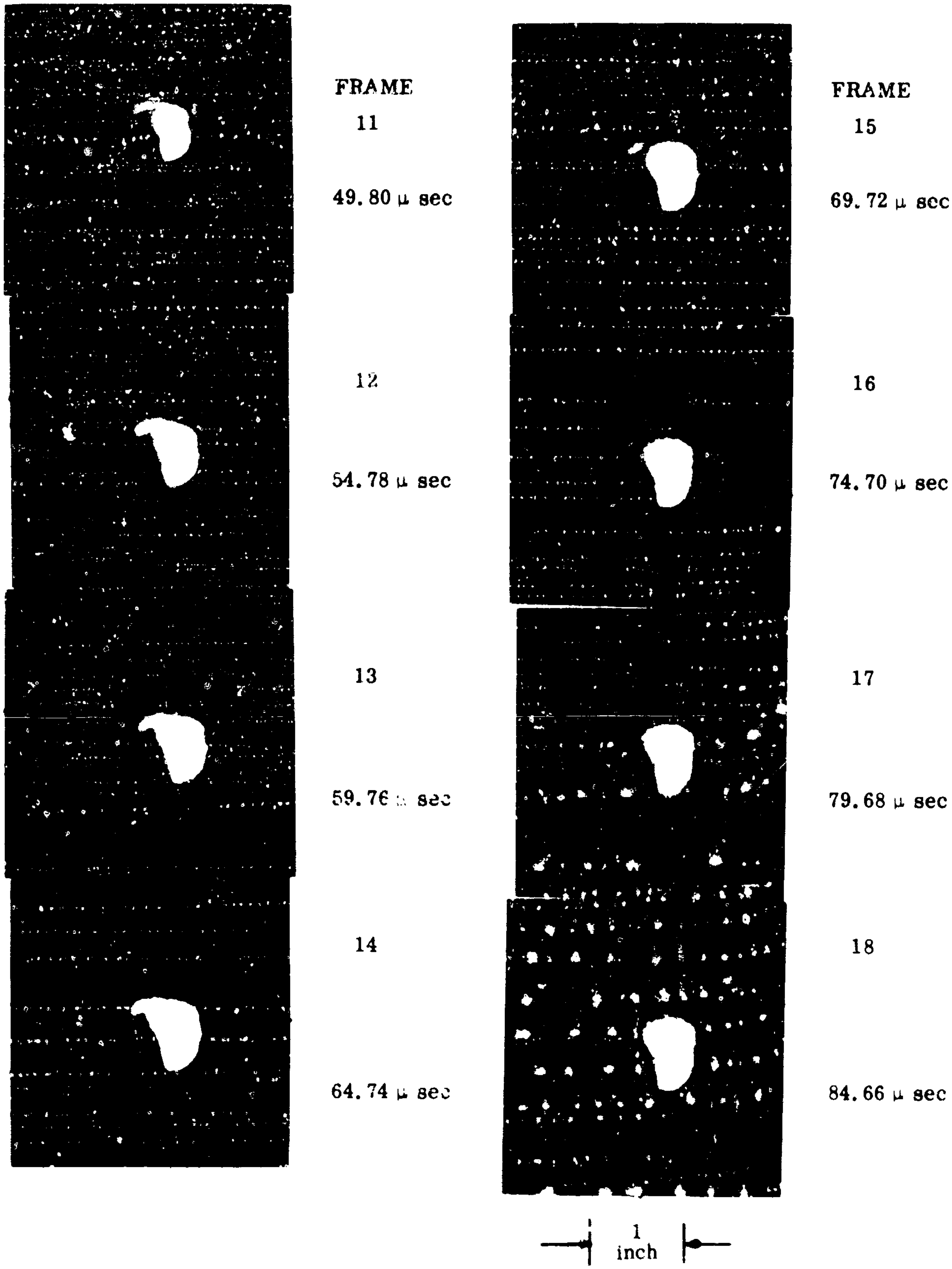

Figure 38b. High-Speed Photographs of Plasma Growth
(Log 24, 201,000 fps)

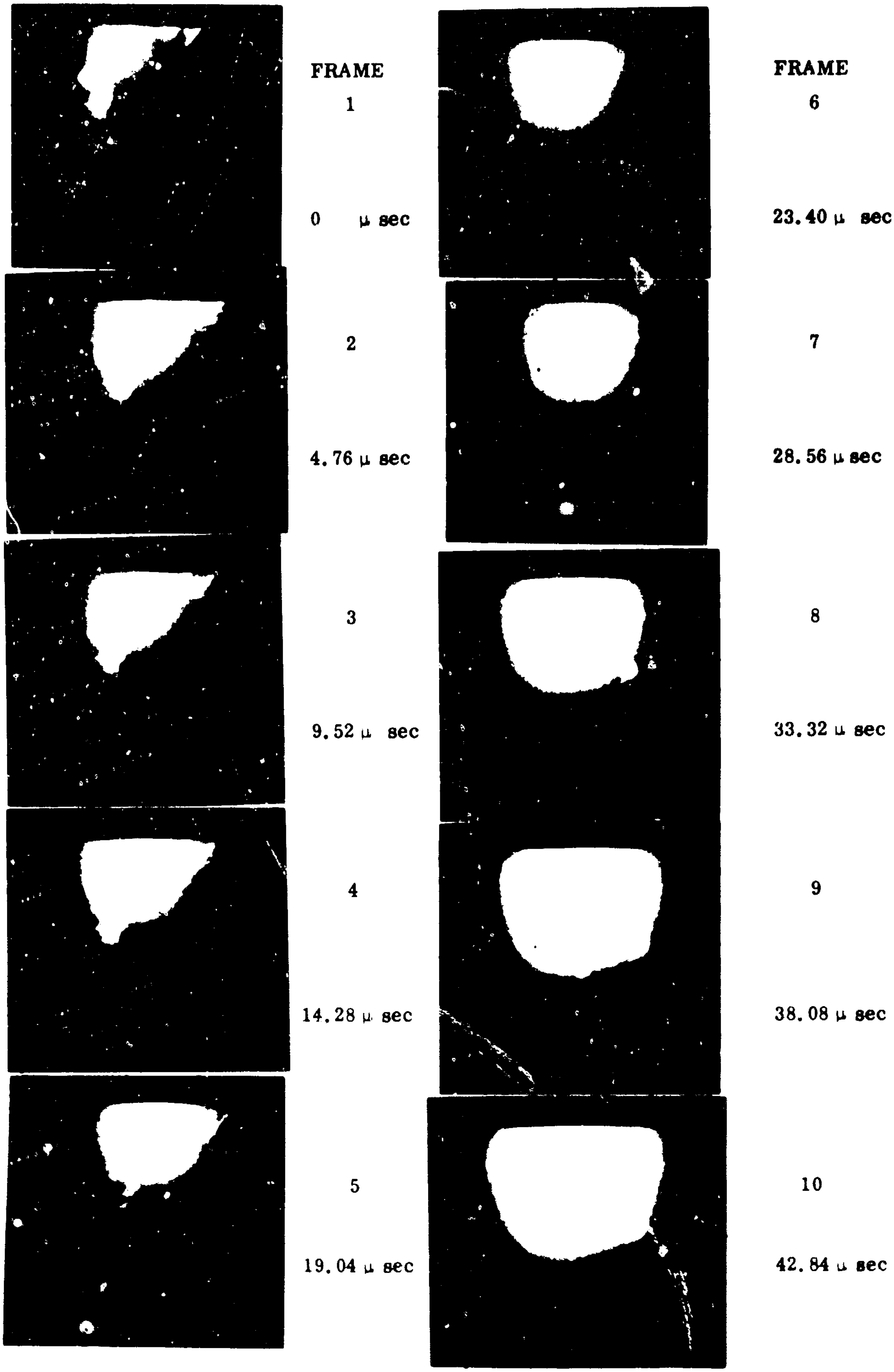

Figure 39a. High-Speed Photographs of Plasma Growth
(Log 54, 210,000 fps)

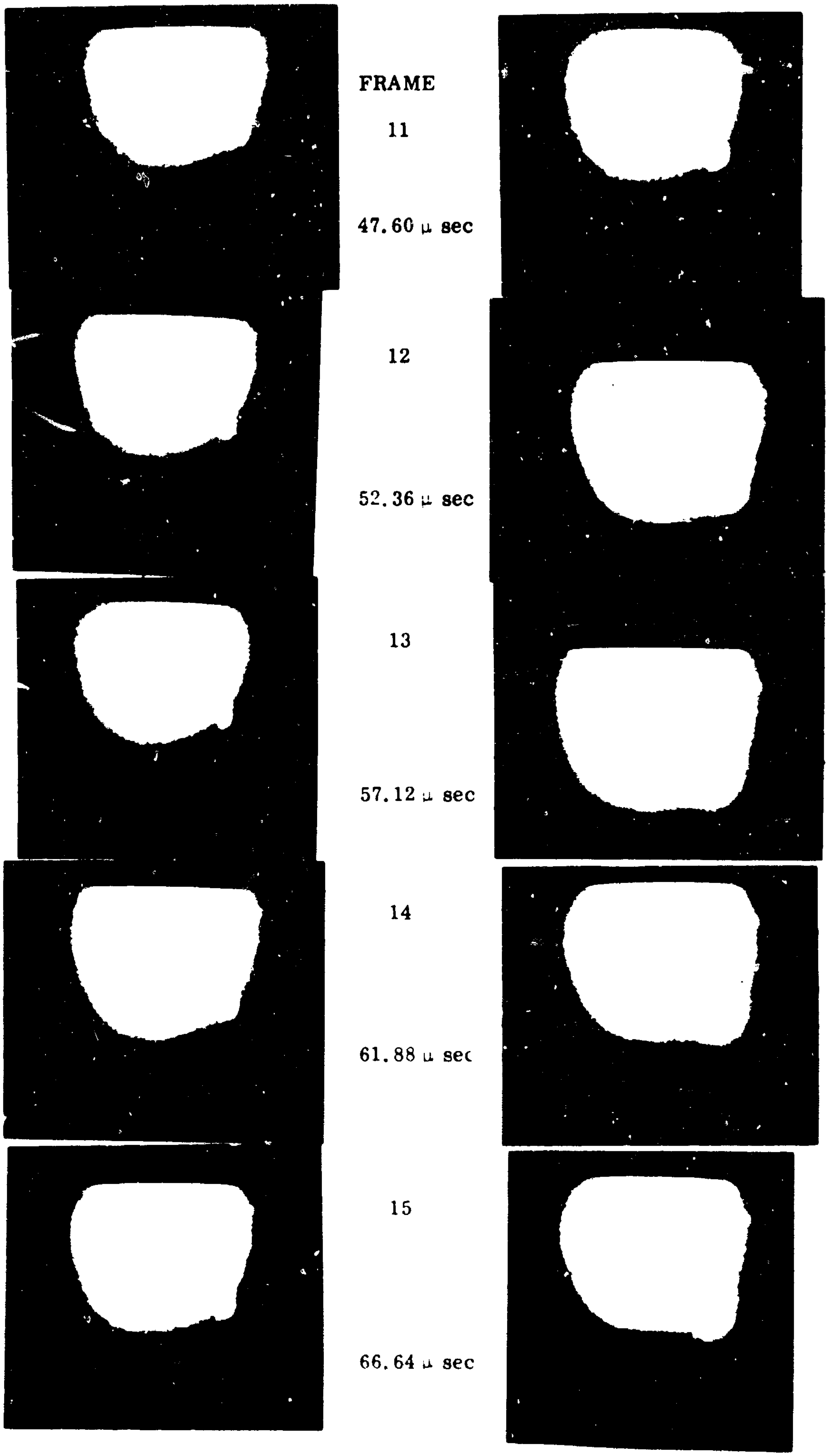

Figure 38b. High-Speed Photographs of Plasma Growth
(Log 54, 210,000 fps)

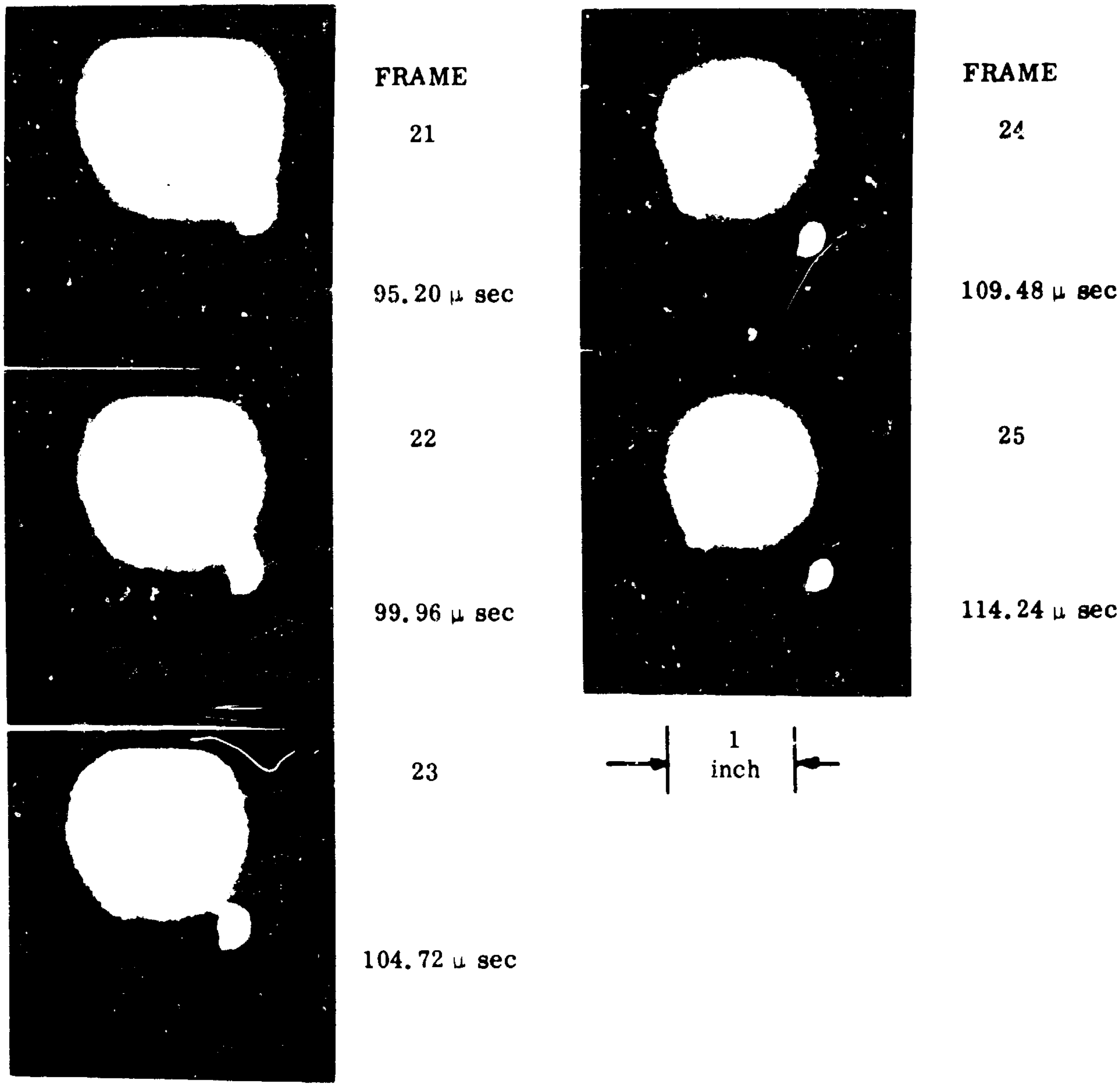

Figure 39c. High-Speed Photographs of Plasma Growth
(Log 54, 210,000 fps)

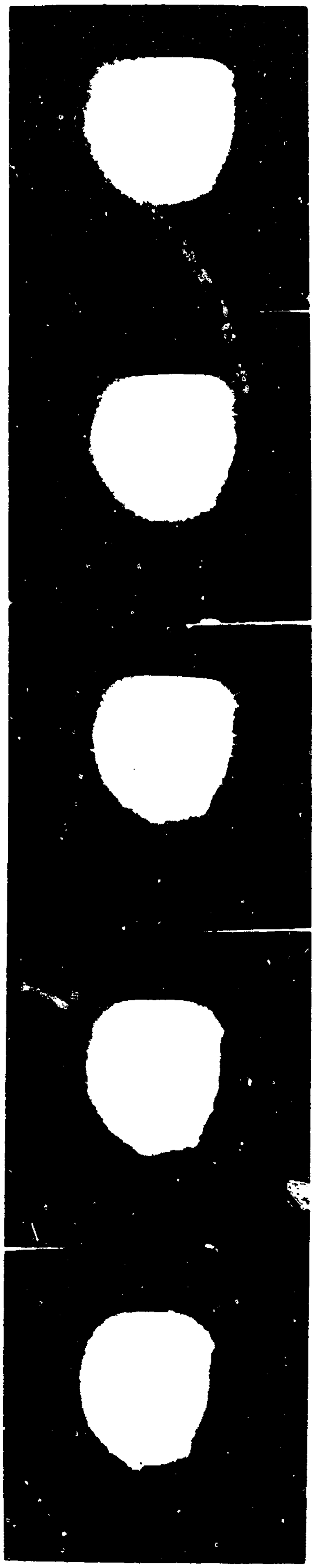

FRAME	
1	0 µ sec
2	4.95 µ sec
3	9.90 µ sec
4	14.85 µ sec
5	19.80 µ sec

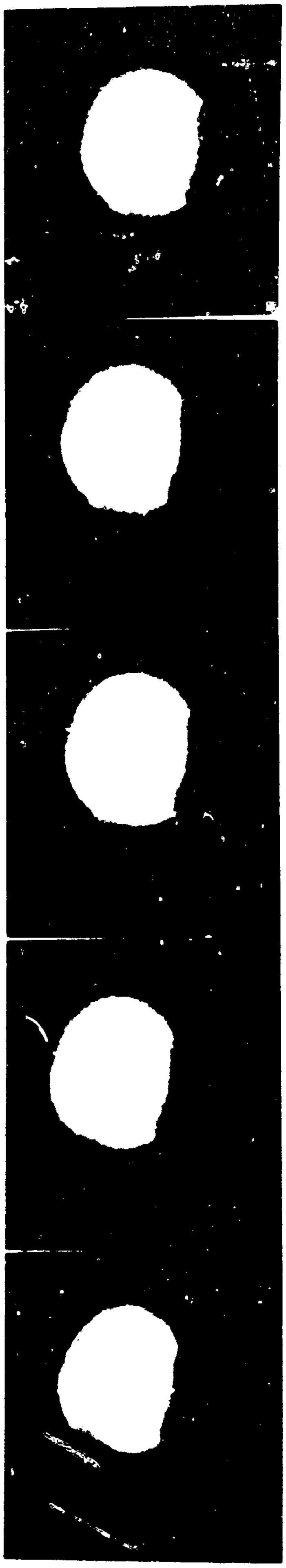

FRAME	
6	24.75 µ sec
7	29.70 µ sec
8	34.65 µ sec
9	39.60 µ sec
10	44.55 µ sec

Figure 40a. High-Speed Photographs of Plasma Growth
(Log 23, 202,000 fps)

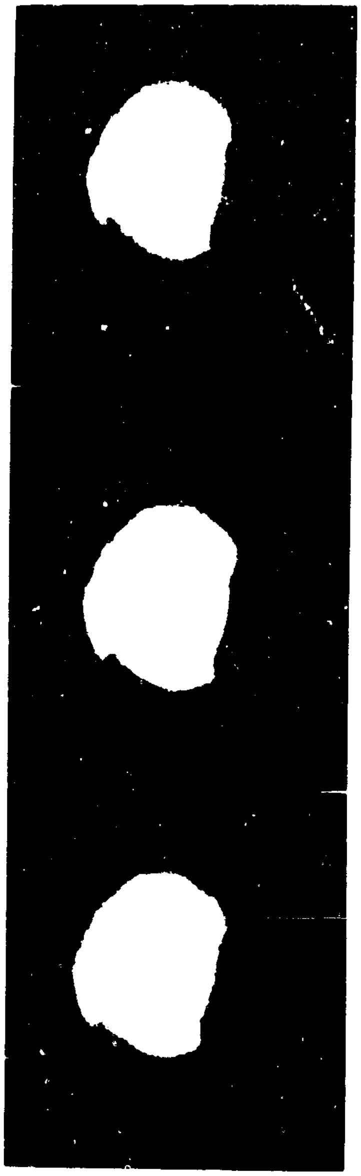

FRAME

11

49.50 μ sec

12

54.45 μ sec

13

59.40 μ sec

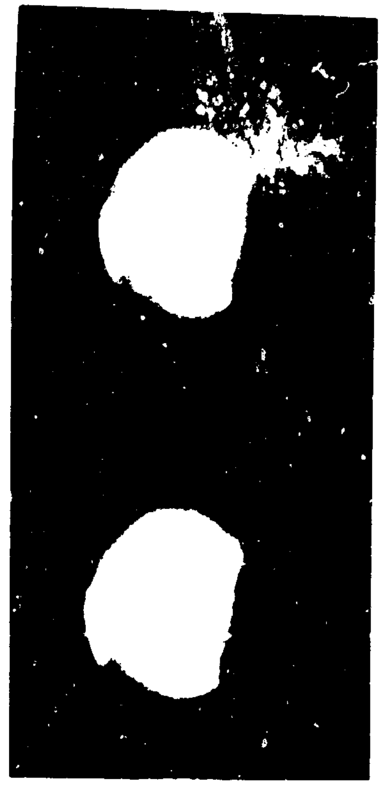

FRAME

14

64.35 μ sec

15

69.30 μ sec

1 inch

Figure 40b. High-Speed Photographs of Plasma Growth
(Log 23, 202,000 fps)

have observed similar streamers in coaxial electrodes containing an aqueous sodium chloride solution. Using a Schlieren technique with backlighting they observed that the first nonluminous streamer, of the number of nonluminous streamers formed, which joined the two electrodes is the streamer in which plasma breakdown occurs. The plasma then propagates rapidly along the streamer going from one electrode to the other. Since the present photographic study was concerned with the evaluation of symmetry of the discharge, photographs were taken by sighting along the axis of symmetry of the electrode assembly. It was, therefore, not possible to observe the streamers connecting the two electrodes such as observed by Mel'nikov.

The discharge shown in Figures 39a, b, and c is particularly interesting. The first frame shows a large number of luminous streamers distributed around the periphery of the electrodes and some localization of the plasma at about eleven o'clock in the picture. The luminosity of the plasma increases with time. In Frame 5, plasma is also seen to localize at about five o'clock in the picture. This localization is more evident in Frame 6. This second region of plasma increases in size while the main luminosity is emitted from the plasma located at eleven o'clock. The luminosity of the main plasma region drops after about 95.2 microseconds (Frame 21) and the outline of the electrode can then be seen with the main plasma appearing like a quarter moon and the second discharge increasing in luminosity and being positioned peripherally about 180 degrees relative to the main discharge region. Unfortunately, the light probe viewing this discharge was accidentally displaced and essentially no light was registered by the probe (Figure 34). The fact that plasma may exist at more than one peripheral location during a given discharge suggests that a nearly symmetrical plasma discharge may be possible.

The last sequence shown, Figures 40a and b, were taken without a neutral density filter on the camera. From the information contained in Figure 35, it is seen that this photographic sequence shows the plasma after the current has been completely discharged and the light intensity of the plasma is rapidly decaying to zero. The self-luminosity of the plasma is sufficient to outline the electrode and the luminous region occupied by the plasma around the electrode. It was initially believed that the darkened circular band to the left of the luminous region represented a pressure wave being propagated into the water and made visible in the manner of a shadowgraph. However, measurements of the rate of radial growth of this region between Frames 6 and 15 indicates a velocity of about 340 ft/second. Because this velocity is considerably lower than the acoustic velocity, it is believed that the darkened band represents the outer extremity of the inner region of radially expanding plasma. The luminosity exterior to this band is due to the presence of plasma having a larger radial extent than the plasma interior to the band but displaced along the axis of the electrode being viewed. Such a double region of radially expanding plasma is seen clearer in Figures 36a and 36b. There is a good possibility that such interfaces of plasma are generated each time the electric current passes through zero during current oscillations. The phototube shows a small inflection point in the light intensity when the current passes through zero. This latter observation was reported in Reference 21 and is shown in Figures 22 and 23 of Reference 12. It is perhaps of interest to note at this point that plasma acceleration studies in a vacuum have also shown the generation of a new mass of plasma each time the electric current passes through zero[11].

Inductance changes due to changes in the geometry of the plasma are also evident from the photographs presented in Figures 36 through 40. If the conductivity of the plasma should remain constant, it would appear that the plasma resistance should also change because of changes in the area through which current flows. Such an observation, however, does not check with the findings of Caulfield[7] or with those of Skvortsov, Komel'kov and Kuznetsov.[5] As the edges of the electrode assembly are not sharply defined, it is not possible to make reliabl displacement measurements from which the radial and peripheral velocity of the plasma could be accurately evaluated.

Unlike magnetically-driven plasma sheets in inverse pinch geometries being studied in a vacuum, the underwater plasma generated by a 3000 joule discharge was not found to be axisymmetric with respect to the electrodes. Evidently, the large inertia of the water surrounding the electrodes inhibits the peripheral spreading of the discharge at the energy levels that have been studied.

In addition to the high speed framing camera photography described above, a rotating mirror camera was used to obtain streak photographs of the electrical discharge. Figure 41 shows the arrangement of equipment that was used. High speed streak photographs were taken with and without a slit positioned on the discharge. Figure 42 shows a typical discharge in a darkened room. A glass plate was also positioned on the surface of the water to eliminate surface ripples in the water. Figure 43 shows a typical photograph obtained at 602 rps. The axis of rotation of the mirror is parallel to the two interelectrode faces of the acoustic generator (see Figure 44). Therefore, any expansion of the plasma would be seen in Figure 43 as light expanding normal to the line marked C_L in Figure 44. The interpretation of Figure 43 can be better understood by reference to Figure 44 which schematically illustrates the position of the mirror relative to the electrode and plasma motion.

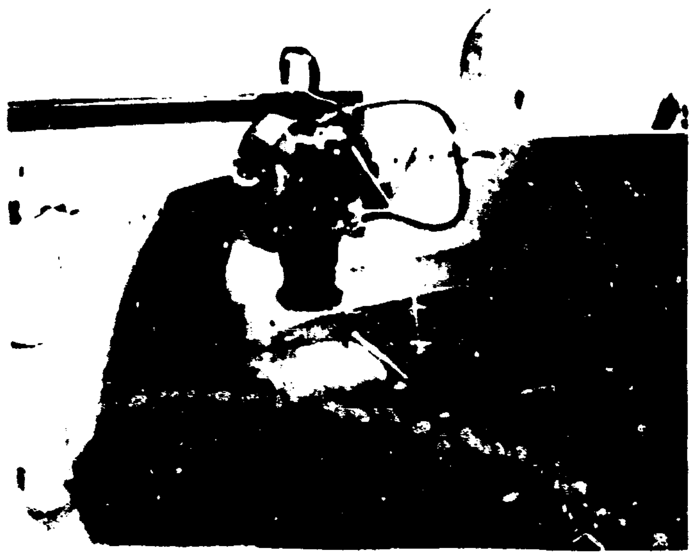

Figure 41. Rotating Mirror Camera

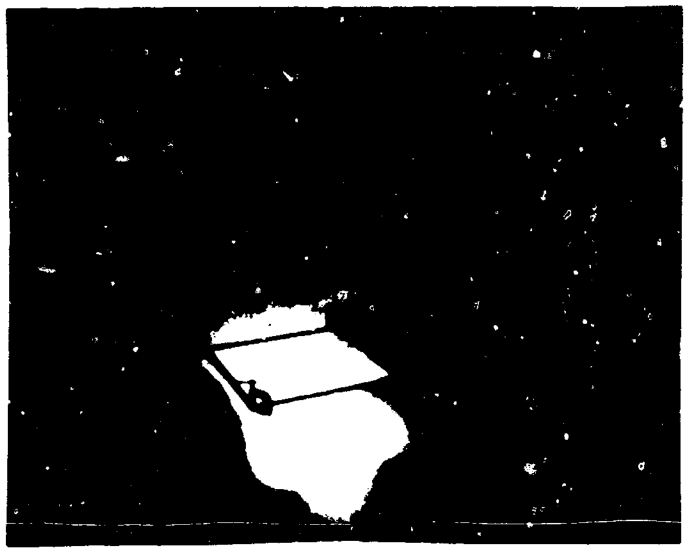

Figure 42. Typical Discharge

Figure 43. Typical Streak Photograph (0.77 mm/μ sec writing speed)

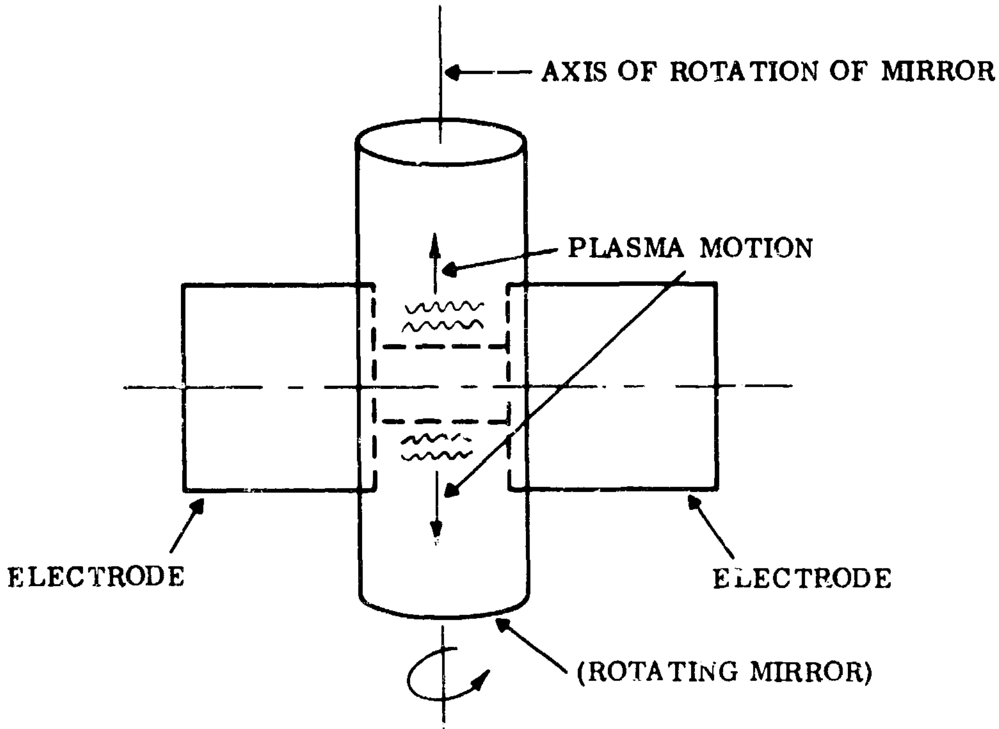

Figure 44. Schematic Illustration of Phenomena

From Figure 43 one can see that for a period of about 50 μ seconds there exists initially an essentially constant diameter of plasma whose light intensity increases with time. At the end of this period there is a rapid expansion of the plasma column normal to the axis of the electrode assembly. Since a reference dimension is not available in the photograph, the velocity of expansion or the radial extent of this expansion cannot be evaluated with certainty, an attempt was made to obtain two reference marks on the film a known distance apart. Two spaced wires did not manifest themselves on the exposed film. While it is suspected that the two visible horizontal lines (see arrow in Figure 43) are the supporting bolts (see Figure 41) of the electrode assembly (and known to be a certain distance apart), it has been clearly established that these are the bolts and, therefore, velocities cannot be reliably evaluated.

All of the streak photographs that were taken showed a sudden expansion ("explosive-like") in the plasma column after the initial period of constant width (initiation period) of the luminous column. A phototube was used to examine the variation in light intensity of the plasma in order to supplement the information obtained with the streak photographs.

In general it was concluded that the streak photographs were not as informative as the framing camera results described above.

2. Light Pulse-Current Variation Correlation

The use of a phototube to view the luminosity variation of the plasma bubble represents a simple tool for obtaining supplementary diagnostic information. One of the interesting studies was to examine the variation of the light intensity radiated by the luminous bubble as a function of the discharge voltage and electric current.

Figure 41 shows the voltage variation (across the ignitron) and the light probe output for a given discharge. It is seen that upon closing the ignitron the bank voltage (10 KV) appears across the electrodes of the generator. A linear "leak-off" of voltage occurs for about 150 μ seconds before the "explosive" discharge occurs (just prior to the "discharge" only about 5.5 KV remains across the ignitron). The light probe shows no evidence of light during this 150 μ seconds discharge initiation period. Only during the roughly 25 μ seconds long discharge period is light seen by the phototube. It has been previously established that the Rogowski coil detects current only during this rapid voltage drop. While current flows during the initiation period, its magnitude is too small to read with the Rogowski coil.

Figures 46 through 52 show the current and light probe reading for voltages varying from 11 KV to 40 KV. The light intensity is seen to commence with the flow of current through the plasma. The light output increases as the magnitude of the current increases. It appears that the light intensity increases for a few microseconds, even after the current reaches peak amplitude and starts to decrease. Each time the current passes through zero, the light probe output is seen to experience an inflection. A similar result has been observed in other pulsed plasma experiments[12].

By referring to Figures 36a and 36b which were obtained with the framing camera, we can note that a second radially expanding region of plasma becomes visible after about 25 μ seconds. This time would correspond roughly to the time the discharge current passes through zero and a new region of plasma is created by the electric discharge as suggested by phototube studies. The perturbations in the light intensity, therefore, do appear to be associated with perturbations in the plasma bubble motion and perhaps, therefore, explain in part the difference in the shape of the pressure signals generated by either oscillatory or critically damped discharges.

It is interesting to note that a resemblance exists in the appearance of the light probe output and the pressure signal when a critically damped current exists, or when the current oscillates through one or more cycles.

Voltage
(5 kV/cm)

Light

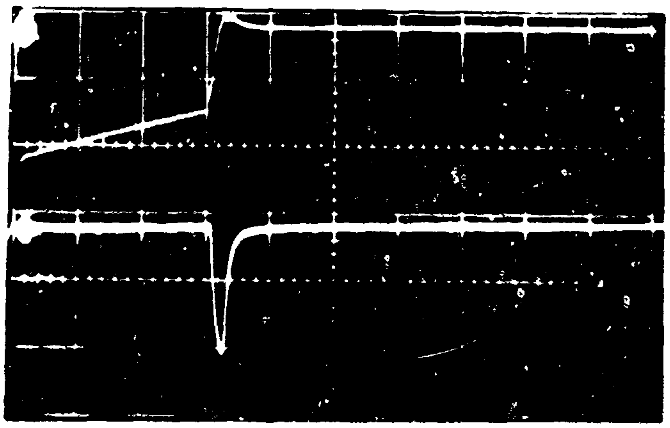

Time (50μ sec/cm)

Figure 45. Voltage-Light Probe Trace

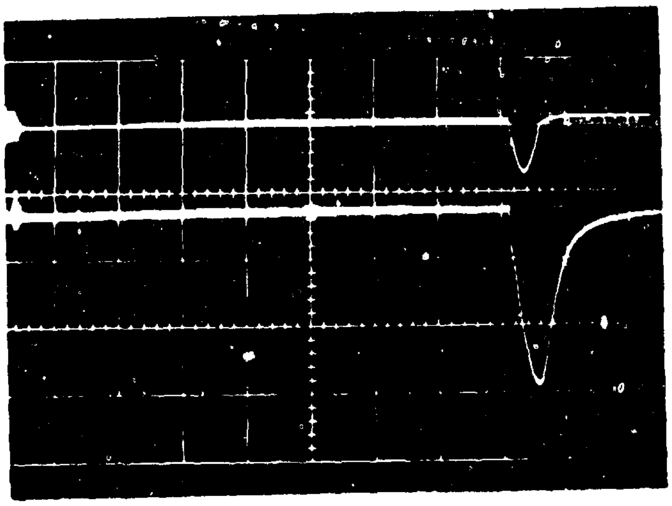

Time (20 µ sec/cm)

Figure 46. Current and Light Probe Reading (11 KV)

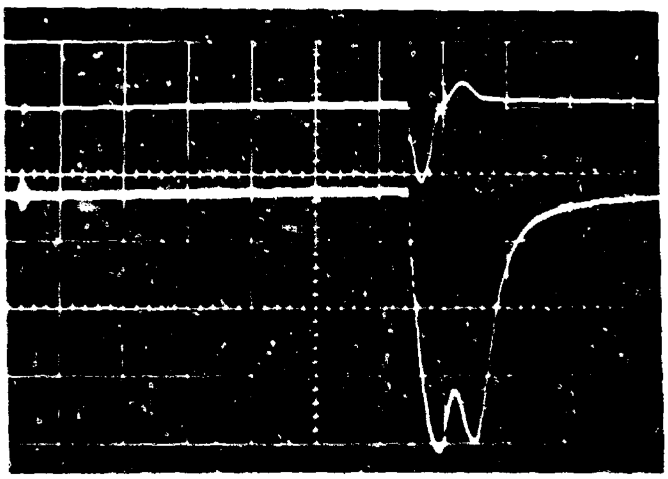

Time (20 µsec/cm)

Figure 47. Current and Light Probe Reading (12 KV)

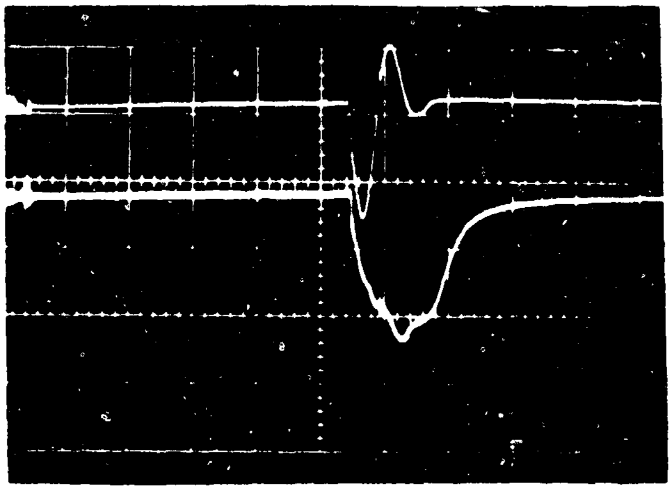

Current

Light

Time (20 µ sec/cm)

Figure 48. Current and Light Probe Reading (14 KV)

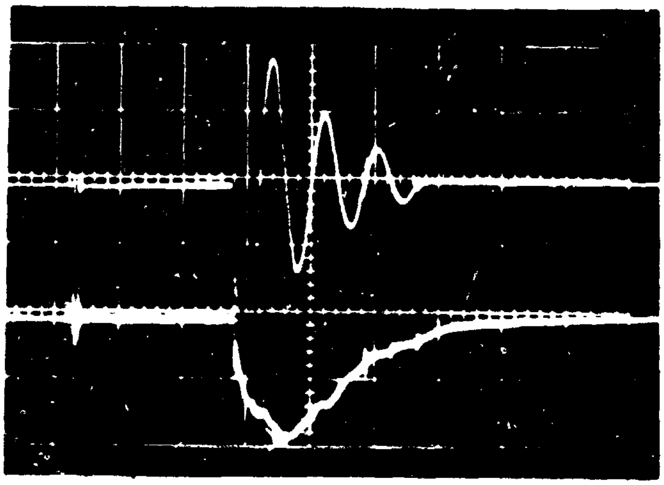

Current

Light

Time (20 µ sec/cm)

Figure 49. Current and Light Probe Reading (15 KV)

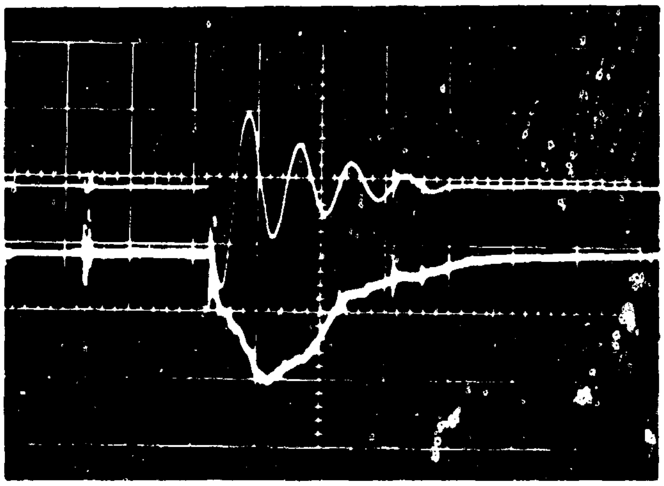

Time (20 μ sec/cm)

Figure 50. Current and Light Probe Reading (20 KV)

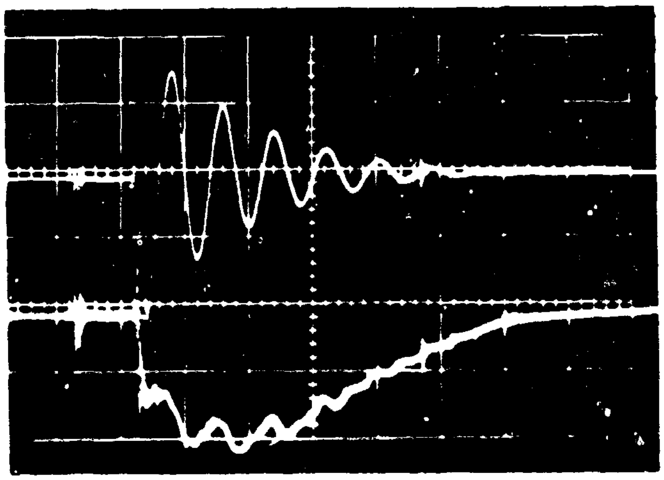

Time (20 μ sec/cm)

Figure 51. Current and Light Probe Reading (25 KV)

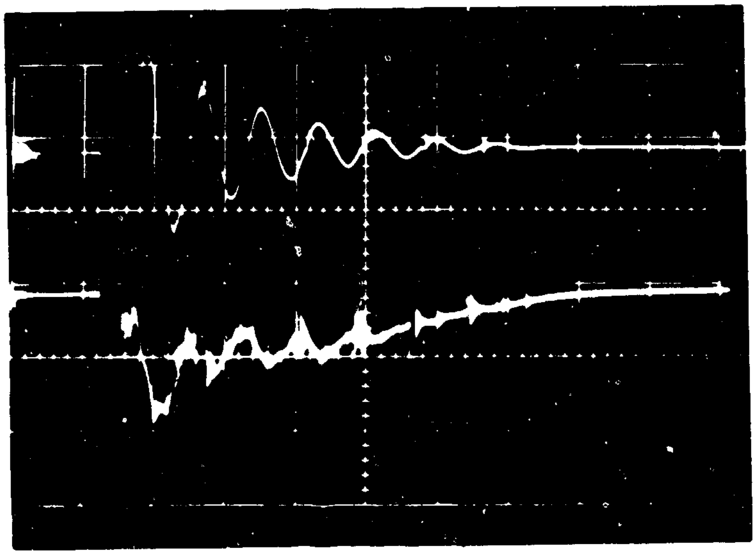

Time (20 μ sec/cm)

Figure 52. Current and Light Probe Reading (40 KV)

F. ACOUSTIC WAVEFORM SHAPING

Studies were carried out of the effect of varying current waveform on the shape of the initial acoustic pulse in order to explore the feasibility of altering the frequency spectrum or imparting a "signature" shape. Both fresh water and salt water discharges were examined. The staggered multi-capacitor energy storage system described in Section IIB was used for this study. Briefly, the firing at controlled time spacing of up to three of the 15 μfd capacitors provides sufficient control to generate a fair variety of single and multiple pulse discharges encompassing a fairly wide range of discharge current wave shapes.

An important difference, which affected the study of multiple pulse discharges, was found between fresh water and salt water. Figure 53 shows two examples of the voltage versus current resulting from delayed discharges of two capacitors. The fresh water case shows that once the initial discharge has effectively been quenched, reapplication of voltage does not lead to an immediate strong discharge;

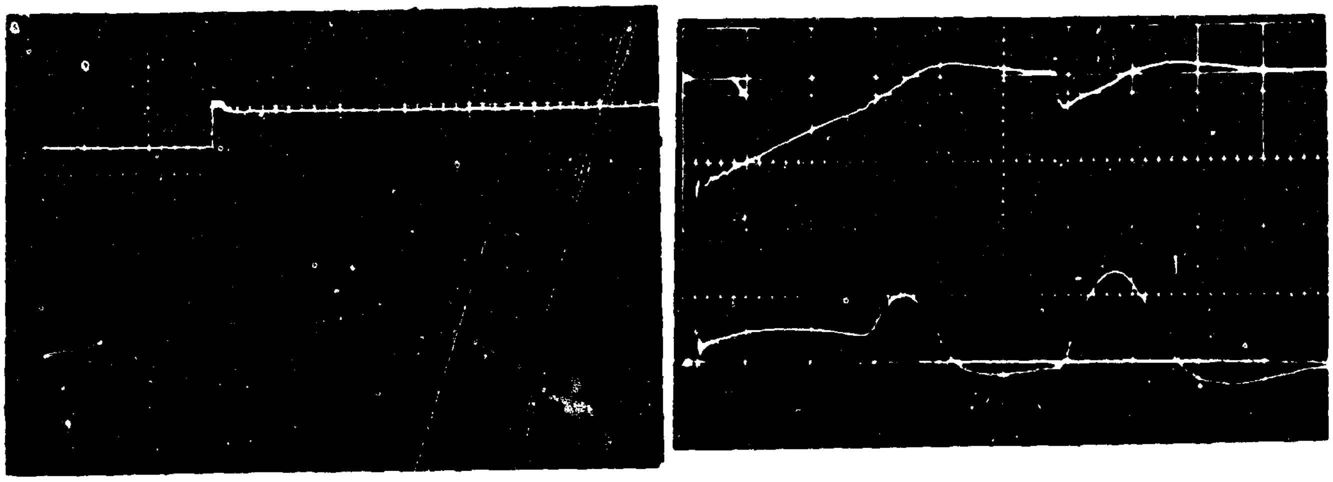

Upper trace - voltage = 10kV/div
sweep = 100 μ sec/div
Lower trace - current = $2x10^4$ amps/div
sweep = 10 μ sec/div
Seoond capacitor delay - 22 μ sec

Shot A33, S = 0 ‰

Upper trace - voltage = 10kV/div
Lower trace - current = $1x10^4$ amps/div
sweep = 10 μ sec/div
Second capacitor delay - 58 μ sec

Shot B117, S = 32 ‰

Figure 53. Two Capacitor Discharges in Fresh and Salt Water

but rather a new induction period (270μ seconds here) is required. Because of the oscilloscope sweep speed chosen, only the first current peak was recorded here. This result represents a severe limitation on use of multiple discharges in fresh water, restricting their practical use to cases where there is overlapping of the currents from the two capacitors. No such limitation is found for the salt water case; in general, immediate development of a strong discharge from the second capacitor was always observed. The fact that the gas bubble formed from the discharge has a life in the order of milliseconds means that it must be present on the electrodes. Hence, the gas bubble in salt water appears to have a low breakdown level in contrast to that found in fresh water.

A series of tests using the same total stored energy in the capacitor system to generate a variety of current wave forms was executed. Examples of the resultant voltage, current, and pressure waveforms are presented in Figure 54. As can be immediately seen, the results in terms of significant alteration of the shape of the primary pressure pulse radiated are largely negative. A reduction of the peak pressure is apparently associated with the reduction in the initial electric current resulting from lower initial voltage.

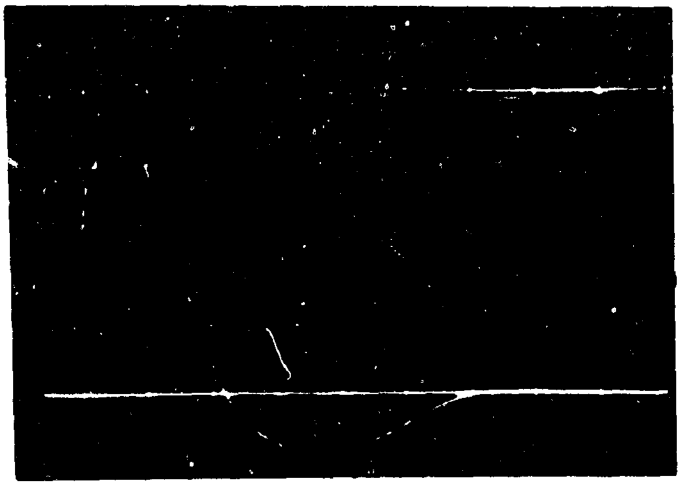

Upper, voltage = 10 kV/div
Lower, current = 10^4 amps/div
Sweep = 5 μsec/div

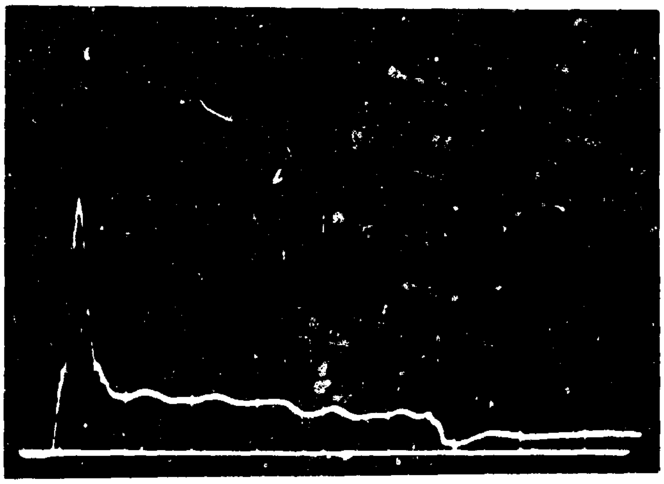

Pressure = 60 psi/div
Sweep = 50 μsec/div
Range = 1 yard

Shot A92 - One Capacitor, 17 kV

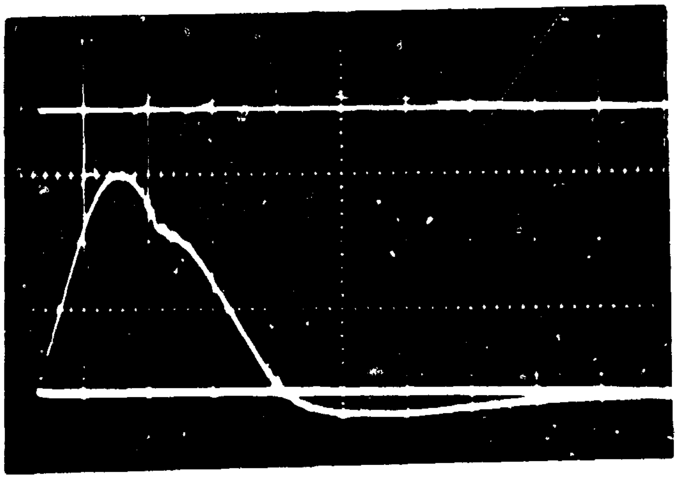

Upper, voltage = 10 kV/div
Lower, current = 10^4 amps/div
Sweep = 5 μsec/div

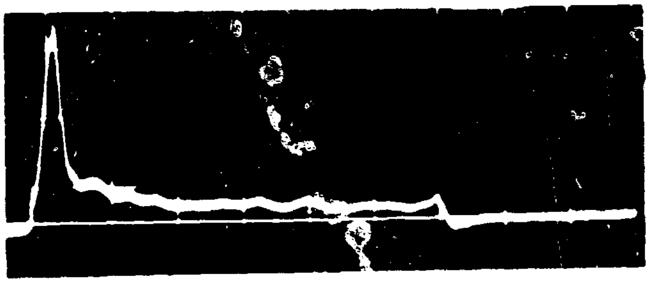

Pressure = 60 psi/div
Range = 1 yard
Sweep = 50 μsec/div

Shot A88 - Two Capacitors 15kV and 8 kV

FIGURE 54a. CURRENT WAVEFORM SHAPING IN FRESH WATER

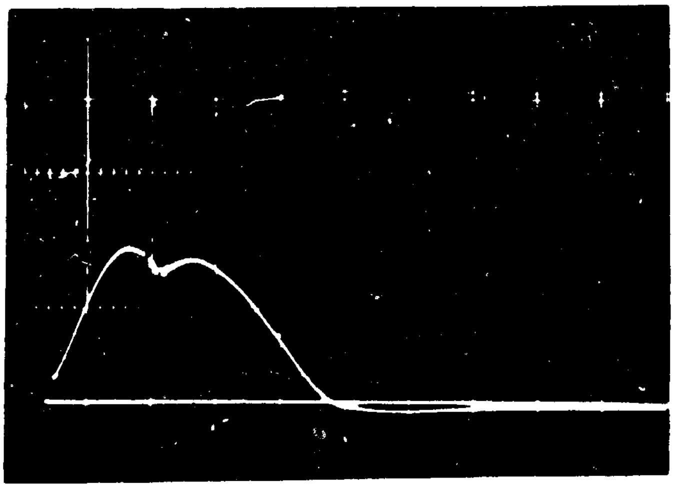

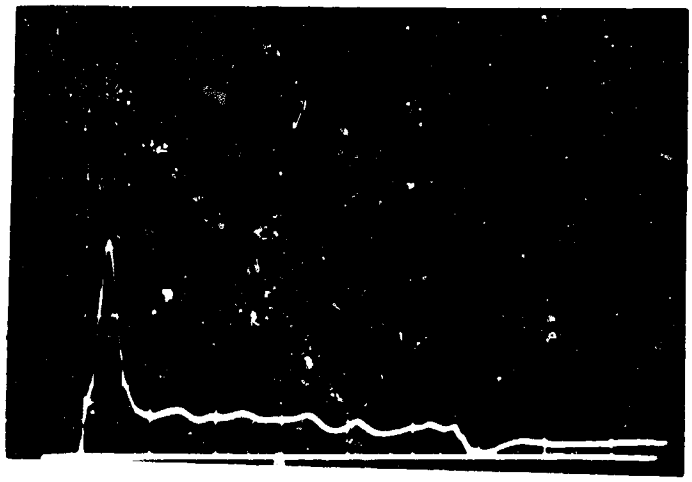

Upper, voltage = 10 kV/div
Lower, current = 10^4 amps/div
Sweep = 5 μsec/div

Pressure = 60 psi/div
Sweep = 50 μsec/div
Range = 1 yard

Shot A91 - Two Capacitors; 12 kV and 12 kV

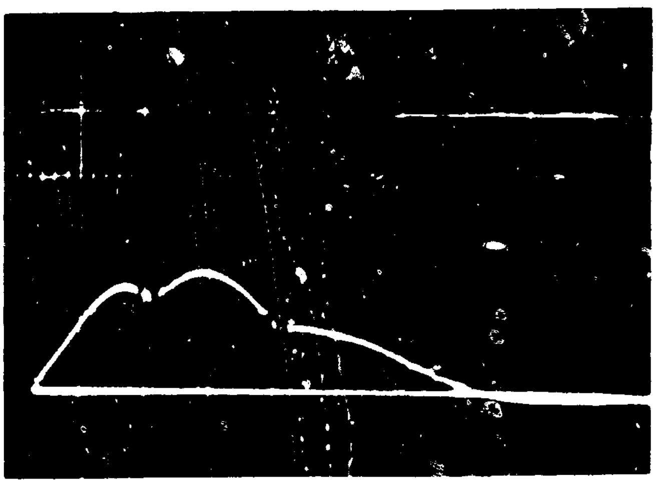

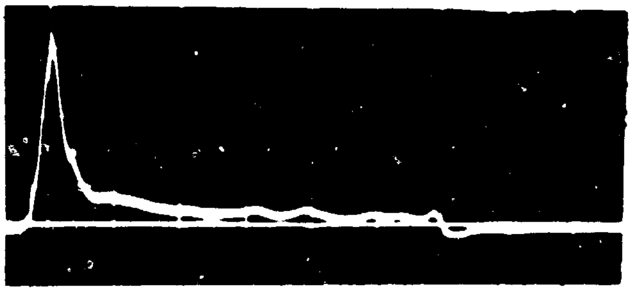

Upper, voltage = 10 kV/div
Lower, current = 10^4amps/div
Sweep = 5 μsec/div

Pressure = 60 psi/div
Sweep = 50 μsec/div
Range = 1 yard

Shot A86 - Three Capacitors; 10 kV, 10 kV and 9.5 kV

FIGURE 54b. CURRENT WAVEFORM SHAPING IN FRESH WATER

The results of a similar series of shots in salt water solution VI (S approximately 32%) are shown in Figure 55. The pressure traces were taken on a more expanded time scale than in the fresh water series. The initiation period of the discharge and its associated pressure signal are evident. It can be seen that considerably more success in imparting different "signatures" to the acoustic pulse was achieved in salt water. Inspection of shot B 127, for example, shows a time correspondence between the two current peaks corresponding to the two strong discharges and the two humps in the pressure record. The second current peak appears to generate a considerably weaker signal despite its considerably greater energy; this effect is generally observed and probably serves to explain the negative results of the wave shaping attempts in fresh water. Apparently energy deposition in the expanding gas bubble produces relatively less acceleration of the water interface, due either to remoteness of the latter or a larger mass of vapor in the bubble. Shaping of this portion of the waveform thus requires proportionally greater energy expenditure.

Figure 56 shows the result of a band-averaged calculation of the energy spectrum of shots B 127 and B 128 (Figure 55b); since the average level of signal was somewhat different, the abscissae have been normalized by the total energy in the part of the pulse recorded. A definite, though small, change in the distribution is evident; however, the effects would be made more dramatic and carried into a more useful frequency regime if the pulse spreading were further broadened.

In general, it can be stated that some qualitative success was achieved in shaping the waveform of the acoustic pulse in salt water through use of delayed multicapacitor discharges emitted by one source. The effects so far investigated affect principally the frequency region above 10 kc. Little success was achieved in fresh water, in part due to an observed tendency of the discharge to resist reignition after cessation of the first capacitor's current. The results obtained suggest that varying the frequency content of the acoustic pulse radiated is perhaps more efficiently carried out by discharging in sequence several closely spaced discrete sources rather than sequentially energizing a singular source.

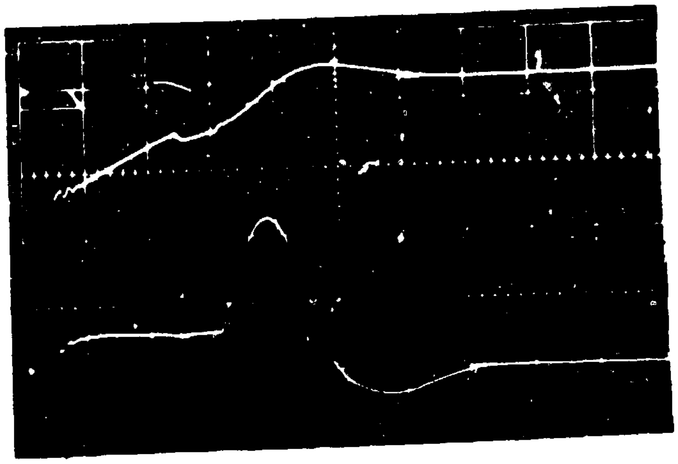

Upper, Voltage = 10kV/div
Lower, current = 10^4 amps/div
Sweep = 10 μsec/div

Pressure = 49 psi/div
Range = 2 feet
Sweep = 20 μsec/div

Shot B116 - Two Capacitors: 16 kV and 10 kV

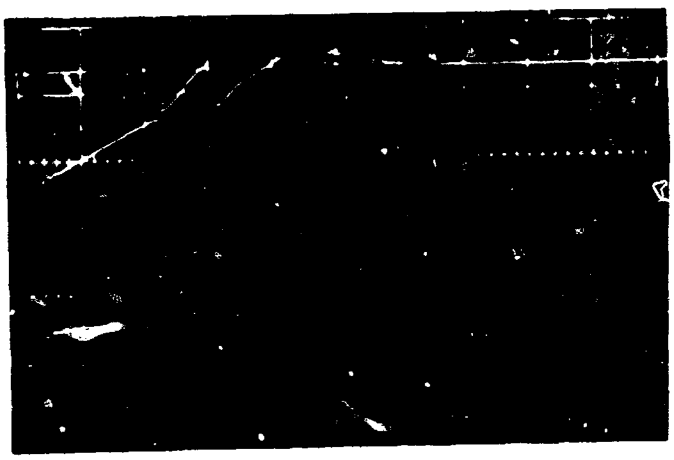

Lower, current = 10^4 amps/div
Upper, voltage = 10 kV/div
Sweep = 10 μsec/div

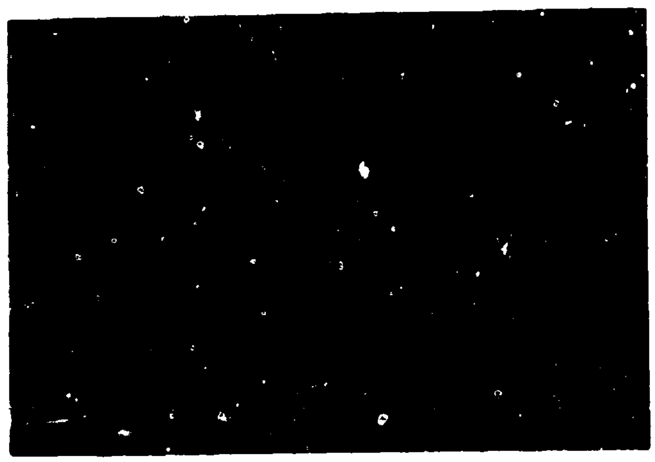

Pressure = 48 psi/div
Range = 2 feet
Sweep = 20 μsec/div

Shot B124 - Two Capacitors: 18 kV and 15 kV

Figure 55a. Current Waveform Shaping in Salt Water

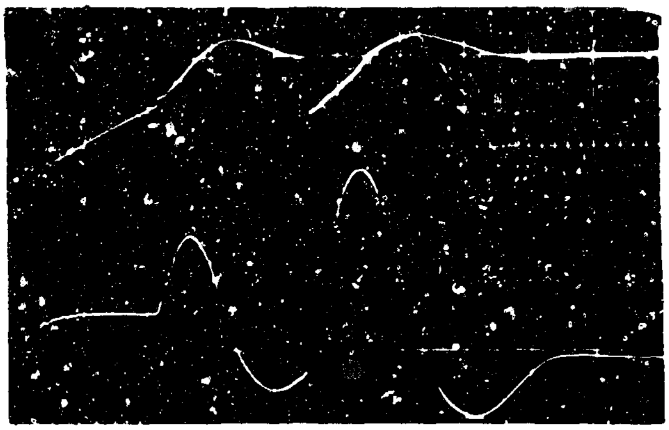

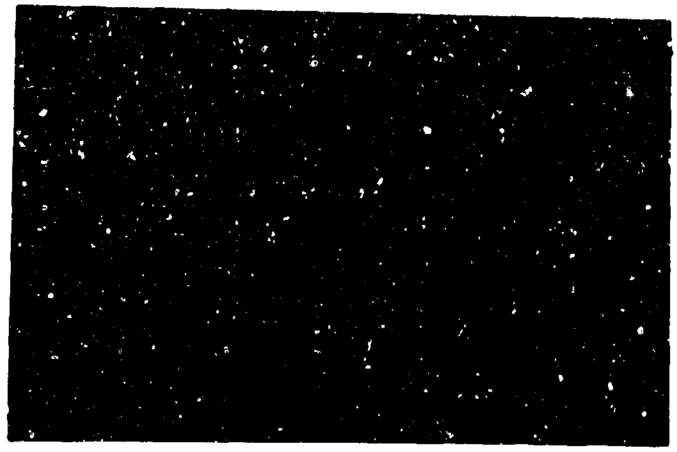

Upper, voltage = 10 kV/div
Lower, current = 10^4 amps/div
Sweep = 10 μsec/div

Pressure = 48 psi
Range = 2 feet
Sweep = 20 μsec/div

Shot B127 - Two Capacitors: 18 kV and 18 kV

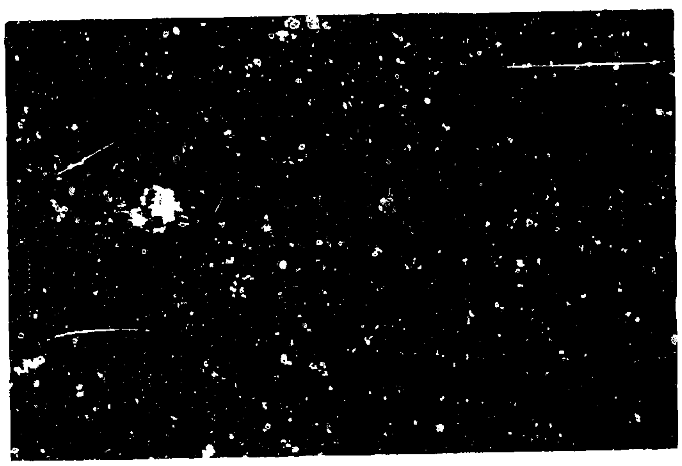

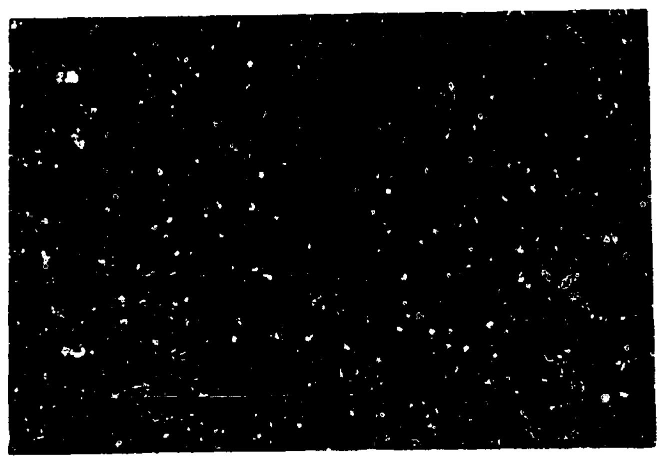

Upper, voltage = 10 kV/div
Lower, current = 10^4 amps/div
Sweep = 10 μsec/div

Pressure = 48 psi/div
Range = 2 feet
Sweep = 20 μsec/div

Shot B128 - Two Capacitors: 18 kV and 18 kV

Figure 55b. Current Waveform Shaping in Salt Water

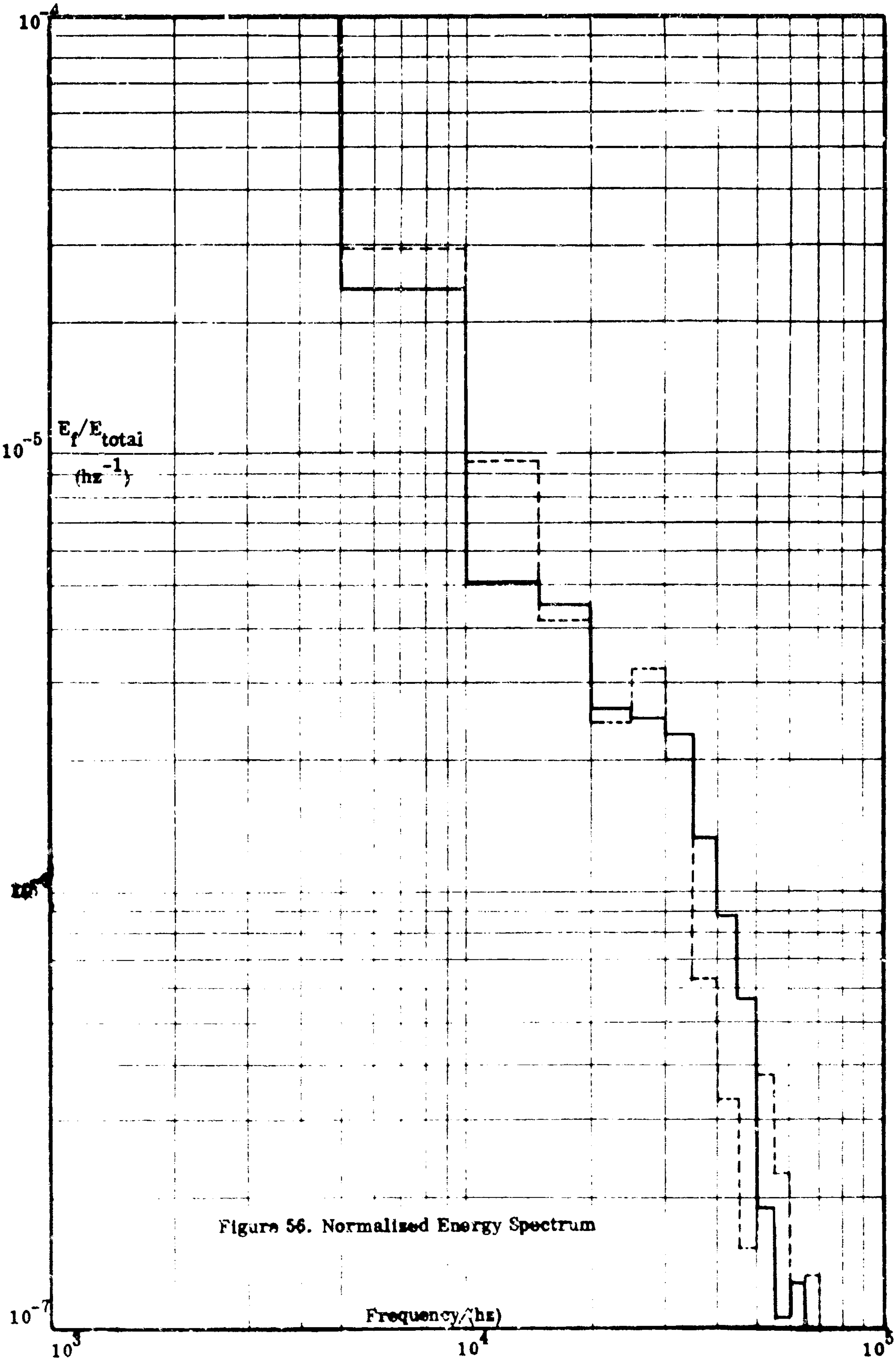

Figure 56. Normalized Energy Spectrum

SECTION IV

CONCLUDING REMARKS

A. COMPARISON OF ELECTRIC DISCHARGES WITH OTHER SOURCES

Impulsive sound sources achieve, through rapid and efficient energy deposition, very high peak pressures in acoustic signals containing one, or at the most, a few aperiodic pulses. These acoustic pulses are produced by rapid acceleration of the water surface in the vicinity of the source; a variety of mechanisms have been employed, and these may be grouped as follows:

1) rapid generation or release of high pressure permanent (non-condensable) gas. Underwater explosions and the various air guns employing fast release valving are examples of this group.

2) rapid generation of a high pressure (and temperature) water vapor bubble through vaporization of the water near the transducer surface. The various open underwater electrical discharge devices, including the type described in this report, are included in this category; the principal distinction from the first group lies in the condensable nature of the water vapor bubble, which disappears almost immediately upon implosion.

3) acceleration of a solid wall or boundary in contract with the water. A wide variety of devices, differing in the means employed for accelerating the wall, exist; these means include electromagnetic ("Boomer", pinger), contained explosions or combustion, and contained electrical discharges.

4) generation of a cavitation bubble which, on implosion, produces a strong pressure pulse as the water decelerates near the end of the implosion process. Rapid motion of a plate or piston has been used to produce the cavitation; a related technique is the rupture of evacuated glass spheres.

Common to the acoustic signals from all these devices is an initial very intense pressure pulse, containing the greater part of the acoustic energy generated by the initial outward motion of the water. Return of the water towards its initial configuration leads to a long weak negative (expansion) pulse immediately followed by a strong implosion pulse as the water reaches minimum radius (complete condensation, usually, for electric discharge devices), generated by the sudden positive acceleration.

The two strong pulses contain most of the energy, and determine, by their shape and spacing, the frequency spectrum of the impulsive signal. An ideal impulsive spike generates a flat frequency spectrum signal;for real signals (as above), the low frequency spectrum will be enhanced by contributions from frequencies harmonically related to the period between the pulses, and the high frequency content will be governed by the shape of the pulses, tailing off the more rapidly as the pulse is broadened from ideal spike shape.[13,14]

It is of particular interest to examine the differences that may be expected between electrical discharges and explosions in this regard. Initial conditions in both the electrical discharge arc channel and the gas sphere resulting from the underwater detonation of a chemical explosive are, for usual energies, sufficiently high that a shock front discontinuity is developed.[4,8] Theoretical determination of the pressure profile behind this front has been extensively worked out for explosives in the work summa rized by Cole including the effects of three dimensional geometry, non-linear propagation, and motion of the expanding bubble. The assumption was made in this work that initial conditions corresponding to complete energy release of the explosion at constant volume provided a good approximation, due to the fact that since in water the sound speed behind a shock front exceeds the shock front velocity, pressure information on the early details of the expansion process tends to be absorbed into the front. The same considerations would seem applicable to underwater electrical discharges to the same approximatetion in view of the generally small duration of energy deposition (typically under 50 microseconds).

McGrath[15-17] has performed an extensive comparison of electrical discharges (wire stabilized) and explosions, specifically directed to ascertaining whether the peak pressure and decay rate obey the same scaling laws for the two classes of acoustic sources. He assumed that the energy deposited in the water through the arc resistance was equivalent to the energy of detonation of the explosive, and hence related to its weight. Application of corrections for circuit energy losses, initiating wire vaporization energy and instrumentation response characteristics led to the conclusion that the function E/r (equivalent to the commonly used $W^{1/3}/R$ parameter for explosives) correlated the peak pressure of electric discharges well and gave reasonable correspondence to explosive sources; both cases were found to be represented by curves of the form $p_m = a(E^{1/3}/r)^b$, where p_m is the peak pressure, r the distance from the source, and E the energy released.

The discrepancy between the two classes in this correlation was of the order of 40% in the pressure (higher for the electrical discharge); in view of the wide range of energy involved, this agreement is remarkable. At least some of the discrepancy may be accounted for by the possibility that McGrath's correction for energy used in vaporization of his initiating wire over-compensated due either to partial vaporization or to availability of a part of this energy for acoustical pulse generation.

McGrath obtained similar agreement between electrical discharges and underwater explosions in the rate of pressure decay behind the initial shock front in terms of the Kirkwood-Bethe theory,[4] although the scatter was somewhat larger in accord with the difficulties in measuring the very small (microsecond) time intervals obtained at the close ranges of laboratory scale experiments. Using the parameter $W^{1/3}$ (equivalent to energy), where W is the weight of explosive and making the conversion of electrical energy into equivalent weight be obtained:

$$\tau / W^{1/3} = 58\,(W^{1/3}/R)^{-0.22} \quad \text{explosives}$$ [18]

$$\tau / W^{1/3} = 70\,(W^{1/3}/R)^{-0.22} \quad \text{electric discharges}$$

where τ = time constant of decay (assumed exponential)

These results provide reasonable substantiation for the hypothesis that the form of the initial shock wave (and thrus its contribution to the source spectrum) is governed principally by the total amount of energy released into the water; in the case of explosives this corresponds to the detonation energy, and for electrical discharges the energy dissipated in the arc resistance. Contributions to the spectrum from the imploding gas bubble may be expected to differ due to the different nature of the gas or vapor involved, thus affecting both the time of collapse and the intensity of the signal radiated; these contributions may be expected primarily at the lower frequencies.

B. SUMMARY

Operation of the inverse pinch geometry in underwater electrical discharges, viewed as acoustic sources, has been evaluated. The basic characteristics of the signal radiated (e.g., distance dependence, waveform, etc.) are similar to general underwater discharges and explosive sources. Critical dependence of the energy efficiency on the electrical damping characteristics of the discharge circuit (including the discharge itself) was found. However, high speed optical investigations disclosed that, under the achievable energy and configuration limitations, it was not possible to produce a discharge of the desired cylindrical symmetry.

Auxiliary investigations demonstrated that the configuration produced satisfactory strong(arc-like) discharges in water equivalent in salinity to sea water; however, the increased energy loss during initiation of the arc, due to the higher conductivity of the water, tended to decrease overall efficiency in saline solutions. It was also demonstrated that near field acoustic signals may be shaped to a considerable extent by tailoring the waveform of the electrical discharge (with significantly decreased energy efficiency, however).

REFERENCES

1. Anderson, O.A., H.P. Furth, J.M. Stone, and R.E. Wright, "Inverse Pinch Effect," Physics of Fluids, 1 (6), 489-494, (1958).

2. Vlases, G.C., and Jones, D.L., "Blast Waves from an Inverse Pinch Machine," Physics of Fluids, 9 (3), 478-485, (March, 1966).

3. Dietrich, G. "General Oceanography," Interscience, 1957.

4. Cole, Robert H., Underwater Explosions, Princeton University Press, 1948.

5. Skvortsov, Yu. V., V.S. Komel'kov and N.M. Kuznetsov, "Expansion of a Spark Channel in a Liquid," Zh. T.F., 30 (10), 1165-1177, October 1960; Sov. Phys. - Tech. Phys. 5, 1100 (1960).

6. Pastukhov, V.N., "Initial Stage of an Electrical Discharge in Water," Sov. Physics - Technical Physics, Vol. 13, No. 2, August 1968, pp. 232-234.

7. Caulfield, D.D., "Predicting Sonic Pulse Shapes of Underwater Spark Discharges," Deep-Sea Research, 1962, Vol. 9, pp. 339-348, Pergamon Press.

8. Martin, E.A., "Experimental Investigation of a High-Energy Density, High Pressure Arc Plasma," J. Applied Phys., 31 (2), 255-267, 1960.

9. Bazhenova, T.V., and R.I. Soloukhin, "Pressure Field Occurring in Water During an Electrical Discharge," Publishing Office of the Academy of Sciences of the USSR in "Physical Gasdynamics", 1959. Available in "Physical Gasdynamics", (Ed. in Chief-Predvoditelev), Pergamon Press, New York, 1961, pp. 144-153.

10. Mel'nikov, N.P., Ostroumov, G.A., Stoyak, M. Yu, "Formation of Electrical Breakdown in Aqueous Sodium Chloride Solutions," Sov. Phys. - Technical Phys., Vol. 9, No. 5, November, 1964, pp. 730-733.

11. Guman, W.J., McIlroy, W., "Study of Pulsed Underwater Sound Projector," Second Semi-Annual Status Report, FHR 2220-2, PCD-TR-65-27, December, 1965, Fairchild Hiller Corp., Republic Aviation Division, Farmindale, New York.

12. Pearson, J., Cavalconte, C., Guman, W.J., Granet, I., "The Design, Fabrication and Test of a Pulsed-Pinch Plasma Engine for Space Applications," Engineering Aspects of Magnetohydrodynamics, Edited by C. Mannal and N. Mather, Columbia University Press, New York, 1962.

13. Weston, D.E., "Underwater Explosions as Acoustic Sources," Proc. Phys. Soc. 76 (2), 233 (1960).

14. Weston, D.E., "Explosive Sources," in "Underwater Acoustics," Vol. 1, Ed. V.M. Albers; Plenum Press 1961.

15. McGrath, J.R., "Scaling Underwater Exploding Wires," J. Applied Physics 37, (12), 4439-4443, 1966.

16. McGrath, J.R., "Scaling Underwater Exploding Wires, NRL Report 6266, December 17, 1965.

17. McGrath, J.R., "Underwater Exploding Wires," Naval Oceanographic Office Informal Report, IR No. 67-87, November, 1967.

18. Arons, A.B., "Underwater Explosion Shock Wave Parameters at Large Distances from the Charge," J. Acoustical Soc. Am. 26, 343, (1954).

SUPPLEMENTARY BIBLIOGRAPHY

Nakao, Y., and Sakamoto, S., "Research on Underwater Spark Discharge," Electrical Engineering in Japan, 87, (5), 83-90, (1967).

Schmied, H., "Die elektrische Unterwasserentladung als Stosz-Schaligenerator hober Leistung," Acustica, 19 (2), 107-108 (1967/1968).

Roi, N.A., and Frolov, D. P., "On the Electroacoustical Efficiency of a Spark Discharge in Water," Doklady AN SSSR 118, 683, (1958); Sov. Phys. - Doklady 3, 118 (1958).

Ioffe, A. I., Naugol'nykh and Roi, N.A., "On the Initial Stage of an Electrical Discharge in Water," Zh. prikl. mekh. i tekh. fiz, 4, 108 - 113, (1964).

Arsent'yev, V. V., "Theory of Impulsive Discharges in a Liquid Medium," Zh. prikl. mekh itekh. fiz, 5, 51-57 (1965).

Naugol'nykh, K. A., and Roi, N. A., "Electrical and Hydrodynamical Characteristics of an Impulsive Corona in Water," Soviet Physics - Acoustics, 13 (3), 352-359, (1968).

Okun, I. Z., "Use of Dimensional and Similarity Methods in Investigating Pulse Discharge in Water," Sov. Phys.-Tech. Phys., 12 (9), 1267-1273 , (March 1968).

Guman, W. J., "Study of an Inverse-Pinch Electric Discharge Sound Source," U. S. Navy Journal of Underwater Acoustics, Vol. 17, No. 3, pp. 511-521 (July 1967).

Naugol'nykh, K. A., and Roi, N. A., "On the Relationships Between Hydrodynamic and Electrical Characteristics of a Discharge in a Liquid," Doklady AN SSSR 168 (3), 556, (1966).

Fillipov, N. V., Zhurin, V. V., Sulyayev, V. A., "Electrical Discharge in Water," Inzhenernyy Zhurnal, Vol. 2, No. 4, 341-343, (1962), available as FTD-TT-63-385/ 1 and 2, Foreign Technology Division, Air Force Systems Command, Wright Patterson Air Force Base, Dayton, Ohio.

Rust, H. H., Drubba, H., Praktische Anwendung des Unterwasserfunkens als Impulsschallgeber fur die Echolotung, Z. Ang. Physik V - Band, Heft 7, pp 251-252 , (1953).

Gardner, S., Electoacoustic Properties of the Underwater Spark Discharge Report 5480, Edo Corporation, College Point, N. Y. (1 June 1961).

Drubba, H., Rust, H. H., The Underwater Spark as an Acoustic Impulse Source, Archiv fur Electrotechnik, Vol. 7, pp 429-440, (1953).

McGrath, J. R., Some Mathematical Aspects of Underwater Explosions Caused by Exploding Wires, Informal Report IR No. 67-63, Naval Oceanographic Office, Washington, D. C., (August 1967).

Yutkin, L. A., Gol'tsova, L. I., Method of Obtaining High and Ultrahigh Pressures and Devices for its Realization, AFFTD TT-64-965, Foreign Technology Division, Air Force Systems Command, Wright Patterson AFB, Dayton, Ohio, (15 February 1965).

Bailitis, E., The Sound Pulse from a Spark Discharge in a Fluid, Z. f. Angew Physik einschliesslich Nukleonik, 9, Heft 9, pp 424-434 (1957).

Wright, H., Underwater Electrodeless Spark Sound Source, Technical Report, AVSSD-0359-67-CR Contract NONR 4389 (00), 10 October 1967. Avco Space Systems Division, Avco Corporation, Lowell, Massachusetts.

Vorotnikova, M. I., Effect of Rate of Heat Release in Electrical Explosions in Water on the Distribution of the Explosion Energy, Zh. prikl. mekh i tekh. fiz. 2, 110 (1962).

Vaughan, W. J., Underwater Shock Waves formed by Exploding Wires, NRL Report 5901 (April 30, 1963).

PROJECT REPORTS AND PUBLICATIONS

Semi-annual Status Reports:

No. 1	Report No. RAC 2229-1, 1 June 1965
No. 2	Report No. FHR 2229-2, 1 December 1965
No. 3	Report No. FHR 2229-3, 20 June 1965 (also available as Technical Report FHR 2292-3A, December, 1966.
No. 4	Report No. FHR 2229-4, 30 June 1967
No. 5	Report No. FHR 2229-5, 31 December 1967

Publications:

"Study of an Inverse-Pinch Electric Discharge Sound Source," by William J. Guman, U.S. Navy Journal of Underwater Acoustics, 17 (3), 511-521, (July, 1967), Unclassified.

APPENDIX 1

INSTANT OCEAN

Synthetic Sea Salts Analysis

	% by weight
$NaCl$	65.270
$MgSO_4$	16.318
$MgCl_2$	12.770
$CaCl_2$	3.266
KCl	1.738
$NaHCO_3$	.4966
KBr	.06753
$SrCl_2 \cdot 6H_2O$	.04692
$MnSO_4 \cdot H_20$	.009384
$Na_2HPO_4 \cdot 7H_2O$	.009384
$LiCl$	.0002346
$Na_2MoO_4 \cdot 2H_2O$	.0002346
$Na_2S_2O_3 \cdot 5H_2O$	.0002346
$Ca(C_6H_{11}O_7)_2$	.0001564
$Al_2(SO_4)_3$	.0001126
$RbCl$	.00003754
$ZnSO_4 \cdot 7H_2O$	.00002402
KI	.00002252
$CoSO_4$	.00001251
$CuSO_4 \cdot 5H_2O$	.000002502
	99.99 %

UNCLASSIFIED

Security Classification

DOCUMENT CONTROL DATA - R & D

(Security classification of title, body of abstract and indexing annotation must be entered when the overall report is classified)

1. ORIGINATING ACTIVITY (Corporate author) Fairchild Hiller Corp/Republic Aviation Division Power Conversion Department Farmingdale, New York 11735	2a. REPORT SECURITY CLASSIFICATION Unclassified 2b. GROUP

3. REPORT TITLE

Studies of an Electric Discharge Underwater Sound Source

4. DESCRIPTIVE NOTES (Type of report and inclusive dates)

Final Report 1 December 1964 - 31 October 1968

5. AUTHOR(S) (First name, middle initial, last name)

Dr. William J. Guman
Dr. Burton G. Humphrey, Jr.

6. REPORT DATE	7a. TOTAL NO OF PAGES	7b. NO OF REFS
	100	18

8a. CONTRACT OR GRANT NO Nonr 4741(00) b. PROJECT NO	9a. ORIGINATOR'S REPORT NUMBER(S) PCD-TR-68-16, FHR 2229-7
c. d.	9b. OTHER REPORT NO(S) (Any other numbers that may be assigned this report) PC088R0004

10. DISTRIBUTION STATEMENT

Distribution of this docuement is unlimited.

11. SUPPLEMENTARY NOTES	12. SPONSORING MILITARY ACTIVITY Office of Naval Research, Code 468 Acoustics Programs Washington, D.C. 20360

13. ABSTRACT

Operation of the inverse pinch geometry in underwater electrical discharges, viewed as acoustic sources, has been evaluated. The basic characteristics of the signal radiated (e.g., distance dependence, waveform, etc.) are similar to general underwater discharges and explosive sources. Critical dependence of the energy efficiency on the electrical damping characteristics of the discharge circuit (including the discharge itself) was found. However, high speed optical investigations disclosed that, under the achievable energy and configuration limitations, it was not possible to produce a discharge of the desired cylindrical symmetry.

Auxiliary investigations demonstrated that the configuration produced satisfactory strong (arc-like) discharges in water equivalent in salinity to sea water; however, the increased energy loss during initiation of the arc, due to the higher conductivity of the water, tended to decrease overall efficiency in saline solutions. It was also demonstrated that near field acoustic signals may be shaped to a considerable extent by tailoring the waveform of the electrical discharge (with significantly decreased energy efficiency, however).

DD FORM 1473

UNCLASSIFIED

Security Classification

KEY WORDS	LINK A		LINK B		LINK C	
	ROLE	WT	ROLE	WT	ROLE	WT
Underwater Acoustic Source						
Underwater Electric Discharges						
Sound Source						